DYNAMICAL SENSITIVITY ANALYSIS OF TROPICAL CYCLONE STEERING AND GENESIS USING AN ADJOINT MODEL

By

Brett T. Hoover

A dissertation submitted in partial fulfillment of

the requirements for the degree of

Doctor of Philosophy

(Atmospheric and Oceanic Sciences)

at the

UNIVERSITY OF WISCONSIN – MADISON

2010

Abstract

The adjoint of a numerical weather prediction (NWP) model calculates the sensitivity of a pre-defined "response function" of the model verification state with respect to small perturbations of the model state at earlier times. For response functions describing the growth or behavior of tropical and extratropical systems, these *sensitivity gradients* provide a wealth of dynamical information that would be difficult or impossible to obtain otherwise. An investigation into the dynamical sensitivity of a specific aspect of an NWP forecast through dynamical *interpretation* of adjoint-derived sensitivity gradients can be called *dynamical sensitivity analysis*.

Physical interpretation of sensitivity gradients is complicated by several factors. The adjoint model is limited by constraints of linearity and their handling of moisture physics, which are either simplified or absent due to the difficulty of including these routines, often based on "if"-statements, in the linear and adjoint code. Poor choices in defining response functions may result in unrealistic sensitivity gradients; these issues can be difficult to avoid, since even a function that describes the particular forecast aspect of interest very well could be based on auxiliary assumptions that render it useless for calculating sensitivity of that forecast aspect (e.g. a priori knowledge of the exact location of a synoptic-scale feature of the forecast at the end of the model simulation). Finally, interpretation must always be framed in the context of hypothetical changes to a response function due to hypothetical perturbations to a model state; one cannot declare entire regions of the basic state as "important" just because they are collocated with a region of strong sensitivity.

Several NWP models and their adjoints are employed to perform dynamical sensitivity analysis of tropical cyclone (TC) steering and genesis. A methodology is

developed to ensure that physical interpretation of sensitivity gradients is validated at every step of the process. Functions traditionally used to describe TC steering and genesis are tested for their appropriateness as response functions, and systematic problems with several functions are diagnosed, and solutions to those problems are also theorized and tested. Once suitable response functions have been chosen, sensitivity gradients are calculated for the explicit purpose of approaching problems in TC steering and genesis from the perspective of the impact of small perturbations on the growth and development of modeled TCs. Sensitivity gradients of a measure of TC intensity are applied to TC genesis in the eastern Pacific; structures in sensitivity with respect to zonal and meridional flow suggest that some TCs have the capability to grow through barotropic conversion of energy from a persistent low-level zonal jet in the southern portion of the basin.

Acknowledgements

I would like to thank my advisor, Dr. Michael Morgan, for his unparalleled mentorship skills. Somehow Michael knows precisely how to balance providing a supportive research relationship with keeping enough distance from the work to allow his students to learn and grow confident as scientists, as well as being a good friend and an outrageously silly person at heart. My committee members: Dr. Jon Martin, whose enthusiasm and good humor are a constant source of inspiration. Dr. Greg Tripoli, who I wanted on my committee because I knew if I could make *him* satisfied with my work I would have no problems. I had two members exterior to the department, Dr. Grace Wahba and Dr. Chris Davis, whom I thank for taking time out of their busy lives to provide refreshing and different perspectives on my research. I can't imagine having formed a better committee – it was an Olympic All-Stars team without the diva-like in-fighting.

Thanks to my lab-mates and good friends, Nick Bassill and Dianna Nelson, who keep the line between "having fun with friends" and "work-related drudgery" sufficiently blurred so as to make me glad to wake up in the morning and head to work (even on a Sunday). There is nothing more valuable than being able to work alongside people so entertaining and talented. I feel like we're all going places.

I want to thank my mother, who has waited patiently to be able to brag to people about this, and my family at large that worked especially hard to make sure I would be able to get as far as I wanted to go.

If scientists indeed must sit on the shoulders of giants to see further than their predecessors, it is these people who give them a much needed boost.

Table of Contents

Chapter 1: Introduction

1.1 What is an adjoint model?

Given initial and boundary conditions, a numerical weather prediction (NWP) model is a system of partial differential equations used to compute time-tendencies of the atmospheric model state. The nonlinear NWP model can be represented as a function of model state M($\mathbf{x}_{in}$), which takes the initial and boundary conditions as its input ($\mathbf{x}_{in}$) and calculates the future state of that system ($\mathbf{x}_{out}$):

$$\mathbf{x}_{out} = M(\mathbf{x}_{in}) \quad (1).$$

The NWP model is typically nonlinear and includes explicit and parameterized moisture physics. One can derive a tangent linear model (TLM) from this model by linearizing the time-tendency equations about a nonlinear NWP model trajectory, called a *basic state*. Given *perturbations* to the initial conditions of the basic state, the TLM calculates the future state of *perturbations* of the system as these perturbations evolve along the trajectory defined by the basic state:

$$\mathbf{x}'_{out} = \mathbf{L}\mathbf{x}'_{in} \qquad (2),$$

where $\mathbf{x}'$ represents a perturbation to the state vector $\mathbf{x}$, and $\mathbf{L}$ represents the "propagator matrix" of the TLM. The TLM does not calculate how an initial state will evolve to a final state, but instead how perturbations to an initial state will evolve to perturbations of a final state, linearized around a basic state defined by the nonlinear model.

The adjoint model is defined as the transpose of $\mathbf{L}$. The adjoint model is used to calculate *sensitivity gradients* of a *response function*. A response function (R) can be any function of model output ($\mathbf{x}_{out}$) of interest, so long as it is differentiable with respect to $\mathbf{x}$. A

sensitivity gradient is simply the gradient of R with respect to $\mathbf{x}$ $\left(\partial R/\partial \mathbf{x}\right)$. A sensitivity gradient describes how a small change in the model state will change the response function defined at model verification, or the *sensitivity* of R with respect to perturbations of the model state. The adjoint model is initialized with $\partial R/\partial \mathbf{x}_{out}$, and computes sensitivity of R (defined at model verification) with respect to small perturbations of model input $\left(\partial R/\partial \mathbf{x}_{in}\right)$:

$$\frac{\partial R}{\partial \mathbf{x}_{in}} = \mathbf{L}^{\mathrm{T}} \frac{\partial R}{\partial \mathbf{x}_{out}} \qquad (3),$$

where $\mathbf{L}^{\mathrm{T}}$ is the transpose of the TLM propagator matrix. Since the adjoint model is the transpose of the TLM, it operates backward through time; sensitivity of R with respect to perturbations of model *output* is used to calculate sensitivity of R with respect to model *input*.

It is important to keep in mind that the adjoint model is linear, as it is the transpose of the TLM. Furthermore, the adjoint model typically lacks all of the moisture physics found in the nonlinear NWP model. Parameterizations of moisture physics typically depend on "if-traps" where several criteria must be met before the parameterized physics are activated; these sorts of (nonlinear) systems are incredibly difficult to utilize in an adjoint model that propagates *backward* through time.

1.2 Sensitivity Gradients and Singular Vectors

The product of the adjoint model, $\partial R/\partial \mathbf{x}_{in}$, describes how small perturbations to the *initial conditions* of the model will impact a function of the model *output*. Provided a suitable response function can be defined for some aspect of interest (e.g. intensity of a cyclone), sensitivity gradients provide valuable *a priori* information about how sensitive that function is to small perturbations to the initial conditions. Hypothetical perturbations have to be kept small in order to maintain linear evolution required by the adjoint model. It is known

that two model simulations of the same event with almost arbitrarily small differences in their initial conditions can lead to drastically different verification states (Lorenz 1963). This has prompted a less deterministic view of atmospheric prediction and the rise of ensemble forecasting as a way to tease out a probability-distribution of future states rather than relying on a single forecast with one set of initial conditions.

For a given deterministic forecast trajectory, sensitivity gradients provide information concerning the sensitivity of some function of the model forecast state to small perturbations of the initial conditions; rather than using an ensemble method where individual perturbations to every variable at every grid point on every level are evolved in the nonlinear NWP model, the adjoint model calculates similar information with a single model run. Furthermore, sensitivity gradients are produced for individual response functions; it is possible to define multiple response functions to describe several different aspects of the model forecast state and derive sensitivities for each of those response functions independently. Sensitivity gradients produce a wealth of dynamical information that would be difficult or impossible to calculate otherwise; ensemble sensitivities produced with even 90 ensemble members can depart drastically from adjoint-derived sensitivities (Ancell and Hakim 2007).

Adjoint models can also be used to calculate singular vectors, which describe successive, orthogonal perturbations to the model state vector that will grow fastest (linearly) along the basic state trajectory, as measured by the growth of a given energy norm metric. Singular vectors are important in analysis of error growth; errors in the initial conditions of an NWP model that project strongly onto the first few leading singular vectors will rapidly grow and degrade the forecast (Lorenz 1965, Farrell 1990).

To find these most unstable dynamical structures in the linear model, we establish a time period $(0 \le t \le \tau)$ over which we measure the growth of perturbations in terms of some measure of perturbation growth: $\mathbf{z}_t = \mathbf{C}\mathbf{x}_t$, with $\mathbf{x}_t$ representing the model state at time t and $\mathbf{C}$ representing a diagonal matrix of scaling factors transforming the variables in $\mathbf{x}$ into a unified measure of perturbation growth, usually an expression of total energy (ε) such that $\varepsilon_t = \langle \mathbf{x}_t; \mathbf{C}\mathbf{x}_t \rangle = \langle \mathbf{z}_t; \mathbf{z}_t \rangle$. Perturbations $\mathbf{v}_i(z)$ which maximize ε solve the eigenvalue problem:

$$\mathbf{L}_*^{\mathrm{T}} \mathbf{L}_* \mathbf{v}_i = \sigma_i^2 \mathbf{v}_i \quad (4)$$

where $\mathbf{L}_* = \mathbf{C}^{1/2} \mathbf{L} \mathbf{C}^{-1/2}$. The eigenvectors are referred to as the right singular vectors. A full derivation can be found in Gelaro et al. 1998.

Mathematically, singular vectors can also be represented as output of singular value decomposition as applied to the model (Thompson 1998):

$$\mathbf{U}\,\Sigma\,\mathbf{V}^{\mathrm{T}} = \mathbf{G} \quad (5).$$

Here, the model serves as a Green function ($\mathbf{G}$) mapping $\mathbf{x}_{\mathrm{in}}$ to $\mathbf{x}_{\mathrm{out}}$, $\mathbf{V}$ and $\mathbf{U}$ represent singular vectors mapped onto $\mathbf{x}_{\mathrm{in}}$ and $\mathbf{x}_{\mathrm{out}}$, respectively ($\mathbf{U}$ represents the evolved singular vectors at $t = \tau$; $\mathbf{u}_i = \mathbf{L}\mathbf{v}_i$), and Σ is a diagonal matrix of singular values which measure the strength of each singular vector pattern. Singular vectors represent a hierarchy of orthogonal vectors within model state-space that map structures of ε in $\mathbf{x}_{\mathrm{in}}$ to structures of ε in $\mathbf{x}_{\mathrm{out}}$. Because singular vectors are concerned only with the growth of this specified "energy norm", the information gleaned from their calculation is neither focused toward a particular aspect of the forecast state nor easily interpreted physically.

1.3 Dynamical Sensitivity Analysis

While the adjoint model lends itself to problems relating to data assimilation through application of four dimensional variational data assimilation (4DVAR; Lewis and Derber 1985), the adjoint model, being the adjoint of the *dynamical* model (more specifically, a linearized dynamical model), ultimately produces *dynamical* information about the evolution of a simulated atmosphere. This information can be used to identify time-scales of physical processes within the model that are important to the response function (Hall and Cacuci 1983), or to test the sensitivity of model results to changes in chosen model parameters (Hall 1986).

Dynamical sensitivity analysis can be used alongside or take the place of traditional studies wherein an aspect of the initial conditions is changed and the evolution of the simulation is compared to a "control" simulation. These studies are often phrased as "what if" questions; "what if the carbon dioxide of the atmosphere were doubled?" (Hall and Cacuci 1983), or "what if the potential vorticity (PV) of an upper trough were removed or altered in the initial model state?" (Fehlmann and Davies 1997). These kind of experiments are typically focused on how these kinds of changes to the initial conditions will impact a specific aspect of the final model state, such as the genesis or intensity of a midlatitude cyclone; a dynamical sensitivity study using an adjoint model and an appropriate response function can perform a similar analysis without the arbitrariness of altering the initial conditions with no *a priori* knowledge of what parts of the initial conditions the cyclone is most sensitive to (Vukicevic and Raeder 1995, Langland et al 1995).

When performing a dynamical sensitivity analysis of this nature, where the goal is to determine what aspects of the model initial state are most important to the evolution of a feature of the model verification state, care has to be taken to remember exactly what

sensitivity gradients are and what they mean. The sensitivity gradient itself does not provide any information about how an aspect of the basic state impacts the evolution of a response function of the basic state; it only refers to how a *hypothetical perturbation* to the basic state will change the response function. A feature of, say, vorticity in the basic state that exists in a region of strong sensitivity with respect to vorticity cannot be said to be particularly important based on this information alone; technically all this means is that a small change to this feature will yield a large impact, which is not the same as saying that this vorticity feature as-is has an impact on the response function as-is (Langland et al. 1995). It is entirely possible that perturbations to the initial conditions in the location of that vorticity feature have the same impact on the response function whether that vorticity feature is there in a basic state trajectory or not (Langland and Errico 1996); if this is the case, it can hardly be said that the vorticity feature is particularly important to the response function in that trajectory. It only exists in a *region* of importance to the response function.

1.4 Study: Dynamical Sensitivity Analysis of Tropical Cyclones

The following study is a dynamical sensitivity analysis of tropical cyclones (TCs), which focuses on two main elements of TC prediction: sensitivity of TC steering, and sensitivity of TC genesis. Many years of study have been devoted to issues regarding the predictability of these two aspects of TC evolution, as accurate prediction of TC steering (and therefore, track) and genesis are required in order to properly inform and prepare all parties that will be impacted by the passage or landfall of a TC in the near future.

Questions remain about the dynamics of TC steering and genesis, as well as what measures can be taken to optimize the forecast of these events. A detailed dynamical

sensitivity analysis can help answer both of these questions. First, sensitivity gradients can provide new insights into the dynamics that drive TC steering and genesis; a study that makes use of an adjoint model alongside more traditional methods can approach questions about TC evolution from a different perspective. Certainly the *a priori* information provided by an adjoint model about the sensitivity of these features can help focus a study that relies on perturbations of model initial conditions to observe an outcome on the forecasted TC. In addition, the arbitrariness of traditional perturbation studies is lost; not only can you know beforehand where perturbations will have the largest impact, but you have an expectation of how large that impact is. The inner product of the sensitivity gradient with the perturbation to the model initial state vector $\left(\mathbf{x}'_{in}\right)$ provides the expected change in the response function ΔR:

$$\Delta R \approx \left\langle \frac{\partial R}{\partial \mathbf{x}_{in}}, \mathbf{x}'_{in} \right\rangle \qquad (6).$$

Sensitivity gradients also provide information regarding the characteristics of errors that are most influential to the TC forecast (e.g. what $\mathbf{x}'_{in}$ creates the largest ΔR given equation 5); this information is more direct than that provided by singular vectors, because sensitivity gradients derived for a response function *defined* as a function of TC steering or TC intensity reveal perturbations to which variables in which locations will have the strongest impact on those aspects of the forecast *specifically*, rather than which perturbations will grow fastest measured by a vague energy-norm that may or may not correspond to TC steering or intensity.

The following study uses adjoint-derived sensitivity gradients to approach questions about TC steering and genesis from this perspective. What perturbations to model initial conditions have the largest impact on the steering of a TC, and why do they have such a

strong impact? What can sensitivity gradients tell us about TC genesis, especially in the tropical eastern Pacific basin where it is thought that some TCs may grow barotropically from the shear produced by a low-level westerly jet? How can information provided by sensitivity gradients be used to direct adaptive observations to improve the initial conditions of NWP models where they will have the largest impact on TC forecasting specifically? Results of this study bring us closer to answering these important questions, and provide evidence that adjoint models can be used as important dynamical tools as well as data assimilation tools.

These questions are each approached using the same general technique. First, an appropriate response function must be found to define the TC forecast aspect of interest (e.g. steering or intensity). The function must not only be differentiable with respect to the model forecast state and make physical sense of the forecast aspect of interest, but it must also satisfy special requirements to be an appropriate response function for the calculation of *sensitivity* to that forecast aspect. Some functions may work perfectly well to define, say, TC steering, but fail to produce reasonable sensitivities to TC steering. This may be because small perturbations to the model initial state can have profound influence on the response function in ways that have nothing to do with TC steering (chapter 2). In order to make sure the response function is appropriate to the task under consideration, perturbations must be made to the model and the results of those perturbations must be observed, to ensure that the resulting change to the response function (Eqn. 6) is physically manifest as a change to the forecast aspect of interest, and not some other, unforeseen effect.

Once an appropriate function has been defined, the sensitivity gradients are interpreted physically. This is done through a combination of inferences made based on the

physics of the model as well as observing perturbations introduced into the model to verify those inferences. In some cases, one can turn to a simplified model in order to gain more in-depth understanding of specific physical processes. In all cases, the questions posed to the models and the results of experiments must take into consideration the limitations of the model, especially the constraints of linearity and simplified (moisture) physics. It is not desirable to pursue questions relating to highly nonlinear, moist-physics dependent aspects of TC genesis with an adjoint model. However, questions surrounding the possibility for barotropic growth of tropical vortices along a low-level westerly jet can be approached with these models (chapter 5).

A dynamical sensitivity study of TC steering is presented in chapters 2 and 3. First, the appropriateness of response functions defining TC steering is analyzed and tested within a simplified barotropic framework (chapter 2), where problems with an existing response function are observed and a solution to those problems is described. In chapter 3, this response function is applied to several cases of TC steering in the tropical western Pacific, and physical interpretation of adjoint-derived sensitivity gradients is used to gain insight into the kinds of perturbations most important for TC steering (and therefore track) errors. In chapter 4, an analysis of several functions to describe TC intensity/genesis is performed, and then an appropriate function is selected to investigate TC genesis in the tropical eastern Pacific (chapter 5). The goal is to determine if barotropic growth of vortices along a low-level westerly jet is a possible growth mechanism for TCs in this basin, and if there is a way to delineate TCs that grow barotropically from those that grow non-barotropically. Conclusions and directions for future research are provided in chapter 6.

Chapter 2: Validation of a Tropical Cyclone Steering Response Function with a Barotropic Adjoint Model*

Abstract

The steering of a tropical cyclone (TC) vortex is commonly understood as the advection of the TC vortex by an "environmental wind." In past studies, the environmental steering wind vector has been defined by the horizontal and vertical averaging of the horizontal winds in a box centered on the TC. The components of this environmental steering have been proposed as response functions to derive adjoint-derived sensitivities of TC zonal and meridional steering. The appropriateness of these response functions in adjoint sensitivity studies of TC steering is tested using a two-dimensional barotropic model and its adjoint for a 24hr forecast. It is found that these response functions do not produce sensitivities to TC steering, because perturbations to the model initial conditions that change the final-time location of the TC also change the response functions in ways that have nothing to do with the steering of the TC at model verification.

An alternate response function is proposed wherein the environmental steering vector is defined as the wind averaged over the response function box attributed to vorticity outside of that box. By redefining the response functions for the zonal and meridional steering as components of this environmental steering vector, the effect of small changes to the final-time location of the TC is removed, and the resultant sensitivity gradients can be shown to truly represent the sensitivity of TC steering to perturbations of the model forecast state.

* Published under: Hoover, B. T., and M. C. Morgan, 2010: Validation of a tropical cyclone steering response function with a barotropic adjoint model. *J. Atmos. Sci.*, **67**, 1806-1816.

2.1 Introduction

An adjoint *sensitivity* study involves evaluating the change in a specific aspect (called a *response function, R*) of a model forecast state ($\mathbf{x}_f = \mathbf{x}(t_f)$) resulting from arbitrary changes in any of the model control variables at the initial ($t = 0$) or forecast times ($t = \tau$). Such a study calculates the gradient of the response function, $\partial R / \partial \mathbf{x}_\tau$, with respect to the model control variables represented by a state vector ($\mathbf{x}_\tau$).[1] An adjoint model is the most efficient tool for evaluating these forecast sensitivities (Errico 1997).

Conspicuously absent from the many prior applications of adjoint-based sensitivity analysis to tropical and extratropical cyclone issues are synoptic and dynamical interpretations of these sensitivities. When dynamical interpretation of sensitivities *is* provided, often what is offered is merely the observation that the distribution of sensitivities (Vukicevic and Raeder 1995, Wu et al. 2007) or singular vectors (Peng and Reynolds 2006, Chen et al. 2009) is coincident with a synoptic feature. Coincidence of adjoint sensitivities with a synoptic feature alone is insufficient to attribute dynamical significance to the feature (Langland et al. 1995). Langland et al. (1995) demonstrate that the sensitivity fields calculated in their study of an idealized cyclogenesis event in a time-evolving, non-zonal flow were very similar to the same calculation performed for a steady, zonal basic state. While adjoint sensitivities do not provide information regarding whether particular physical processes actually occurred within a basic state (control) forecast trajectory, these sensitivities do provide information concerning the effect of possible perturbations to the

[1] Most often, sensitivities are calculated with respect to the model initial and boundary conditions; however, these dynamical sensitivities may be calculated with respect to the model forecast trajectory, $\mathbf{x}_\tau \quad 0 < \tau < t_f$ as well. For the purposes of this study, references to $\mathbf{x}$ can be inferred to mean $\mathbf{x}_f$ when referring to the response function, while references to $\mathbf{x}$ can be inferred to mean $\mathbf{x}_o$ when referring to sensitivities of the response function.

basic state. It is this particular characteristic of adjoint sensitivities that make them a potentially powerful tool in synoptic case studies (Langland and Errico 1996).

In order for the results of an adjoint sensitivity calculation to have meaning, thorough testing and interpretation is required (Errico and Vukicevic 1992). Such rigorous dynamical interpretation and testing of adjoint-derived forecast sensitivities provides a means of characterizing what the sensitivity fields represent and evaluates how well the response function associated with the sensitivity gradients truly measures its intended forecast aspect. In this study, a specific set of response functions, designed to measure instantaneous TC steering, is considered. It is demonstrated that while the response functions chosen are appropriate for diagnosing steering, the sensitivities calculated with these response functions do not provide insight into the sensitivity of TC steering. A solution to this problem is offered and tested.

Wu et al. (2007) presents an objective targeting strategy whereby a response function is defined to represent the zonal or meridional steering of a TC at model verification:

$$R_1 = \frac{\sum_k \sum_{i,j \in D} u_{i,j,k} \, \Delta x \Delta y \Delta p}{\sum_k \sum_{i,j \in D} \Delta x \Delta y \Delta p} \quad (1)$$

$$R_2 = \frac{\sum_k \sum_{i,j \in D} v_{i,j,k} \, \Delta x \Delta y \Delta p}{\sum_k \sum_{i,j \in D} \Delta x \Delta y \Delta p} \quad (2)$$

R_1 and R_2 represent respectively, the horizontally and vertically averaged zonal and meridional wind in a horizontal domain D and bounded between 850 hPa and 300 hPa (indexed by k). The horizontal domain D, or the "response function box", is defined as the set of all grid points (indexed zonally by i and meridionally by j) in a box 600 km on a side,

centered on the model verification position of the TC. In this way, the response function R_1 (R_2) is the environmental zonal (meridional) wind steering the TC at verification (Chan and Gray 1982). The sensitivity gradients can be combined into a vector:

$$ADSSV = \left(\frac{\partial R_1}{\partial \mathbf{x}}, \frac{\partial R_2}{\partial \mathbf{x}} \right) \quad (3)$$

that represents the vector change in steering of the TC given a unit perturbation to a model state vector, **x**. Wu et al. (2007) calls these vectors "Adjoint-Derived Sensitivity Steering Vectors", or ADSSVs, and uses the vectors in an attempt to understand the influence of dropsondes deployed in a Dropwindsonde Observations for Typhoon Surveillance near the Taiwan Region (DOTSTAR) targeted observation field campaign (Wu et al. 2005) to initialize model forecasts of Typhoon Mindulle (2004). Wu et al. (2007) suggests that because these dropsondes provided data in regions of low sensitivity their assimilation would not have significantly improved track forecasts for Mindulle.

While care has been taken to show that sensitivities using these TC steering response functions are coincident with synoptic features likely important to the steering of a modeled TC (Wu et al. 2009a), this coincidence is insufficient to identify those synoptic features as important. Further, no studies exist that test the validity of these response functions by perturbing the initial conditions of the model in regions of high sensitivity, and determining exactly *how* those perturbations impact the response function. Due to the lack of any rigorous testing of the appropriateness of these response functions and a lack of dynamical interpretation of the sensitivity fields, it is unclear whether these sensitivity gradients appropriately describe sensitivity to TC steering.

Using a 2-D, barotropic, non-divergent, inviscid model on an *f*-plane (see Section 2), it is shown in this study that the response functions previously used to define TC steering

(see Wu et al. 2007, Wu et al. 2009a) are inappropriate for diagnosing TC steering sensitivity. A dynamical interpretation of the sensitivity gradients for R_1 and R_2 in the simplified model provides an explanation of the problem as well as the solution. Section 2 provides a description of the model and the idealized case used in the study. A dynamical interpretation of the sensitivities is provided in Section 3, along with an analysis of perturbations introduced into the model in order to verify the interpretation. In Section 4, a solution to this problem is tested and verified by re-defining the response functions used by Wu et al. (2007) to describe TC steering. Future work using these tools is described in Section 5.

2.2 Model Study

a) The Model

The simplified numerical model used is based upon the two-dimensional, non-divergent inviscid barotropic vorticity equation on an *f*-plane, for which relative vorticity is conserved:

$$\frac{\partial \zeta}{\partial t} + \mathbf{V} \cdot \nabla \zeta = 0 \quad (4),$$

where ζ is the relative vorticity and $\mathbf{V}$ is the horizontal vector wind field with zonal and meridional components u and v respectively. A streamfunction, ψ, which is related to the relative vorticity by $\nabla^2 \psi = \zeta$, is diagnosed from the vorticity distribution using successive over-relaxation. The non-divergent wind field is calculated from the streamfunction:

$$u = -\frac{\partial \psi}{\partial y} \quad (5)$$

$$v = \frac{\partial \psi}{\partial x} \quad (6).$$

The nonlinear model is solved on a centered-difference, discretized *f*-plane, over a closed domain 5235 km across with a grid spacing of 15 km. Homogeneous lateral boundary conditions are imposed on the streamfunction. The model is integrated forward in time using a forward Euler scheme, with a 30s time-step.

b) The tangent-linear and adjoint models[2]

Linearization of (4) about a time-evolving forecast trajectory calculated from (4) yields the tangent linear model:

$$\frac{\partial \zeta'}{\partial t} + \overline{\mathbf{V}} \cdot \nabla \zeta' + \mathbf{V}' \cdot \nabla \overline{\zeta} = 0 \quad (7)$$

where $\overline{\zeta}$ and $\overline{\mathbf{V}}$ are the basic state relative vorticity and wind vector $\overline{\mathbf{V}} = (\overline{u}, \overline{v})$ respectively, and ζ' and $\mathbf{V}'$ are the perturbation relative vorticity and wind vector $\mathbf{V}' = (u', v')$ respectively. The tangent linear model is also solved using a centered in space, forward Euler in time scheme. The adjoint model is developed at the coding level as the line-by-line transpose of the tangent linear model. Tests of the validity and accuracy of the tangent linear and adjoint codes are preformed in sections 3b and 4 c and d. Because the dynamics of the model are expressed in terms of the distribution of relative vorticity, output of the adjoint model is sensitivity with respect to vorticity.

c) Idealized Case

In order to aid dynamical interpretation of adjoint-derived sensitivities of TC steering, the simplest possible idealization was chosen – a TC embedded in a quiescent environment. The nonlinear model was initialized with a Gaussian distribution of vorticity (hereafter referred to as the basic state vortex, or BSV) maximized at the center of the model domain (Fig. 2.1). This vortex is the "TC" in the model. The model is run for 24 hours. Since the

[2] The code and supporting documentation are available from the first author upon request.

only wind in the model domain is symmetric about the BSV center, the state of the model is unchanged for the full 24-hour integration. This 24-hour model trajectory defines the basic-state about which the adjoint model is linearized.

The response function is defined as the average zonal flow in a 1200 km x 1200 km box centered on the BSV at the end of the 24-hour model integration

$$R_1 = \frac{\sum_{i,j \in D} u_{i,j}\, \Delta x \Delta y}{\sum_{i,j \in D} \Delta x \Delta y} \qquad (8).$$

For brevity, the discussion to follow focuses on response functions for zonal steering.

2.3 Description and interpretation of $\partial R_1 / \partial \xi$

a) Dynamics

Before describing the sensitivities of R_1 to vorticity, we consider what perturbations to the model forecast trajectory would change R_1, the average zonal flow in the response function box at forecast hour 24 given the dynamical constraints of the model. The only way to increase R_1 at 24 hours is for positive (negative) relative vorticity perturbations to be found north (south) of the center latitude of the box at that time. Within the context of the linearized model, there are only two processes which can create this state: 1) the basic state flow advects positive (negative) perturbation vorticity north (south) of the BSV position; or 2) the creation of vorticity perturbations associated with the northward advection of the BSV (translation of the TC) by winds associated with vorticity perturbations external to the BSV. The former effect, the basic state advection of perturbation vorticity (second term in the

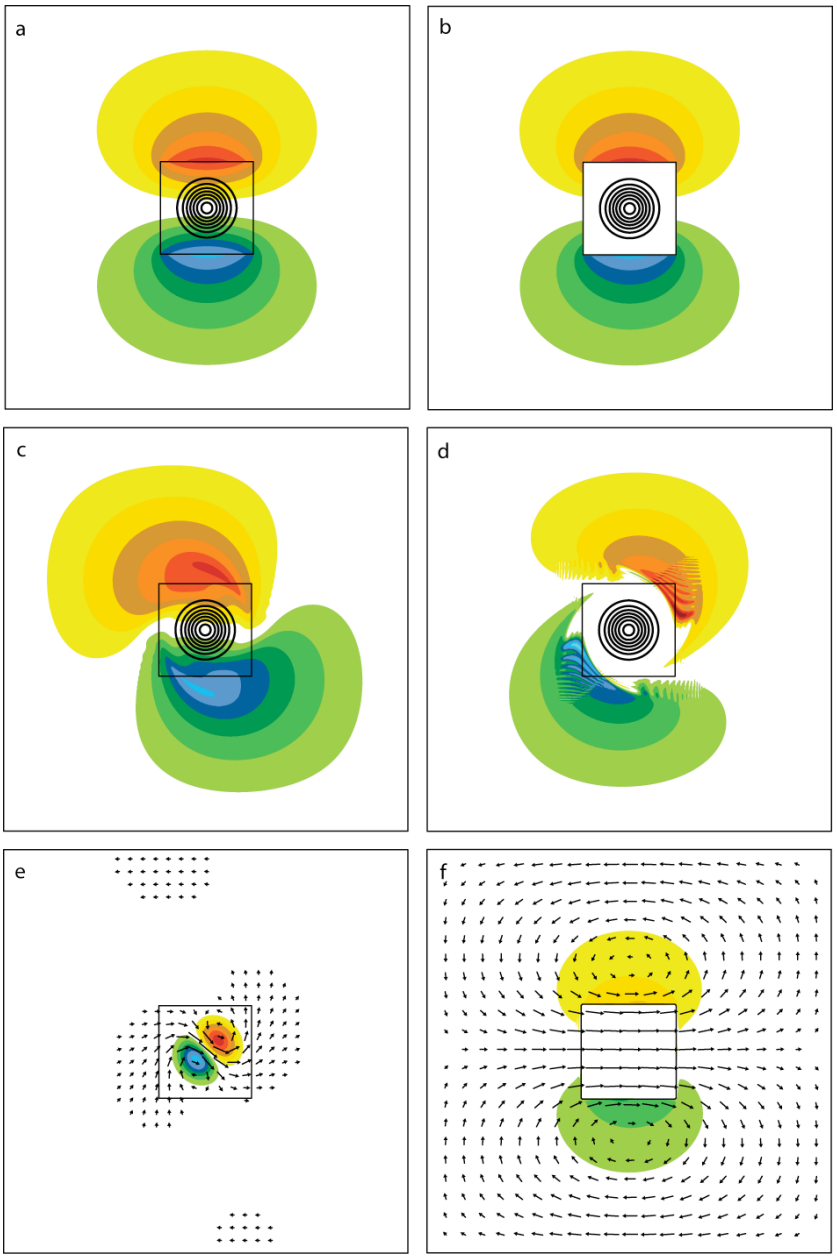

Figure 2.1. Basic state vorticity contoured every $2.0\text{x}10^{-5}$ s^{-1} and sensitivity of R_1 with respect to vorticity shaded every $5.0\text{x}10^{4}$ m at model verification (a) and model initialization (c). The same plots are provided for sensitivity of R_{E1} with respect to vorticity at model verification (b) and model initialization (d). (e) Perturbation vorticity shaded every $5.0\text{x}10^{-6}$ s^{-1} and perturbation winds at model verification after optimal perturbations to increase R_1 were introduced at model initialization. (f) Perturbation environmental vorticity shaded every $5.0\text{x}10^{-7}$ s^{-1} and perturbation environmental winds at model verification after optimal perturbations to increase R_{E1} were introduced at model initialization. Vectors in (f) are an order of magnitude smaller than vectors in (e). The box at the center of the plot corresponds to the boundaries of the response function box. Note that the wavy patterns in sensitivity in panel d are due to the zeroth-order discontinuity in initialized sensitivity (see panel b), and do not negatively impact the results.

linearized model (7)), is the instantaneous steering effect we seek to capture using the adjoint sensitivity diagnosis. The latter effect, an increase in R_1 due to a *northward displacement* of the BSV (manifest as an asymmetric distribution of perturbation vorticity in the box, third term in (7)) is *not a zonal steering* effect. Further, this latter effect represents the integrated response of the imposed vorticity perturbations west and east of the longitude of the BSV advecting that vortex northward rather than the instantaneous response associated with the north-south perturbation vortex dipole.

b) Adjoint sensitivity gradients for R_1

The adjoint model is initialized with the distribution of $\partial R_1 / \partial \zeta$ at the end of the 24-hour model integration (Fig. 2.1a)[3]. These sensitivities describe how a perturbation to vorticity would *instantaneously* change the response function. Sensitivities at this time are positive (negative) to the north (south) of the BSV (Fig. 2.1a). This distribution of sensitivities implies that placing positive (negative) vorticity perturbations north (south) of the response function box increases R_1. Such perturbations correspond to an increase in the zonal flow that would steer the BSV (the "TC") eastward *at this time*.

Integrated backward in time 24h to the model initialization time, $\partial R_1 / \partial \zeta$ has two important features (Fig. 2.1c). First, the maximum positive (negative) sensitivity appears northeast (southwest) of the BSV center. Second, positive (negative) sensitivity now appears west (east) of the BSV center. Each of these two features can be identified with processes in (7): the advection of perturbation vorticity by the basic state wind field (the instantaneous steering effect) and the advection of the basic state vorticity by the perturbation wind field (the primary cyclone displacement effect).

---

[3] $\partial R_1 / \partial \zeta$ is computed by defining $\partial R_1 / \partial u$, $\partial R_1 / \partial v$ directly and computing $\partial R_1 / \partial \zeta$ by using the adjoint of the successive over-relaxation scheme used to compute u, v from ζ.

c) Interpretation

1) INSTANTANEOUS STEERING EFFECT

Sensitivity of R_1 with respect to vorticity at 24 hours is a north-south dipole of positive and negative vorticity centered on the BSV. Because the absolute (and relative) vorticity is conserved on an *f*-plane in the model, at forecast hours prior to 24 hours these vorticity perturbations must be located *upstream* of their final-time locations (Fig. 2.2a). How far upstream the vorticity perturbations must be located to maximize their influence on increasing R_1 is dependent on the length of the adjoint model backward integration, the distance the vorticity perturbation is from the center of the box, and the intensity of the BSV.

Perturbation vorticity northeast and southwest of the BSV at the forecast hour 0 will be advected by the basic state wind field (Fig. 2.2a). At the end of the 24-hour model integration, this perturbation vorticity will be directly north and south of the BSV center (Fig. 2.2b). Therefore, if positive (negative) perturbation vorticity were introduced northeast (southwest) of the BSV at model initialization, the dipole of positive and negative perturbation vorticity would be oriented north/south across the response function box by the end of the model integration. This perturbation vorticity would be associated with a positive zonal perturbation flow in the response function box, increasing R_1.

2) PRIMARY CYCLONE DISPLACEMENT EFFECT

Unlike the instantaneous steering effect, the distribution of perturbation vorticity which would create a northward displacement of the BSV is less obvious because of the dual (possibly competing) effects of the imposed vortices – the vortices will not only perturb the

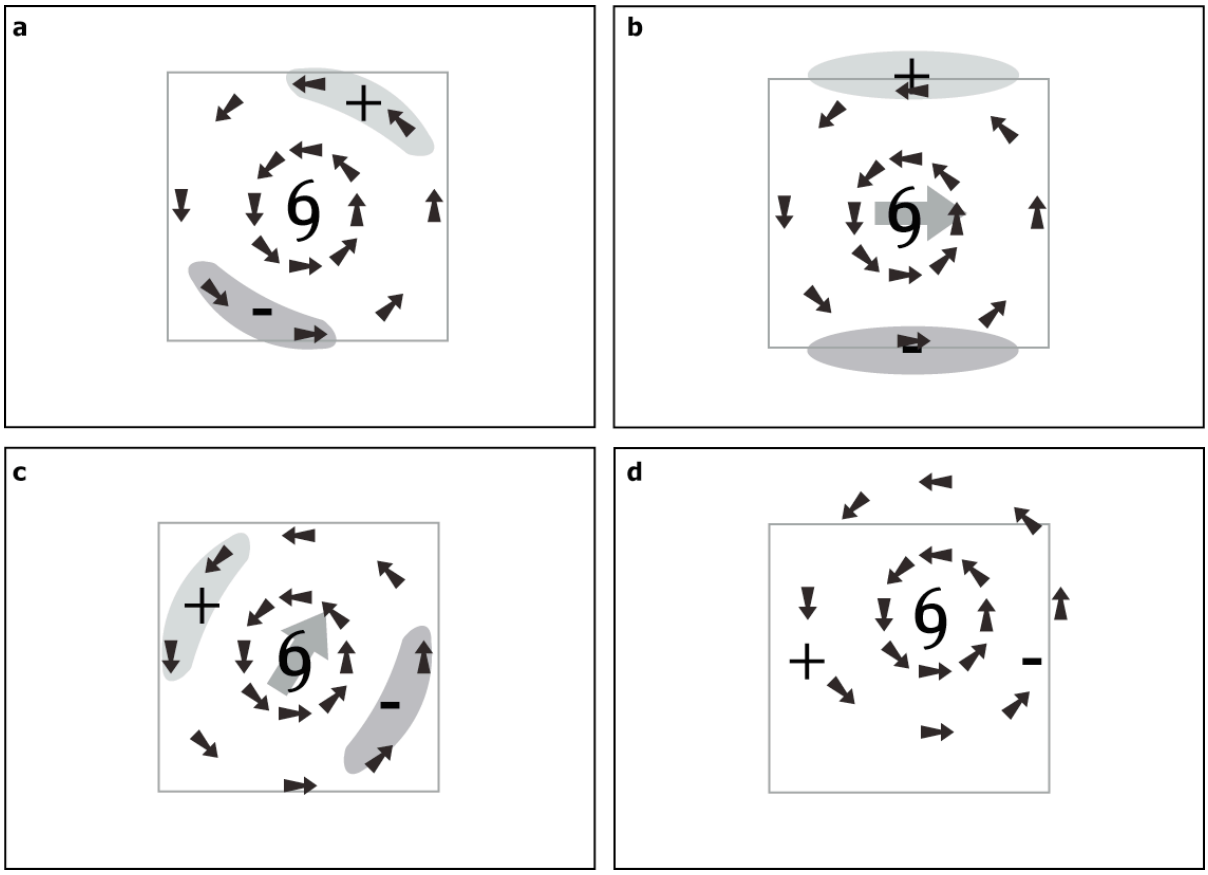

Figure 2.2. (a) Schematic configuration of vorticity perturbations ('+' for positive perturbation, '-' for negative) at initial forward model time placed in regions of maximum sensitivity shown in Fig. 1c; (b) subsequent configuration of vorticity perturbations 24h later that contribute to the *instantaneous* zonal flow within the response function box; (c) configuration of vorticity perturbations contributing to a northeastward "primary cyclone displacement" effect at the forward model initial time; and (d) subsequent configuration of the BSV and vorticity perturbations 24h after the time shown in (c). Note that in (d) the BSV has moved north-northeast of its initial location. Tropical cyclone symbol denotes location of BSV. Black filled arrows indicated flow associated with BSV. Grey filled arrows show direction of flow at vortex center attributed to perturbation vorticity. Shading indicates approximate regions of maximum sensitivity for R_1 that would produce the steering effect (a) and (b) and the PCD effect (c).

location of the BSV, they will also directly contribute to the zonal flow in the box at the time the response function is defined.

In order for perturbation vorticity to advect the BSV northward, the positive (negative) perturbations must be located northwest (southeast) of the longitude of the BSV at some time over the 24h period. In this configuration, the perturbation flow would be from the south over the BSV. Positive (negative) perturbation vorticity placed initially to the west (east) of the BSV would be associated with a southerly perturbation flow, advecting the BSV to the northeast (Fig. 2.2c). By the end of the 24-hour model integration, the BSV is displaced northeast of the center of the response function box (Fig. 2.2d). The symmetric circulation of the BSV contributes positively to the average zonal flow in the response function box, positively influencing R_1.

The dynamical interpretation of the adjoint-derived sensitivity gradients makes the problem with the R_1 clear: the process described by the basic state advection of perturbation vorticity actually impacts the steering of the BSV. Sensitivities associated with this process can legitimately be called sensitivities of TC steering. The sensitivities associated with perturbation advection of basic state vorticity are of another sort. Perturbations to the model initial conditions in regions where these sensitivities are large result in the BSV being advected north of its final-time location in the control forecast and therefore contribute to R_1 in a way that has nothing to do with the zonal steering of the BSV. We call this the primary cyclone displacement (PCD) effect.

While it would be convenient to simply move the averaging box so as to be centered over the new vortex center and thus remove the effect of the displaced cyclone, the response function is chosen as the average zonal wind in a box over a *specific* geographic region.

While the chosen region may be centered directly on the vortex in the *basic state*, and therefore represent the steering of a modeled TC in the basic state, there is nothing preventing vorticity perturbations from advecting the vortex out of the middle of the box. Any comparison, qualitative or quantitative, between these sensitivities and the steering of the modeled TC must keep the averaging box in the same place. The response function box cannot be arbitrarily moved based on *a posteriori* information in order to accommodate the perturbation advection of the BSV.

d) Perturbation test for validation of dynamical interpretation

A test can be performed to validate the above dynamical interpretation for $\partial R_1 / \partial \xi$. Initial vorticity perturbations, designed to increase R_1, may be derived by scaling the sensitivity to the initial distribution of vorticity, $\left.\frac{\partial R_1}{\partial \xi}\right|_{t=0h}$:

$$\xi_0' = \frac{S \left.\frac{\partial R_1}{\partial \xi}\right|_{t=0h}}{\max\left(\left|\left.\frac{\partial R_1}{\partial \xi}\right|_{t=0h}\right|\right)} \quad (9).$$

Here, $\max\left(\left|\left.\frac{\partial R_1}{\partial \xi}\right|_{t=0h}\right|\right)$ is the absolute value of the maximum sensitivity in the model domain at forecast time 0h. An initial perturbation vorticity distribution with maximum perturbation vorticity 2.0x10^{-6} s^{-1} is created by choosing $S = 2.0 \times 10^{-6}$. In this way, perturbation vorticity introduced at model initialization has the same structure as $\partial R_1 / \partial \xi_{t=0h}$ (Fig. 2.1c).

The model is integrated forward 24h with the perturbed initial conditions. At 24 hours, perturbation vorticity and winds, defined as the difference between the perturbed and control (unperturbed) forecast values of vorticity and wind respectively, reveal a dipole of perturbation vorticity in the response function box indicating a northeast translation of the

BSV by the perturbation wind field (Fig. 2.1e). A significant portion[4] of the perturbation flow in the response function box is attributed to the vorticity perturbations ascribed to the translation of the BSV. This result confirms the dynamical interpretation for the fault with $\partial R_1 / \partial \zeta$ - that the assumption that the BSV would remain in the center of the response function box is violated, and some contributions to the change in R_1 have nothing to do with the instantaneous zonal steering of the BSV at 24 hours. In fact, it appears that, for this case, the PCD effect is larger than the instantaneous steering effect.

We can also perform a test to validate the adjoint model's assumption of linearity for this case. The total change in the response function between the perturbed and control runs can be directly calculated by evaluating R_1 for each run and calculating the difference.

$$\Delta R_1 = R_1\big|_{perturbed} - R_1\big|_{control} \qquad (10)$$

Assuming linearity, this value can be approximated by evaluating the inner product of the sensitivity field at model initialization $\partial R_1 / \partial \zeta_{t=0h}$ with the perturbation to initial condition vorticity $\zeta'_{t=0h}$.

$$\Delta R_1 \cong \delta R_1 = \left\langle \frac{\partial R_1}{\partial \zeta_{t=0h}}, \zeta'_{t=0h} \right\rangle \qquad (11)$$

For the case under consideration, $\Delta R_1 = 0.922\ m\ s^{-1}$, while $\delta R_1 = 0.919\ m\ s^{-1}$. The adjoint model was able to account for 99.7% of the change in R_1, indicating that the perturbations evolved linearly in the model, and the adjoint-derived sensitivity gradients are valid.

As Fig. 2.1e shows, the change in R_1 is largely the result of a slight northward displacement of the final-time location of the BSV within the response function box. This

[4] Perturbation zonal flow attributed to the northward displacement of the BSV accounts for 55% of the perturbation zonal flow in the response function box.

does not correspond to an increase in the zonal steering of the BSV at this time. The PCD effect does not appear to be dependent on the physical size of the BSV (not shown).

The strength of the PCD effect is partially dependent on the size of the response function box. The PCD effect is manifest as a dipole of perturbation vorticity in the center of the box with a concomitant perturbation flow pattern described by that vorticity. While a larger response function box would do nothing to reduce the size of this dipole, the contribution of the PCD effect on the average perturbation flow would be smaller for a large response function box than for a small box. However, this cannot serve as a solution to this problem. The PCD effect exists regardless of the size of the response function box. And the box cannot be too large, since the response function is intended to describe the environmental flow *in the vicinity of the TC*.

In the following section, a new response function is introduced in order to provide a solution to this problem, and is tested in the same manner as R_1.

2.4 Proposed solution

a) Environmental steering response function

It has been shown that the response function used to describe TC steering is fundamentally flawed. Perturbations to the final-time location of the TC within the response function box allow for the TC's own symmetric circulation to contribute to R_1 (and R_2) in a way that has nothing to do with the instantaneous steering of the TC. Dynamical interpretation of $\partial R_1 / \partial \zeta$ shows that the PCD effect is manifest as positive (negative) sensitivity with respect to vorticity appearing west (east) of the BSV.

Here, we propose new response functions to define the zonal and meridional steering of a TC, such that the PCD effect is removed from the sensitivity gradients associated with

the new response functions. For a given domain, one can define the "hurricane advection flow" as the balanced flow at the TC center attributed to the potential vorticity (PV) within that domain after the PV of the TC has been removed (Wu and Emanuel, 1995).

For two-dimensional, non-divergent, barotropic flow, the relevant potential vorticity is the absolute vorticity. We designate the vorticity within the response function box (*D*) as vorticity of the BSV, and all of the vorticity outside of the response function box as vorticity of the environment. The partitioning of the full domain vorticity into vorticity of the TC (vorticity in box) and vorticity of the environment is accomplished by the use of a linear environmental projection operator, **E**:

$$\mathbf{E}\zeta_{i,j} = 0 \; if \; i,j \in D \text{ and}$$

$$\mathbf{E}\zeta_{i,j} = \zeta_{i,j} \; if \; i,j \notin D \quad (12),$$

where $\zeta_{i,j}$ represents the grid point representation of the vorticity.

Once the vorticity of the TC is removed, the vorticity of the environment can be inverted to recover the "environmental" wind, $\tilde{\mathbf{V}}: \tilde{\mathbf{V}} = \mathbf{Q}^{-1}(\mathbf{E}\zeta) = \mathbf{k} \times \nabla[\nabla^{-2}(\mathbf{E}\zeta)] = \tilde{u}\mathbf{i} + \tilde{v}\mathbf{j}$, where **Q** is an operator that calculates the two-dimensional, non-divergent wind field from the vorticity distribution and "∇^{-2}" represents the successive over-relaxation inversion operator that calculates streamfunction from vorticity.

We define a new set of response functions to describe the average "environmental" zonal and meridional wind in the vicinity of the TC.

$$R_{E1} = \frac{\sum_{i,j \in D} \tilde{u}_{i,j} \, \Delta x \Delta y}{\sum_{i,j \in D} \Delta x \Delta y} \quad (13)$$

$$R_{E2} = \frac{\sum_{i,j \in D} \tilde{v}_{i,j} \, \Delta x \Delta y}{\sum_{i,j \in D} \Delta x \Delta y} \quad (14)$$

The averaging of the environmental wind $(\tilde{u},\tilde{v})$ is performed in the same manner as the averaging of the full wind in R_1 and R_2. Figure 2.3a is a flowchart describing the procedure used to calculate R_{E1} and R_{E2} given the model state as expressed in terms of vorticity. The adjoint of this procedure, shown in Fig. 2.3b, is used to derive the sensitivity gradients that initialize the adjoint model.

Since all vorticity within the response function box is removed when the environmental wind is calculated, small perturbations to the final-time location of the BSV within the response function box have no effect on R_{E1} and R_{E2}. A translation of the BSV caused by advection by the perturbation wind field is manifest as a dipole of positive and negative perturbation vorticity oriented in the direction of the translation (Fig. 2.1e). As long as the vorticity associated with the TC is not advected *outside* of the response function box, any translation of the TC *within* the box has no effect on the response functions. This assumption is less restrictive than the previous assumption that the TC had to remain in the *center* of the response function box.

b) Adjoint sensitivity gradients for R_{E1}

By construction, the distribution of $\partial R_{E1} / \partial \xi$ that is used to initialize the adjoint model (Fig. 2.1b) is identical to the initialized sensitivity of R_1 (Fig. 2.1a), except that sensitivity of R_{E1} to vorticity is zero within the response function box. Since all vorticity within the response function box is removed in order to calculate $\tilde{u}$, perturbations to vorticity within the response function box can have no effect on R_{E1} at this time.

a

$$\zeta_f \rightarrow \mathbf{E}\zeta_f \rightarrow \mathbf{Q}^{-1}(\mathbf{E}\zeta_f) \rightarrow \tilde{u}_f \ ,\tilde{v}_f \ \rightarrow R_{\mathrm{E1}}, R_{\mathrm{E2}}$$

b

$$\frac{\partial R_{\mathrm{E1}}}{\partial \zeta_f} = \mathbf{E}^* \frac{\partial R_{\mathrm{E1}}}{\partial \tilde{\xi}_f} \leftarrow \frac{\partial R_{\mathrm{E1}}}{\partial \tilde{\xi}_f} = (\mathbf{Q}^{-1})^* \begin{bmatrix} \dfrac{\partial R_{\mathrm{E1}}}{\partial \tilde{u}_f} \\ \dfrac{\partial R_{\mathrm{E1}}}{\partial \tilde{v}_f} \end{bmatrix} \leftarrow \frac{\partial R_{\mathrm{E1}}}{\partial \tilde{u}_f}, \frac{\partial R_{\mathrm{E1}}}{\partial \tilde{v}_f}$$

$$\frac{\partial R_{\mathrm{E2}}}{\partial \zeta_f} = \mathbf{E}^* \frac{\partial R_{\mathrm{E2}}}{\partial \tilde{\xi}_f} \leftarrow \frac{\partial R_{\mathrm{E2}}}{\partial \tilde{\xi}_f} = (\mathbf{Q}^{-1})^* \begin{bmatrix} \dfrac{\partial R_{\mathrm{E2}}}{\partial \tilde{u}_f} \\ \dfrac{\partial R_{\mathrm{E2}}}{\partial \tilde{v}_f} \end{bmatrix} \leftarrow \frac{\partial R_{\mathrm{E2}}}{\partial \tilde{u}_f}, \frac{\partial R_{\mathrm{E2}}}{\partial \tilde{v}_f}$$

Figure 2.3. (a) Flow chart describing how the response functions R_{E1} and R_{E2} are calculated from final time forecast vorticity, ζ_f. **E** is the environmental projection operator. The operator that inverts vorticity and calculates the horizontal wind attributed to that vorticity is $\mathbf{Q}^{-1}$. The horizontal wind field attributed to vorticity outside of the response function box is $\tilde{u}_f, \tilde{v}_f$. (b) Flow chart describing how the initial conditions to the adjoint model, $\partial R_{\mathrm{E1}}/\partial \zeta_f$ and $\partial R_{\mathrm{E1}}/\partial \xi_f$, are calculated from $\partial R_{\mathrm{E1}}/\partial \tilde{u}_f$ and $\partial R_{\mathrm{E1}}/\partial \tilde{v}_f$. Operators **E*** and $(\mathbf{Q}^{-1})$* are the adjoints of **E** and $\mathbf{Q}^{-1}$, respectively. Note that for the zonal environmental wind response function, $\partial R_{\mathrm{E1}}/\partial \tilde{u}_f = 1$ in the response function box, zero elsewhere, and $\partial R_{\mathrm{E1}}/\partial \tilde{v}_f = 0$; while for the meridional environmental wind response function, $\partial R_{\mathrm{E2}}/\partial \tilde{v}_f = 1$ in the response function box, zero elsewhere, and $\partial R_{\mathrm{E2}}/\partial \tilde{u}_f = 0$.

The structure of $\partial R_{E1}/\partial\zeta$ at time $t = 0$ (Fig. 2.1d) looks quite different from that of R_1 (Fig. 2.1c). Maximum sensitivities still appear to the northeast and southwest of the BSV, but the sensitivities west and east of the BSV associated with the PCD effect have vanished. In fact, there is weak sensitivity of the *opposite* sign present west and east of the BSV, compared to the sensitivity of R_1. The differences in the $\partial R_1/\partial\zeta$ and $\partial R_{E1}/\partial\zeta$ fields at adjoint model initialization (Figs. 1c and 1d respectively) appear primarily directly west and east of the BSV (Fig. 2.4a), and are related to the PCD effect.

c) Perturbation test for validation of dynamical interpretation

A test similar to that performed for the dynamical interpretation of $\partial R_1/\partial\zeta$ (section 3b) is performed here for dynamical interpretation of $\partial R_{E1}/\partial\zeta$. The sensitivity gradient of R_{E1} with respect to vorticity is scaled to create an initial condition perturbation vorticity field that will increase R_{E1}. The nonlinear model is then integrated forward 24 hours with the perturbed initial conditions.

The perturbation environmental vorticity and perturbation environmental wind at 24 hours reveal that the perturbations to increase R_{E1} create a uniform zonal perturbation environmental flow in the response function box (Fig. 2.1f). After the perturbation vorticity within the response function box is removed, the vorticity that remains (constituting the "environmental" vorticity) appears as a positive (negative) gyre directly north (south) of the response function box. Inversion of this environmental vorticity yields a zonal perturbation environmental wind in the response function box. Thus, the zonal steering of the TC, defined as the "hurricane advection flow" due to vorticity outside of the response function box, has been increased.

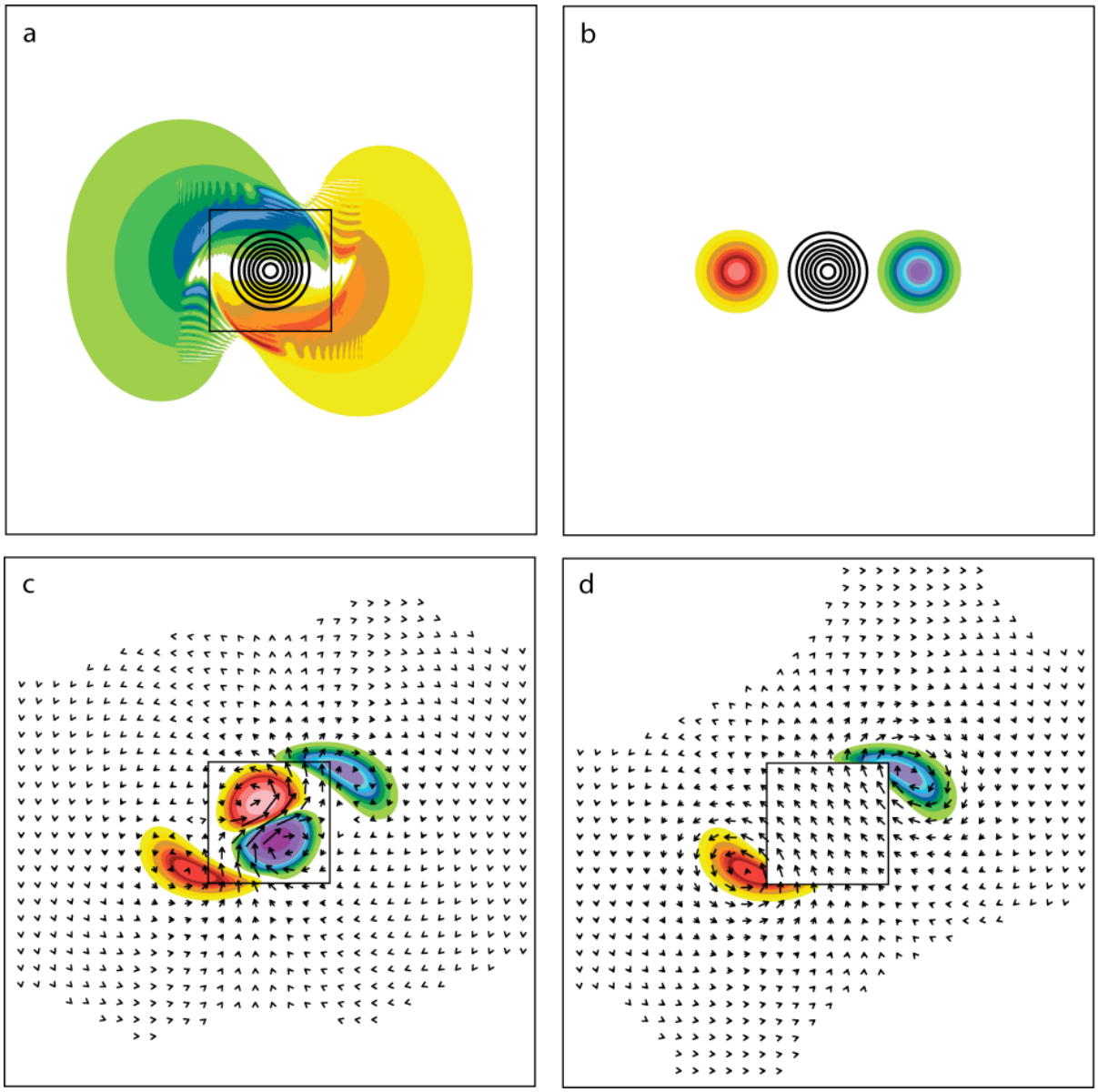

Figure 2.4. (a) Basic state vorticity contoured every $2.0\text{x}10^{-5}$ s^{-1} and difference between $\partial R_{E1}/\partial\xi$ and $\partial R_{1}/\partial\xi$ shaded every $5.0\text{x}10^{4}$ m at model initialization. (b) Basic state vorticity (contoured) and perturbation vorticity shaded every $5.0\text{x}10^{-7}$ s^{-1} at model initialization. (c) Perturbation vorticity (shaded) and perturbation winds at model verification. (d) Perturbation environmental vorticity (shaded) and perturbation environmental winds at model verification. The box at the center of the plot corresponds to the boundaries of the response function box.

A test of linearity similar to that performed for the previous perturbation case is performed. For this case, $\Delta R_{E1} = 0.416\ m\ s^{-1}$, and the approximation of this value assuming linearity is $\delta R_{E1} = 0.420\ m\ s^{-1}$, indicating that the adjoint model accounts for 99.0% of the change in R_{E1}.

d) Elimination of PCD effect in R_{E1}

The reversal in sign between $\partial R_{\mathrm{I}} / \partial \zeta$ and $\partial R_{\mathrm{E1}} / \partial \zeta$ in these regions west and east of the BSV indicates that positive (negative) perturbation vorticity introduced west (east) of the BSV at model initialization *will increase* R_{I} *and decrease* R_{E1}. To show that the PCD effect is eliminated from $\partial R_{\mathrm{E1}} / \partial \zeta$, another perturbation run is performed with a positive (negative) perturbation vortex introduced west (east) of the BSV at the initialization of the nonlinear forward model (Fig. 2.4b). These perturbation vortices have maximum amplitude of 4.5×10^{-6} s^{-1}. Perturbation vorticity and winds are calculated at the end of the 24-hour model integration, and the response functions R_{I} (Fig. 2.4c) and R_{E1} (Fig. 2.4d) are evaluated.

Perturbation vorticity and winds contributing to R_{I} (Fig. 2.4c) show a definite PCD effect. The dipole in perturbation vorticity in the response function box is a clear indication that the BSV has been advected to the northwest by the perturbation wind field by this time. Likewise, the perturbation vortices introduced at model initialization have been advected cyclonically around the BSV by the basic state wind field, appearing to the southwest and northeast of the response function box. The average perturbation zonal wind in the response function box is positive, with $\Delta R_{\mathrm{I}} = 0.101\ m\ s^{-1}$, while $\delta R_{\mathrm{I}} = 0.101\ m\ s^{-1}$, with the adjoint model accounting for 99.6% of the change in R_{I}.

By removing any perturbation vorticity in the response function box, the perturbation environmental vorticity and perturbation environmental winds contributing to R_{E1} (Fig. 2.4d)

reveals a reversal in the direction of zonal flow in the box. All significant perturbation vorticity associated with the PCD effect existed within the response function box. Since all perturbation vorticity in the response function box is removed in order to calculate R_{E1}, the PCD effect has no influence on the calculation of R_{E1}. The perturbation vorticity on the southwest and northeast corners of the response function box constitutes the "environmental" vorticity. This environmental vorticity induces an "environmental" zonal wind which is negative in the response function box, with $\Delta R_{E1} = -0.141\ m\ s^{-1}$. The approximation of ΔR_{E1} assuming linearity is $\delta R_{E1} = -0.138\ m\ s^{-1}$, indicating that the adjoint model could account for 97.9% of the change in R_{E1}.

This analysis validates the dynamical interpretation of $\partial R_1 / \partial \xi$ and $\partial R_{\mathrm{E1}} / \partial \xi$ fields, and how those differences relate to the PCD effect. Sensitivities of R_1 west and east of the BSV are of opposite sign compared to sensitivities of R_{E1} because for the perturbations considered, the PCD effect introduces *positive* perturbation flow in the response function box, while the vorticity that constitutes the "environment" introduces *negative* perturbation flow in the response function box. The PCD effect dwarfs the effect of the environmental vorticity, making ΔR_1 positive. Since the PCD effect is eliminated in the calculation of R_{E1}, only the influence of the environmental vorticity remains, making ΔR_{E1} negative.

This methodology comes with its own limitations. The response function box separates vorticity associated with the TC (vorticity inside the box) from vorticity associated with the environment (vorticity outside the box). Any vorticity of an environmental feature that migrates into the box will be zeroed-out in the response function and not contribute to the "hurricane advection flow" assumed to steer the TC. Thus any interaction of the TC with

its environment that produces environmental vorticity inside of the response function box at model verification will not be manifest in the sensitivities.

2.5 Conclusions

It has been shown that the definition of TC steering as a deep layer mean wind averaged around a TC center is not suitable for defining response functions to calculate adjoint-derived sensitivities of TC steering. The problem is that the deep-layer mean wind averaged around the TC is a measure of the environmental flow that steers the TC only so long as the TC is in the center of the averaging box, such that the symmetric circulation about the TC is removed in the averaging. This definition has been validated when calculating the steering flow for both observed and modeled TCs (Chan 2005). However, when the calculation is used to define a response function for the purpose of calculating adjoint-derived forecast sensitivities of TC steering, the assumption that the TC remains in the same location is often violated. Since the response functions R_1 and R_2 can be influenced by perturbing *either* the environmental flow in the vicinity of the TC (a change to the steering) *or* the final time location of the TC within the response function box (not a change to the steering), these sensitivity gradients do not necessarily correspond to sensitivities of instantaneous TC steering.

A solution is proposed and validated in the context of a two-dimensional, non-divergent barotropic model by defining new response functions that eliminate the PCD effect. By defining the steering of the TC by the "hurricane advection flow", which is an average of the *environmental* flow in the vicinity of the TC rather than an average of the *full* flow, the PCD effect is removed. While R_1 and R_2 require that the TC *remain in the center* of

the response function box, the new response functions R_{E1} and R_{E2} only require that the vorticity associated with the TC *remain within* the response function box.

While the solution presented here has been validated within the context of a barotropic model, the R_{E1} and R_{E2} response functions should be tested in real TC simulations using a full-physics NWP model and that model's adjoint. Clearly, issues regarding the validity of the assumption of linearity in such a model will include issues of the effect of diabatic processes that are not present in the simple model. While the relationship between the adjoint-derived sensitivity gradients and the physics of the tangent-linear model cannot be as clear in a full-physics model as they are in the simple model, it is expected that the dynamical interpretations of sensitivity gradients provided in this study will be a helpful corollary in a more complicated adjoint model. Real TCs are steered by a complexly-evolving environment that can itself be sensitive to small changes to the initial conditions; in such a case one would expect the steering flow of the TC to be sensitive to the TC vortex as well as to relevant aspects of the environment. The results of this ongoing work will be provided in a future study.

A future application of this methodology includes the use of these adjoint-derived sensitivities to define targets for targeted observations with the explicit goal of improving TC track prediction. Dynamical sensitivities of TC steering to model initial conditions provide the requisite *a priori* information about where perturbations to the initial conditions of an NWP model will have the strongest effect on TC steering *specifically*. In order to apply this technique in an operational context, it would be necessary to determine an appropriate response function box size. The box needs to be large enough to accommodate the migration

of the TC as a result of perturbations to the initial conditions, but small enough to produce meaningful results.

Dynamical sensitivities alone are insufficient to make well-informed choices about adaptive observation targeting. Dynamical sensitivity must be combined with information about the uncertainty in the initial conditions and information about how a given observation would be assimilated into the initial conditions. Coupling the output of an adjoint model with the adjoint of a data assimilation system would allow for the calculation of sensitivities of a response function to (individual) observations (Langland and Baker, 2004). By combining *a priori* information about the dynamical sensitivity to the model state, the uncertainty in the initial conditions, and the impact of a given observation assimilated into the initial conditions, sensitivities of an appropriate response function for TC steering can be utilized in a truly objective targeting strategy to improve TC track forecasting.

Acknowledgements

This material is based upon work supported by the National Science Foundation under grant No. 0529343 and the Office of Naval Research under grant N000141610563PR.

Chapter 3: Dynamical Sensitivity Analysis of Tropical Cyclone Steering Using an Adjoint Model

Abstract

Through the use of an adjoint model, one can calculate the adjoint-derived sensitivity of the steering of a simulated tropical cyclone (TC) to various aspects of a model forecast trajectory. This calculation, providing a priori information about how small perturbations to the model's initial conditions will impact the steering of the TC at some future time, provides a wealth of dynamical information about the importance of synoptic-scale features and associated processes to the steering of a modeled TC that is difficult or impossible to obtain by other means. Regions of strong sensitivity to cyclone steering are regions where, if errors in the forecast state exist, those errors would have the largest effect on TC steering. However, without a dynamical understanding of why the steering of a simulated TC is sensitive to changes in these regions, errors in the methodology of implementing an adjoint model for calculating these sensitivities may result in sensitivity gradients that do not represent sensitivity of TC steering at all, and without a strong dynamical interpretation of these sensitivities, these errors may escape notice.

An adjoint model is employed for several cases of simulated TCs in the west Pacific to determine the dynamical significance of regions for which sensitivity to TC steering is found to be particularly strong. It is found that the region of subsidence upstream of a passing midlatitude trough can play a crucial role in the development of perturbations that strongly impact a recurving TC. A dynamical interpretation of this relationship is described and tested.

3.1 Introduction

Previous studies of the relative importance of synoptic-scale features and processes to TC steering in a numerical weather prediction (NWP) model have used adjoint models to calculate singular vectors, which determine regions where perturbations will grow most rapidly (Langland 2005; Buizza et al. 2007; Cardinali et al. 2007; Peng and Reynolds 2006; Chen et al. 2009). A more useful application of adjoint models to dynamical sensitivity analysis of TC steering is the calculation of sensitivity of TC steering itself, which requires a response function that describes the steering of the TC. Dynamical sensitivities of TC steering to model initial conditions provide the requisite *a priori* information about where perturbations to the initial conditions of an NWP model will have the strongest effect on TC steering *specifically*. In addition, the inner product of the sensitivity gradient and the perturbations to initial conditions provides an estimate for *how much* improvement can be expected.

TC motion is primarily caused by advection of the TC by the flow of the surrounding environment (Chan and Gray 1982; Flatau et al. 1994; Chan 2005). While mechanisms exist that cause the TC to move independent of this environmental "steering flow" (Fiornio and Elsberry 1989; Carr and Elsberry 1990; Wu and Emanuel 1993), the steering of the TC by its environment is the dominant contribution, especially for steady TC motion (Chan et al. 2002). Moreover, ambiguities exist in the designation of what constitutes the "environment" of a TC that makes its definition non-unique (Flatau et al. 1994). The relationship of a TC with respect to a complexly evolving environment and how the environment steers the TC has been a subject of modeling research for many years (e.g. Holland 1983; Shapiro 1992; Wu and Wang 2000; Chan et al. 2002).

By providing high-resolution, four-dimensional, nearly dynamically consistent data sets, NWP model simulations can provide insight into the relative importance (steering-wise) of various synoptic-scale features in the environment of the TC. To this end, much of the research using NWP models comes in the form of impact studies, which involve comparing a simulation in which the initial conditions have been perturbed to a "control" run in order to diagnose the importance of specific weather phenomena on a verifying forecast. These impact studies can usually be phrased as "what if?" experiments, such as "what if the potential vorticity (PV) of an upper trough (Fehlmann and Davies 1997) or a tropical cyclone (McTaggart-Cowen et al. 2004) were removed or altered in the initial model state?" Often these impact studies are characterized as a more robust "sensitivity study" by perturbing the initial conditions in multiple ways in order to keep the results from seeming anecdotal. The major drawback of this methodology is that it can never be known *a priori* what kinds of perturbations will have the most impact, and as a result, the study must include many perturbations to many variables in many locations in order to be considered a sensitivity study – an expensive proposition both in terms of time and computational resources.

Alternatively, robust sensitivity analysis can be performed with the adjoint of a NWP model. The adjoint of a NWP model is the transpose of the tangent-linear model, linearized about a full-physics, nonlinear trajectory from the NWP model. A sensitivity study can be performed by defining some specific aspect of the forecast of interest as a *response function* ($R(\mathbf{x}_f)$), which must be first-order differentiable with respect to the model forecast verification state ($\mathbf{x}_f$). The gradient of R with respect to the model forecast verification state is integrated backward through time using the adjoint model to compute the gradient of that same response function (still defined at forecast verification) with respect to the model state

at earlier times. Most often, these gradients are computed with respect to the model initial conditions; with these "sensitivity gradients", the adjoint model provides an economical means by which to determine how small perturbations to the initial conditions would impact the chosen response function (Errico 1997).

While these sensitivity gradients have practical application to tasks such as 4-Dimensional Variational Data Assimilation (Lewis and Derber 1985), adjoint models provide valuable *a priori* information about the dynamical sensitivity of any aspect of the model verification state with respect to past states that is difficult or impossible to derive otherwise. Attempts have been made to reconcile calculated sensitivity gradients with the large-scale dynamics of the model simulation (Langland et al. 1995, Kleist and Morgan 2005), and several studies have used adjoint models alongside NWP models to evaluate the relative importance of synoptic-scale features in the basic state to the development of extratropical cyclones (Vukicevic and Raeder 1995, Langland et al. 1995).

While some work has been done to produce sensitivity gradients of TC steering (Wu et al. 2007, Wu et al. 2009a), the methodology employed has suffered due to lack of rigorous testing and dynamical interpretation of the resultant sensitivity gradients (Hoover 2009, Hoover and Morgan 2010); it is important to keep in mind that sensitivity gradients provide information on how *changes to* the initial conditions will result in *changes to* the response function, and the results cannot be used explicitly to determine if a particular aspect of the initial conditions contributes most to the response function in the basic state (Langland et al. 1995, Langland and Errico 1996).

This study focuses on dynamical interpretation of adjoint-derived sensitivity gradients for the steering of simulated TCs. Small perturbations to the initial conditions of an NWP

model can change the evolution of the TC environment, having a substantial impact on how the environment steers the TC. An NWP model and its adjoint are employed to analyze the sensitivity of the steering of a TC to the initial conditions from this perspective. Several cases of west Pacific TCs in a variety of environments are employed to produce some generalized evaluations of the synoptic features in the environment to which TC steering is most sensitive.

Section 2 provides a description of the model and cases used in the study. A description of the methodology is provided in Section 3. An analysis of sensitivity gradients is provided and tested in Section 4. Directions for future study are provided in Section 5.

3.2 Model Simulations

a) The Model

We employ the Navy Operational Global Atmospheric Prediction System (NOGAPS) global spectral model (Hogan and Rosmond 1991, Rosmond et al. 2002) at T159 resolution and 30 vertical (sigma-) levels to establish the basic state around which the NOGAPS adjoint model (Rosmond 1997) is linearized. The adjoint model is initialized with sensitivity gradients given a response function defined as a measure of the environmental flow that steers the TC (see Section 3) and run at the same resolution.

The NOGAPS model was chosen for several reasons. The study of synoptic-scale influences on TC steering necessarily means we are focusing on large-scale, even global-scale, features. The use of a global spectral model eliminates the influence of boundary conditions that could plague a regional grid-point model. Many adjoint models do not make use of moisture-physics schemes used in the nonlinear, full-physics NWP model, because the adjoint of these routines is difficult to produce (Errico 1997); however, the NOGAPS adjoint

model employs the physics schemes responsible for *large-scale* precipitation. This feature, combined with the information concerning moisture-physics provided by the full-physics basic state (Kleist and Morgan 2005), makes the NOGAPS adjoint model attractive for sensitivity studies focusing on tropical environments.

b) Cases

Four cases of west Pacific TCs were chosen, which describe a variety of environments and synoptic-scale interactions that produce widely varying TC tracks. The cases can be separated into three categories. Simulations of Typhoon Meari (2004) and Typhoon Choi-Wan (2009) describe environments under which the TC experiences significant recurvature, with meridional or nearly-meridional tracks caused by interaction with a midlatitude trough. A simulation of Typhoon Longwang (2005), on the other hand, provides a case of a steady, zonal track. Finally, a simulation of Typhoon Parma (2009) provides a peculiar case wherein the TC remains essentially motionless for 108 hours; this case also appears to include a binary interaction between Typhoon Parma and Typhoon Melor to its east.

For each case, a 36hr simulation is performed with the NOGAPS model, and sensitivity gradients are integrated backward 36 hours to model initialization. The 108 hour simulation of Typhoon Parma (2009) is cut into three 36hr sections, and sensitivity gradients are calculated for steering of the TC at the end of each section. Table 3.1 is a list of the

Simulation	Begins	Ends
Typhoon Meari (2004)	0000 UTC 24 September	1200 UTC 25 September
Typhoon Longwang (2005)	0000 UTC 30 September	1200 UTC 01 October
Typhoon Choi-Wan (2009)	0000 UTC 18 September	1200 UTC 19 September
Typhoon Parma (2009): 1	1200 UTC 02 October	0000 UTC 04 October
Typhoon Parma (2009): 2	0000 UTC 04 October	1200 UTC 05 October
Typhoon Parma (2009): 3	1200 UTC 05 October	0000 UTC 07 October

Table 3.1. Beginning and ending time for each 36-hour simulation. The 108-hour simulation of Typhoon Parma (2009) is divided into three 36-hour sections for the purposes of calculating TC steering sensitivities for the end of each 36-hour section.

beginning and ending times for each model simulation. The model is initialized with 1^o x 1^o Fleet Numerical Meteorological and Oceanographic Center (FNMOC) analyses[5].

3.3 Methodology

A modified version of the ADSSV (Wu et al. 2007, Wu et al. 2009a,b) technique is employed to determine how small perturbations to the initial conditions of the model simulation will impact the steering of the TC 36 hours in the future. We wish to isolate the asymmetric flow over the TC attributed to the environment that steers the TC; this is usually done by averaging the horizontal winds over some horizontal domain centered on the TC and over some vertical depth (Chan and Gray 1982, Velden and Leslie 1991) to remove the symmetric circulation of the TC, leaving the residual to constitute the "environmental flow". However, since the adjoint model can only determine how *changes to* the initial conditions will produce *changes to* the response function, and the average flow in this domain can be greatly changed by perturbing the model so as to cause a (small) displacement of the TC from the center of the domain, this technique will not adequately produce sensitivities to TC steering by the environment (Hoover 2009).

Instead, we can isolate the environmental flow by calculating it directly. If the response function box is chosen so as to provide a separation between vorticity and divergence associated with the TC (vorticity and divergence *inside* of the response function box) and vorticity and divergence associated with the environment (vorticity and divergence

[5] Data for this project is from the Fleet Numerical Meteorological and Oceanographic Center (FNMOC) and the United States Global Data Assimilation Experiment (USGODAE). Available at: http://www.usgodae.org/ftp/outgoing/fnmoc/models/nogaps

outside of the response function box), we can define the environmental flow within the response function box as the wind induced by the vorticity and divergence of the environment:

$$\tilde{\mathbf{V}} = \mathbf{Q}_z^{-1}\left(\tilde{\xi}\right) + \mathbf{Q}_d^{-1}\left(\tilde{\delta}\right) = \mathbf{k} \times \nabla\left[\nabla^{-2}\left(\tilde{\xi}\right)\right] + \nabla\left[\nabla^{-2}\left(\tilde{\delta}\right)\right] = \tilde{u}\mathbf{i} + \tilde{v}\mathbf{j} \quad (1)$$

where $\tilde{\mathbf{V}}$ is the environmental wind vector, $\mathbf{Q}_z$ ($\mathbf{Q}_d$) is an operator that calculates the two-dimensional non-divergent (irrotational) wind field from the environmental vorticity $\tilde{\xi}$ (divergence $\tilde{\delta}$), and "∇^{-2}" represents the inversion operator that calculates streamfunction (velocity potential) from vorticity (divergence). By removing the vorticity and divergence associated with the TC in computing the environmental wind, the effects of small displacements of the TC from the center of the domain do not influence the calculation provided the vorticity and divergence associated with the TC at least remain within the response function box (Hoover and Morgan 2010).

Two response functions are defined to describe the averaged zonal and meridional environmental flow in the vicinity of the TC:

$$R_1 = \frac{\sum_{i,j,k \in D} \tilde{u}_{i,j,k} \Delta x \Delta y \Delta z}{\sum_{i,j,k \in D} \Delta x \Delta y \Delta z} \quad (2) \text{ and}$$

$$R_2 = \frac{\sum_{i,j,k \in D} \tilde{v}_{i,j,k} \Delta x \Delta y \Delta z}{\sum_{i,j,k \in D} \Delta x \Delta y \Delta z} \quad (3),$$

where the summation is carried out over every grid point (indexed zonally by *i*, meridionally by *j*, and vertically by *k*) in the horizontal and vertical bounds of the response function box (*D*) on the Gaussian grid onto which the spectral representation of variables is interpolated.

The response function box is defined as all points within a 15^{o}x15^{o} box centered on the final-time location of the TC in the basic state trajectory, between the 0.9873 and 0.2740 sigma levels, corresponding roughly to the 990hPa-300hPa levels. In this way, R_1 (R_2) represents the deep-layer mean environmental zonal (meridional) flow in the vicinity of the TC. A similar approach to this technique has been applied in modeling studies wherein the PV of the TC is removed and the remaining PV inverted to recover the environmental "hurricane advective flow" steering the TC (Wu and Emanuel 1995).

Sensitivity is calculated for the zonal (R_1) and meridional (R_2) components of the steering separately. These sensitivities can be combined into a vector:

$$\mathbf{V}_{ADSSV} = \left(\frac{\partial R_1}{\partial \mathbf{x}}, \frac{\partial R_2}{\partial \mathbf{x}} \right) \quad (4),$$

which describes how small changes to the model state ($\mathbf{x}$) will change the direction and magnitude of the steering of the TC at the end of the 36hr simulation. These vectors are called Adjoint-Derived Sensitivity Steering Vectors (ADSSV; Wu et al. 2007), and can be computed with respect to any model state variable at any time in the simulation, or with respect to a number of derived variables (Kleist and Morgan 2005). For the purposes of this study, we will focus on sensitivity with respect to vorticity, $\mathbf{V}_{\xi} = \left(\frac{\partial R_1}{\partial \xi}, \frac{\partial R_2}{\partial \xi} \right)$, because vorticity is a quasi-conserved variable (as opposed to, say, temperature) which simplifies interpretation of the sensitivity gradients.

3.4 Analysis

a) Typhoon Meari (2004) – Typhoon/Midlatitude Trough Interaction

Figure 3.1a is a plot of the position of Typhoon Meari (2004) every six hours in a 36hr NOGAPS simulation initialized at 00 UTC 24 September 2004, with the NHC best track analysis overlaid. The model appears to capture the direction and speed of Meari quite accurately, maintaining a track that takes Meari northwest toward mainland China. The reason for the recurvature is clear; Meari appears to be steered by a midlatitude trough just upstream and a weak subtropical high to the east for the entirety of the model simulation (Fig. 3.1b-d).

Sensitivities are computed with respect to vorticity; Figure 3.2 is a plot of $\partial R_1/\partial\zeta$, $\partial R_2/\partial\zeta$, and $\mathbf{V}_\zeta$ valid at model initialization near tropopause level. Some portions of the sensitivity fields appear to be quite simple to dynamically interpret. The strong negative sensitivity of zonal steering southeast of the response function box (Fig. 3.2a) makes sense in a purely advective, barotropic framework. Introducing *anticyclonic* vorticity in this region would create a large, anticyclonic gyre with westerly winds on its north side. If this feature were to persist for 36 hours, it would induce positive zonal environmental flow in the response function box at model verification. Note that this region of sensitivity is not positioned to the southwest of the TC, which would allow such a perturbation to be advected to the east by the TC itself, to arrive at an optimal position just south of the response function box by the end of the simulation. This sensitivity appears to be collocated with an already existing region of negative vorticity in the subtropical ridge; this is in stark contrast to the results of an idealized TC in a barotropic model, in which sensitivity is simply placed upstream of the circulation about the TC (Hoover and Morgan 2010), and is the result of using the adjoint of a full-physics NWP model to simulate a real TC embedded within a complexly evolving environment.

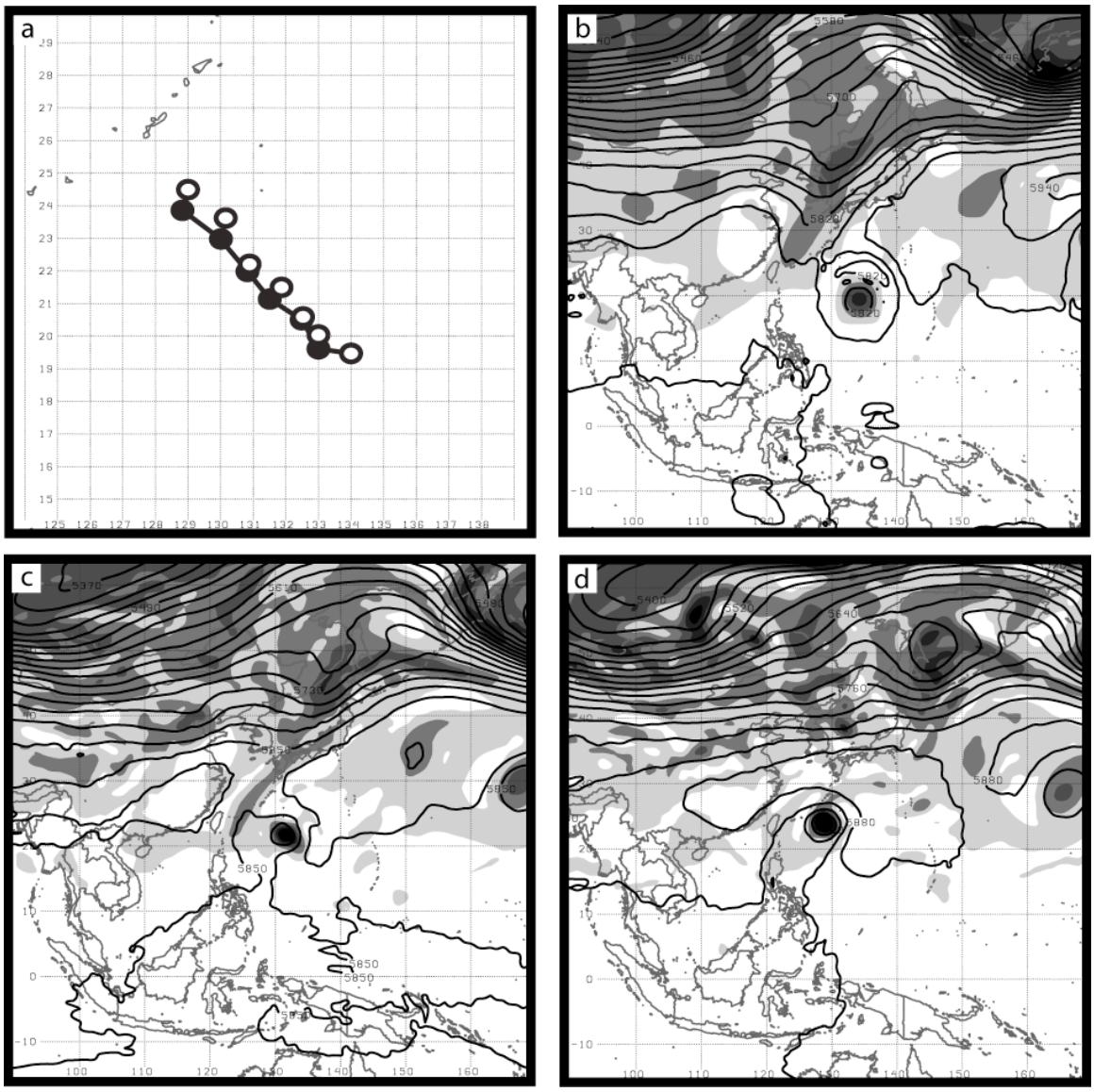

Figure 3.1. (a) Track of Typhoon Meari (2004) in 36hr simulation initialized at 00 UTC 24 September 2004. Black dots indicate the location of minimum sea level pressure every six hours. White dots indicate TC location according to NHC best track analysis. Geopotential height (black contours every 30 m) and absolute vorticity (shaded every $5x10^{-5}$ s^{-1}) at 500 hPa at (b) model initialization (c) 18 hours and (d) 36 hours.

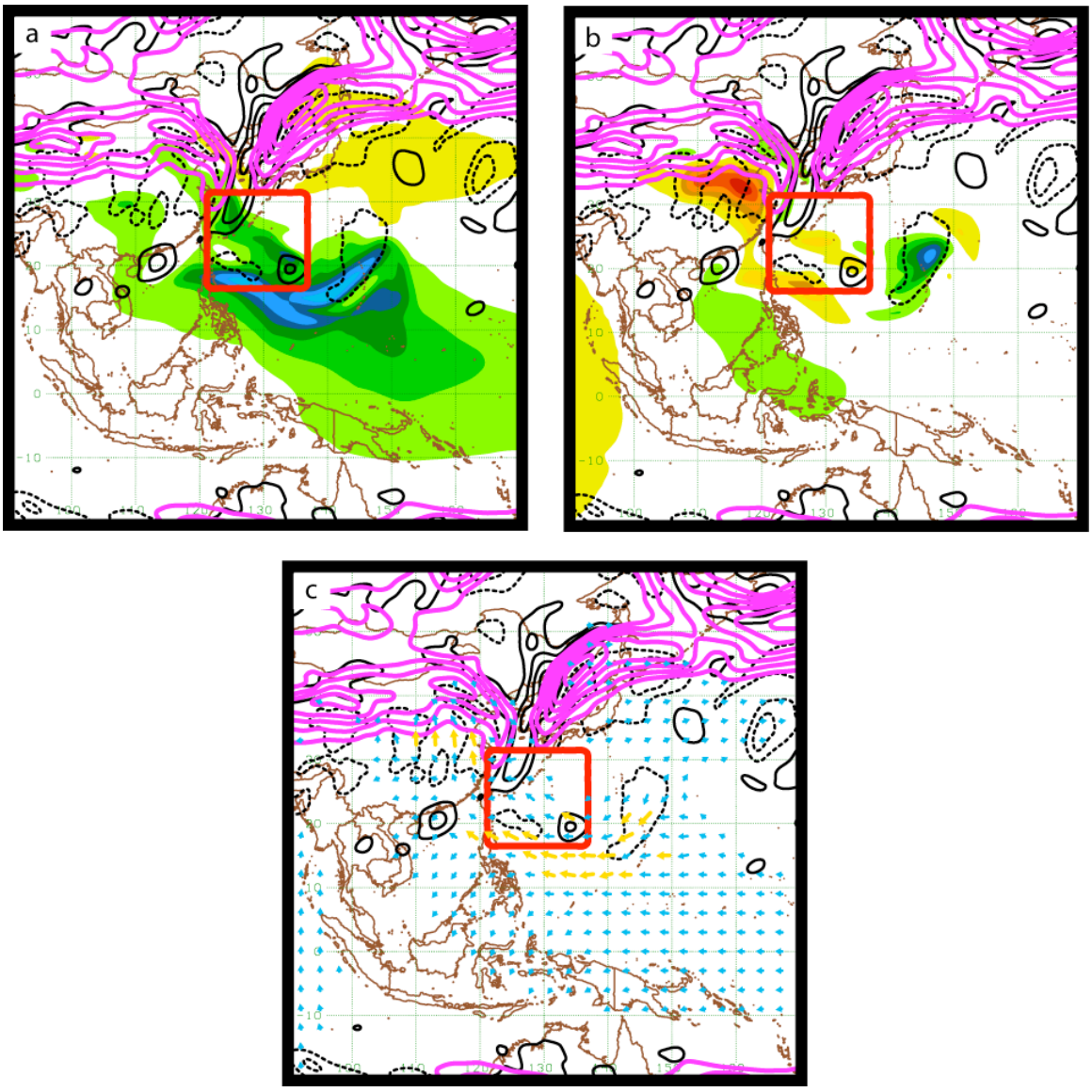

Figure 3.2. Sensitivity of steering of Typhoon Meari (2004) with respect to vorticity at the 0.2740-sigma level, corresponding roughly to the 300mb level assuming a sea level pressure of 1000mb. (a) Sensitivity of the zonal component of steering with respect to vorticity $\left(\partial R_1/\partial\zeta\right)$ (shaded, cool colors negative), basic state vorticity (black contours every 4 s^{-1}, negative contours dashed) and basic state isotachs (magenta contours every 6 ms^{-1} equal to or greater than 24 ms^{-1}) in the forecast with unperturbed initial conditions. (b) Sensitivity of the meridional component of steering with respect to vorticity $\left(\partial R_2/\partial\zeta\right)$. (c) ADSSV representing the magnitude and direction of perturbation steering with respect to vorticity $\mathbf{V}_\zeta = \left(\partial R_1/\partial\zeta, \partial R_2/\partial\zeta\right)$. All sensitivities are computed for steering by the environmental flow in a response function box (red contour) 36 hours into the model simulation.

A very strong region of sensitivity of meridional steering is found upstream of the TC, just south of the polar jet and upstream of the midlatitude trough (Fig. 3.2b). In fact, the vorticity ADSSV appears to be strong in this region (Fig. 3.2c), indicating that a small perturbation to the vorticity in this region would have a large impact on the steering of the TC; in this case, a positive (negative) perturbation would add a southerly (northerly) component to the steering of the TC 36 hours in the future.

Similar results were found by Wu et al. (2009a) when using their ADSSV technique to investigate the role of TC/trough interaction with Typhoon Shanshan (2006). While it was intimated in that study that the coincidence of these features indicates that the midlatitude trough is of great importance to the steering of Shanshan, it is important to remember what these sensitivity gradients actually mean. Sensitivity gradients valid at model initialization only describe how the response function will change as a result of perturbations added to a model's initial conditions. While it may be seductive to conclude a synoptic-scale feature must be important to the steering in the *basic state* because of the coincidence of that feature (such as the vorticity of the midlatitude trough) and sensitivity of steering to vorticity, this is not necessarily the case. A feature of the basic state may be in a region of high sensitivity that would exist in that location whether that particular feature of the basic state were present or not; Langland et al. (1995) found that sensitivity of cyclone intensity to temperature in an idealized channel model appeared very similar regardless of whether a cyclone actually developed in the basic state. It should also be noted that while the sensitivity is near the trough, and may be within the trough when looking at geopotential height, the sensitivity is actually slightly *upstream* of the vorticity of the trough.

The sensitivity in this region may in fact correspond to important interactions between Meari and the midlatitude trough. Alternatively, the sensitivity may be do to some other process that takes place near the trough but isn't directly related to the strength of the trough. The only way to be sure is to perturb the vorticity in the initial conditions and observe the result. Small perturbations to the vorticity in the initial conditions where the sensitivity is positive in this region show an interesting result (Fig. 3.3). The initial perturbation vorticity (Fig. 3.3a) is advected downstream and is stretched when it enters the subsidence in the lee of the midlatitude trough (Fig. 3.4), creating a strong vortex that appears just west of the response function box at model verification (Fig. 3.3b).

If one were to compute the vorticity and divergence of the environment and invert it to recover the environmental flow, a vortex appears just west of the response function box, inducing a strong southerly component to the environmental flow in the box (Fig. 3.3c). A cross-section through the box (Fig. 3.3d) shows that this positive contribution to the meridional steering extends from the middle troposphere to the top of the response function box.

A simple test can be performed to determine how much of the result obtained from the nonlinear model is predicted by the adjoint model. One can calculate the change in response function ΔR between a (control) run with unperturbed initial conditions and a run with perturbed initial conditions by calculating R in both simulations and calculating the difference:

$$\Delta R = R_{perturbed} - R_{control} \qquad (5).$$

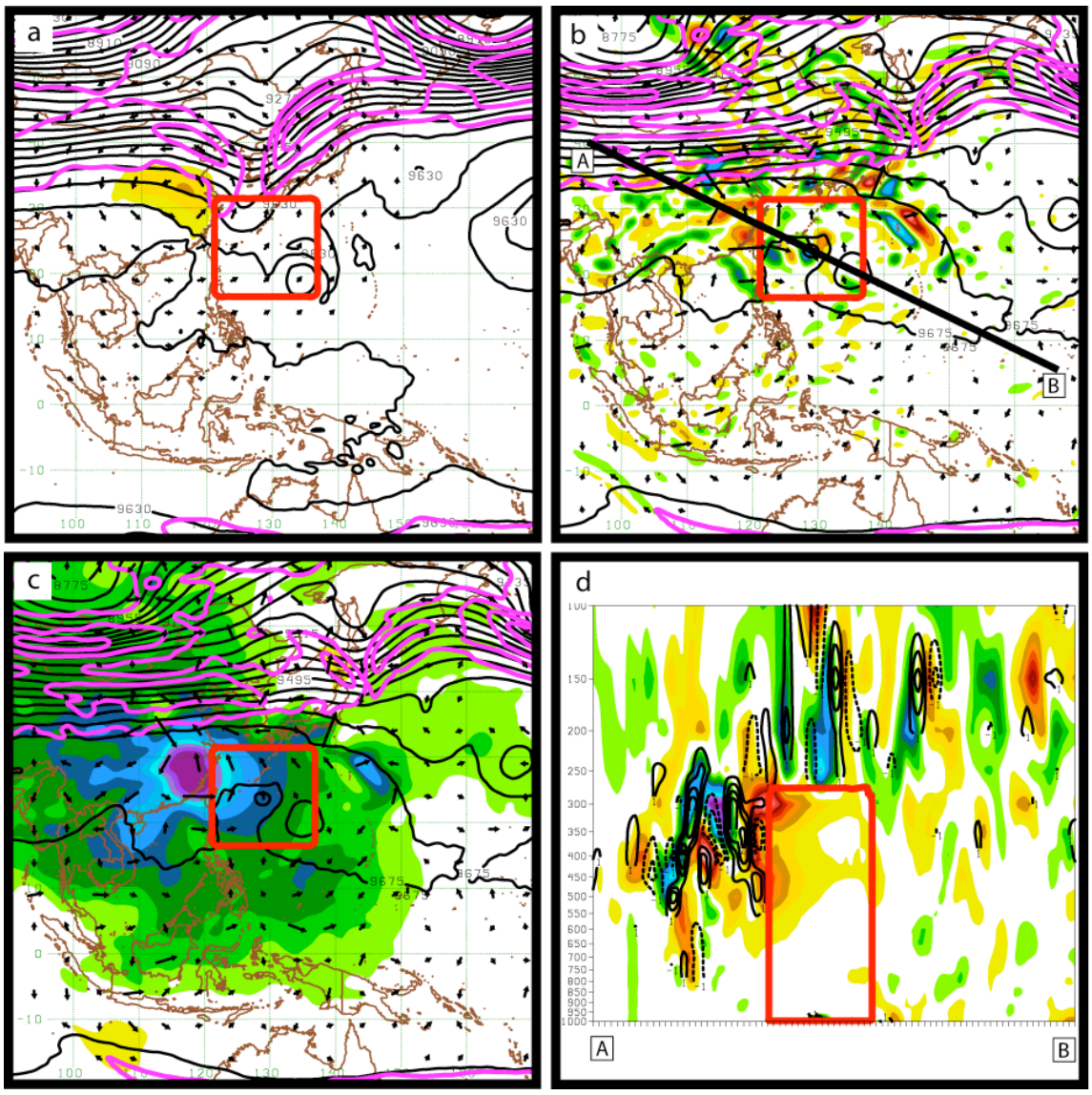

Figure 3.3. Perturbation experiment for Typhoon Meari (2004) simulation. (a) Initial condition perturbation vorticity (shaded every $5x10^{-6}$ s^{-1}, cool colors negative), perturbation winds, and basic state geopotential height (black contours every 45 m) and basic state isotachs (magenta contours every 12 ms^{-1} greater than or equal to 24 ms^{-1}) at 300mb. (b) 36hr perturbation vorticity (shaded every $1x10^{-1}$ s^{-1}), perturbation winds, and basic state heights and isotachs at 300mb. (c) 36hr perturbation environmental winds, streamfunction (shaded), and basic state geopotential height and isotachs. (d) Cross-section from A to B of perturbation environmental vorticity (contour every $1x10^{-5}$ s^{-1}, negative contours dashed) and perturbation environmental meridional flow (shaded every 0.5 ms^{-1}). The red contour in each plot corresponds to the response function box location.

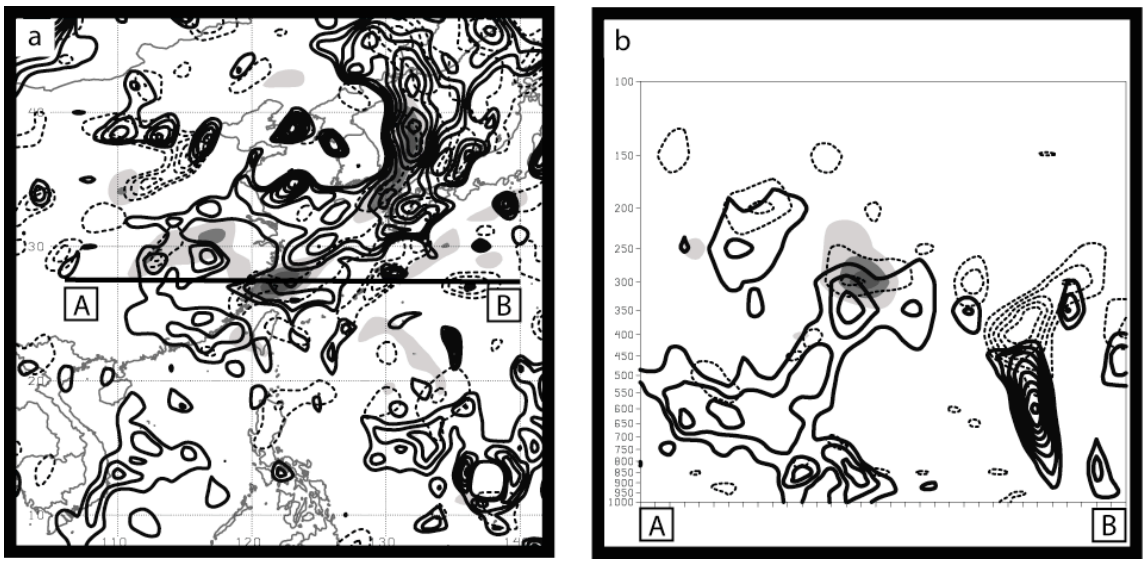

Figure 3.4. Perturbation experiment for Typhoon Meari (2004) simulation. (a) Perturbation vorticity (shaded every $2x10^{-5}$ s^{-1}), basic state vertical motion (solid contours every 0.5 $\mu b\ s^{-1}$, and basic state convergence (dashed contours every 1 s^{-1}) at 300mb valid 24 hours into the simulation. (b) Cross section from A to B of perturbation vorticity (shaded every $2x10^{-5}$ s^{-1}), basic state vertical motion (solid contours every 0.5 $\mu b\ s^{-1}$, and basic state convergence (dashed contours every 1 s^{-1}) at 300mb valid 24 hours into the simulation.

This value can be approximated, assuming linearity and the simplified physics of the adjoint model, by calculating the inner product of the sensitivity gradient $\partial R/\partial \mathbf{x}_0$ and the perturbation to initial conditions $\mathbf{x}_0'$:

$$\Delta R \approx \delta R = \left\langle \frac{\partial R}{\partial \mathbf{x}_0}, \mathbf{x}_0' \right\rangle \quad (6).$$

For the case under consideration, the average perturbation environmental meridional flow in the response function box, ΔR=0.301 m s^{-1}. The adjoint model approximates a value of δR =0.275 m s^{-1}, meaning that the adjoint model was able to account for the change in the response function for this perturbation with an accuracy of 91.3%.

b) Tyhoon Choi-Wan (2009) – Typhoon/Midlatitude Trough Interaction

The interaction of Typhoon Choi-Wan (2009) with a midlatitude trough creates a recurving track that steers the TC northward to northeastward for the entire simulation; the track and speed of motion are well represented by the model (Fig. 3.5a). Choi-Wan has a synoptic environment very similar to Meari, with a midlatitude trough initialized north and upstream of the TC, and a subtropical ridge to the east at 0000 UTC 18 September 2009 (Fig. 3.5b). Unlike with Meari, the midlatitude trough largely stays north of the TC for the entire simulation, with very little direct contact with the TC itself (Fig. 3.5c-d). The subtropical ridge is stronger in this case, steering the TC northward and eventually eastward as the TC enters midlatitude westerly flow.

Sensitivity of steering with respect to vorticity near tropopause level (Fig. 3.6) reveals similar characteristics to those found for Meari. Although $\mathbf{V}_\xi$ appears to be larger in magnitude, especially in the immediate vicinity of the TC, a region of strong sensitivity again appears north and upstream of the TC. This region is again collocated with strong

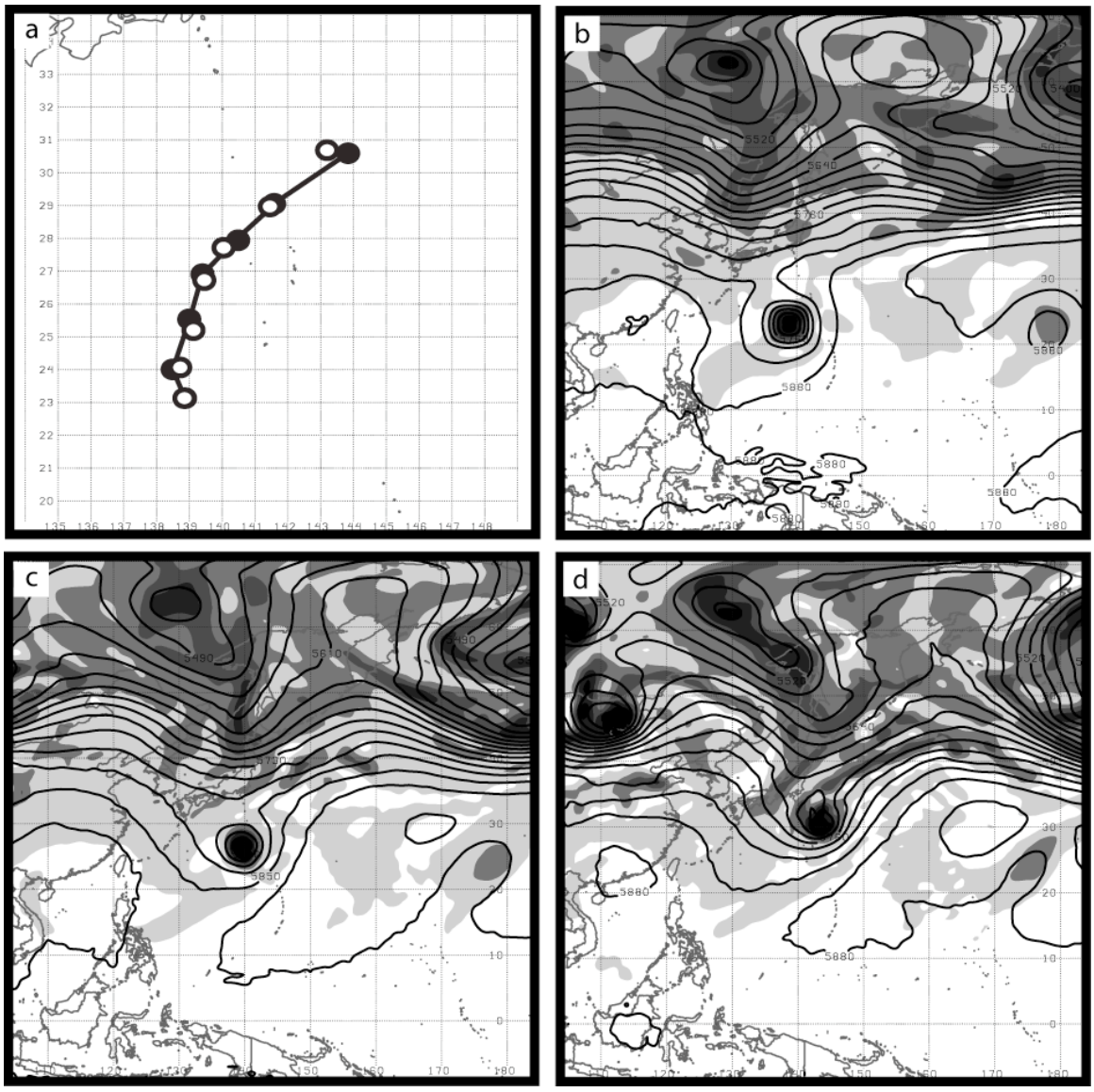

Figure 3.5. (a) Track of Typhoon Choi-wan (2009) in 36hr simulation initialized at 00 UTC 18 September 2009. Black dots indicate the location of minimum sea level pressure every six hours. White dots indicate TC location according to NHC best track analysis. Geopotential height (black contours every 30 m) and absolute vorticity (shaded every $5x10^{-5}$ s^{-1}) at 500 hPa at (b) model initialization (c) 18 hours and (d) 36 hours.

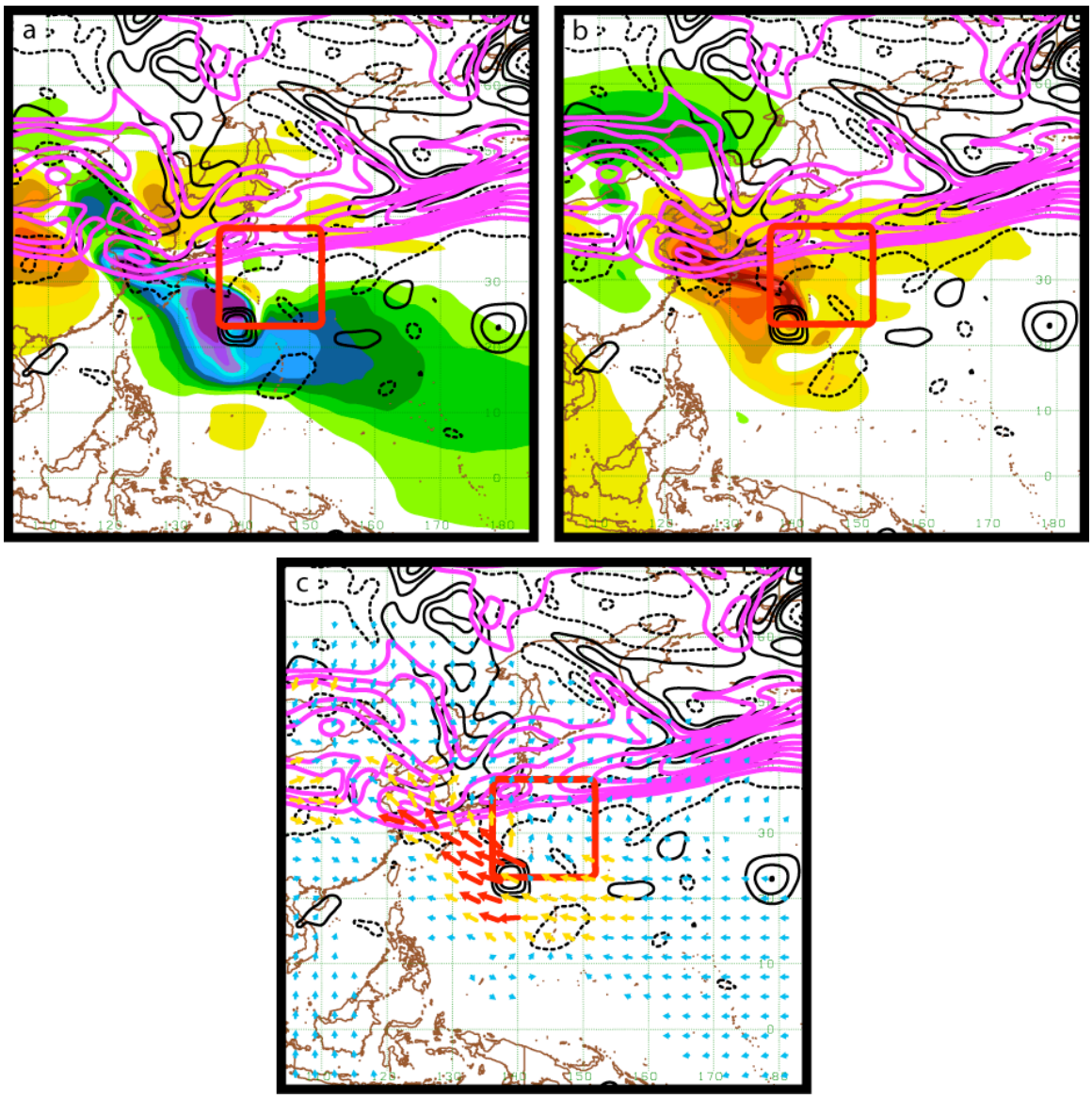

Figure 3.6. Sensitivity of steering of Typhoon Choi-Wan (2009) with respect to vorticity at the 0.2740-sigma level, corresponding roughly to the 300mb level assuming a sea level pressure of 1000mb. (a) Sensitivity of the zonal component of steering with respect to vorticity $\left(\partial R_1/\partial\zeta\right)$ (shaded, cool colors negative), basic state vorticity (black contours every 4 s^{-1}, negative contours dashed) and basic state isotachs (magenta contours every 6 ms^{-1} equal to or greater than 24 ms^{-1}). (b) Sensitivity of the meridional component of steering with respect to vorticity $\left(\partial R_2/\partial\zeta\right)$. (c) ADSSV representing the magnitude and direction of perturbation steering with respect to vorticity $\mathbf{V}_\zeta = \left(\partial R_1/\partial\zeta, \partial R_2/\partial\zeta\right)$. All sensitivities are computed for steering by the environmental flow in a response function box (red contour) 36 hours into the model simulation.

subsidence in the lee of the passing midlatitude trough. This feature of the ADSSV is consistent throughout the middle and upper troposphere and follows the subsidence region throughout time (see Fig. 3.10b). Given the similarity of the sensitivities, as well as the similarity of the environment, it is safe to assume that this feature of the sensitivity exists for the same reason in both simulations; a perturbation of the vorticity in this region would be stretched within the subsidence in the lee of the midlatitude trough, causing the perturbation vortex to intensify as it is carried downstream. At model verification, the vortex would be situated so as to have a strong impact on the environmental steering of the TC as it has been defined in this study.

c) Typhoon Longwang (2005) – Steady Zonal Track

Typhoon Longwang (2005) is provided as an example of a TC that undergoes steady, zonal steering for the entirety of the simulation (Fig. 3.7a). Steered primarily by a dominating subtropical ridge to the north (Fig. 3.7b-d), the ridge prevents Longwang from experiencing any meaningful interaction with passing midlatitude systems. We therefore may expect that sensitivities to steering may be of smaller magnitude, and localized to the immediate environment of the TC and the subtropical ridge. One can imagine that any small perturbation to the vorticity upstream of the TC would be caught up in the westerly flow of the midlatitudes, be carried north of the subtropical ridge, and have little if any impact on the steering of Longwang.

Steering sensitivity near tropopause level appears to have all of these qualities (Fig. 3.8). Zonal steering sensitivity (Fig. 3.8a) shares many characteristics of zonal steering sensitivity for the case of an idealized, barotropic vortex (Hoover and Morgan 2010) embedded in a mean easterly steering flow. Maximum positive (negative) sensitivity appears

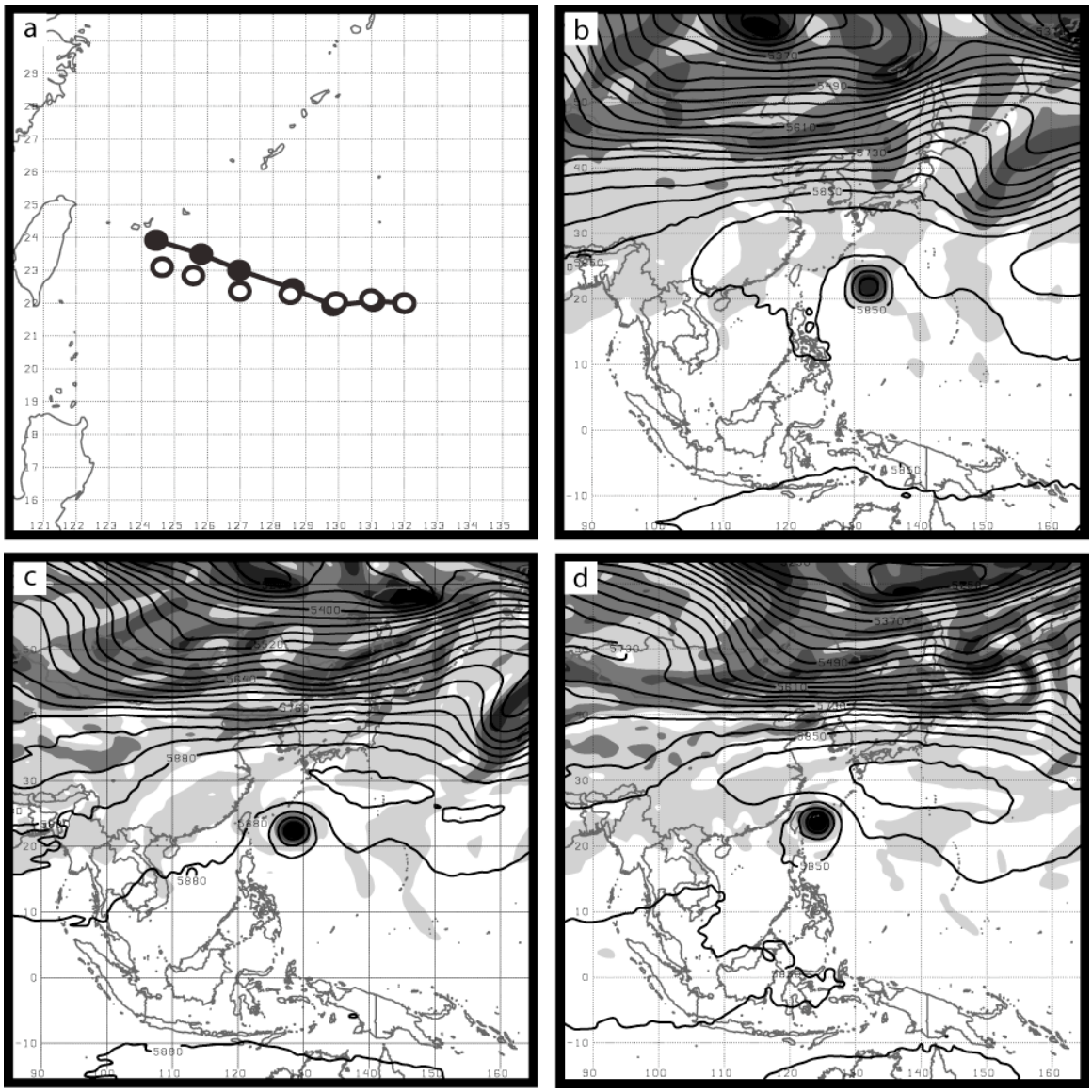

Figure 3.7. (a) Track of Typhoon Longwang (2005) in 36hr simulation initialized at 00 UTC 30 September 2005. Black dots indicate the location of minimum sea level pressure every six hours. White dots indicate TC location according to NHC best track analysis. Geopotential height (black contours every 30 m) and absolute vorticity (shaded every $5x10^{-5}$ s^{-1}) at 500 hPa at (b) model initialization (c) 18 hours and (d) 36 hours.

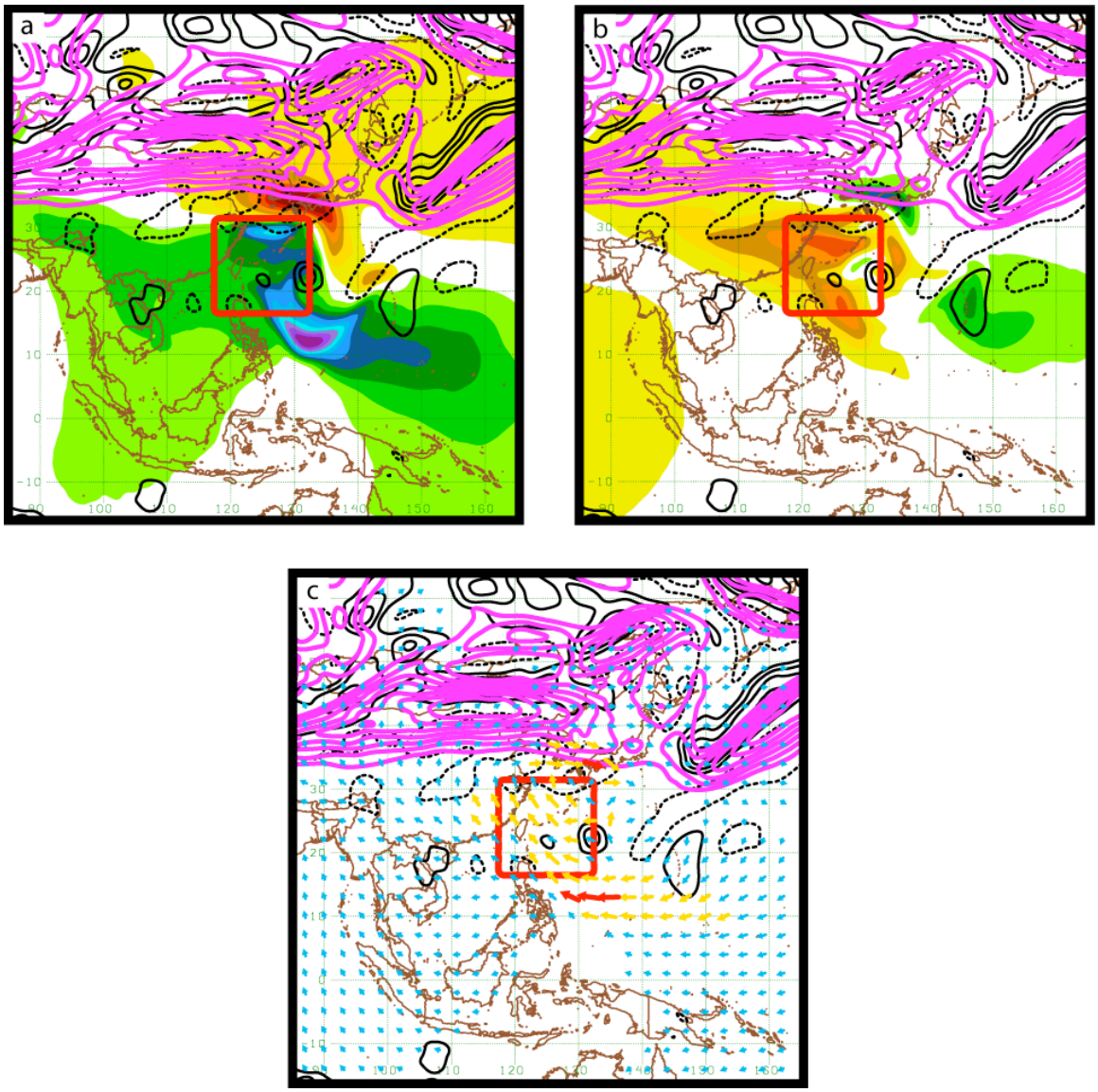

Figure 3.8. Sensitivity of steering of Typhoon Longwang (2005) with respect to vorticity at the 0.2740-sigma level, corresponding roughly to the 300mb level assuming a sea level pressure of 1000mb. (a) Sensitivity of the zonal component of steering with respect to vorticity $\left(\partial R_1/\partial\zeta\right)$ (shaded, cool colors negative), basic state vorticity (black contours every 4 s^{-1}, negative contours dashed) and basic state isotachs (magenta contours every 6 ms^{-1} equal to or greater than 24 ms^{-1}). (b) Sensitivity of the meridional component of steering with respect to vorticity $\left(\partial R_2/\partial\zeta\right)$. (c) ADSSV representing the magnitude and direction of perturbation steering with respect to vorticity $\mathbf{V}_\zeta = \left(\partial R_1/\partial\zeta, \partial R_2/\partial\zeta,\right)$. All sensitivities are computed for steering by the environmental flow in a response function box (red contour) 36 hours into the model simulation.

northeast (southwest) of the TC, localized near the TC, where vorticity perturbations of the same polarity can be advected to be situated just north (south) of the response function box and provide a westerly environmental current. Strong negative sensitivity also appears within and south of the subtropical ridge. ADSSV outside of this small, localized region is very small (Fig. 3.8c).

d) Typhoon Parma (2009) – No TC Motion/Binary Interaction

Typhoon Parma (2009) is an abnormal case wherein the TC began a southeasterly track across the northern Philippines but quickly stalled and remained essentially stationary for several days (Fig. 3.9a). Flanked on either side by a ridge, there is little in Parma's environment to advect the cyclone away from this position (Fig. 3.9b). While a passing midlatitude trough could provide a means to force Parma to recurve and move northeastward, Parma also appears to interact with Typhoon Melor (2009) as the two cyclones move closer to each other between 36-72 hours into the 108 hour simulation (Fig. 3.9d-f), which would induce a binary interaction opposing the advection of Parma by the midlatitude trough. As Melor recurves and moves into the midlatitudes (Fig. 3.9g-h), Parma again finds itself between two ridges and does not move from its position.

The 108hr basic state trajectory provided by the NOGAPS model is divided into three 36hr-long pieces, and a sensitivity analysis is performed for the steering at the end of each piece (36hr, 72hr, and 108hr respectively) with respect to model conditions 36hrs previous (model initialization, 36hr, and 72hr respectively). This is done for two reasons. First, a 108hr trajectory is far too long to allow for the assumption of linearity required to use the adjoint model, while small perturbations can behave linearly in a moist, nonlinear NWP model simulation for upwards of 36hrs (Errico and Vukicevic 1992). Secondly, Parma

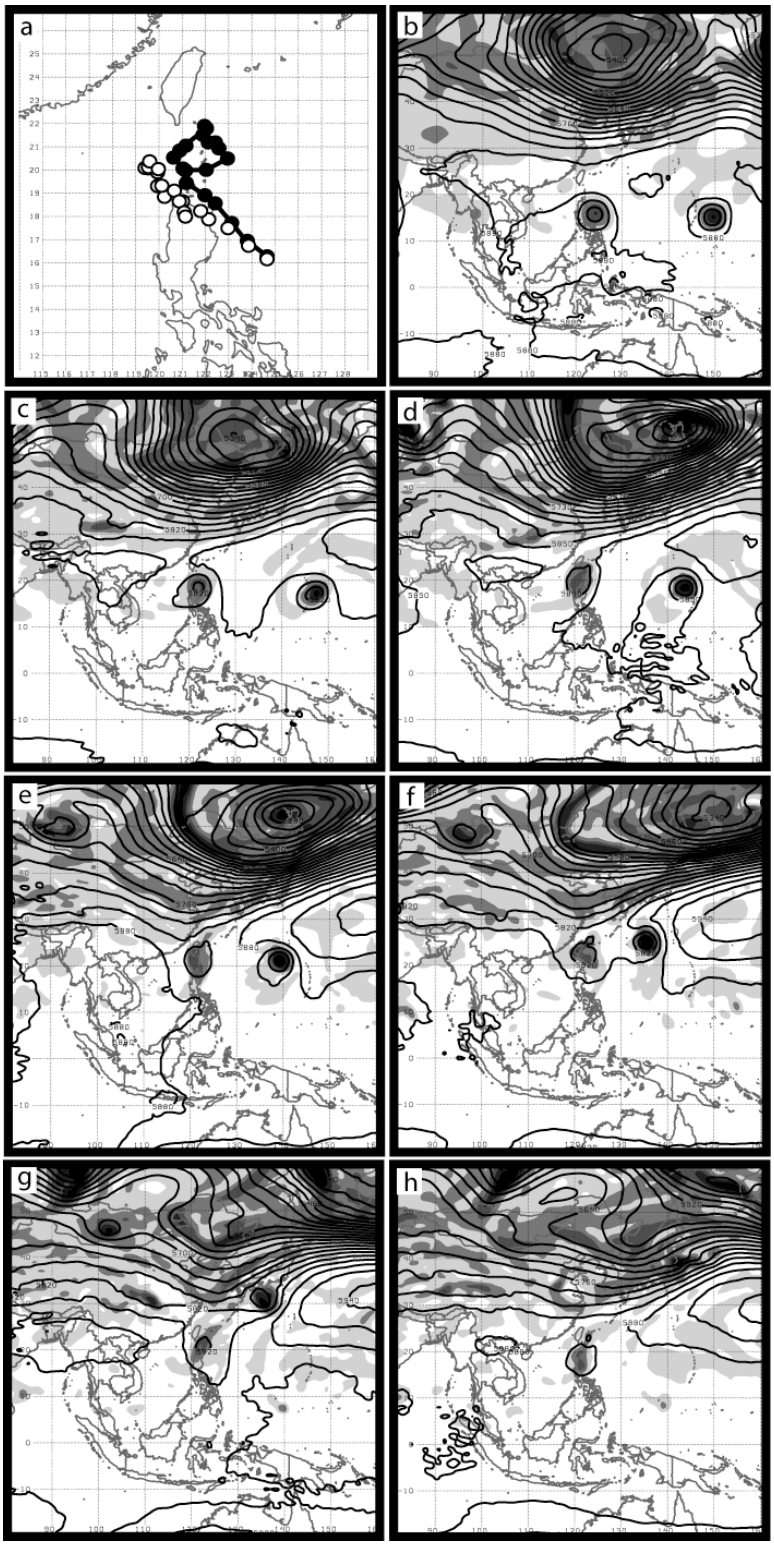

Figure 3.9. (a) Track of Typhoon Parma (2009) in 108hr simulation initialized at 12 UTC 02 October 2009. Black dots indicate the location of minimum sea level pressure every six hours. White dots indicate TC location according to NHC best track analysis. Geopotential height (black contours every 30 m) and absolute vorticity (shaded every $5x10^{-5}$ s^{-1}) at 500 hPa at (b) model initialization (c) 18 hours (d) 36 hours (e) 54 hours (f) 72 hours (g) 90 hours and (h) 108 hours.

appears to experience three environmental regimes throughout the 108hr simulation: an initial stall after moving to the northwest over the northern Philippines (0-36hr), binary interaction with Typhoon Melor (36hr-72hr), and post-interaction with Melor (72hr-108hr). Evaluating the sensitivity of the steering of Parma at these different times provides a survey of information about the relative influence of the major synoptic features near Parma on TC steering for the entirety of the 108hr simulation.

A comparison of ADSSV in the mid-troposphere at these three times (Fig. 3.10) shows the relative sensitivity of Parma to the vorticity of Melor, the midlatitude trough, and the two flanking ridges throughout the simulation. Note that ADSSV in the first two time periods (Fig. 3.10 a,b) diverge over Melor, with northerly ADSSV south of Melor and southerly ADSSV to the north. From this it can be deduced that small perturbations in vorticity around Melor (or the position of Melor itself) have a substantial impact on the meridional portion of Parma's steering, with the strongest sensitivities appearing for steering at 72hrs into the simulation (when Melor and Parma are closest to one another and the binary interaction is likely strongest).

The physical interpretation of these ADSSV is relatively simple. Parma and Melor exist at or very nearly at the same latitude; any contribution to Parma's steering through a binary interaction with Melor will therefore be in the (negative) meridional direction. A southerly component, for example, can be induced by placing a positive (negative) vorticity perturbation north (south) of Melor 36hrs earlier (Fig. 3.10b). The effect of these perturbations would be to induce *westerly flow* over Melor, *increasing* the distance between Parma and Melor, and therefore *decreasing* the strength of their binary interaction. Since Parma is positioned west of Melor, this would decrease the strength of the northerly winds

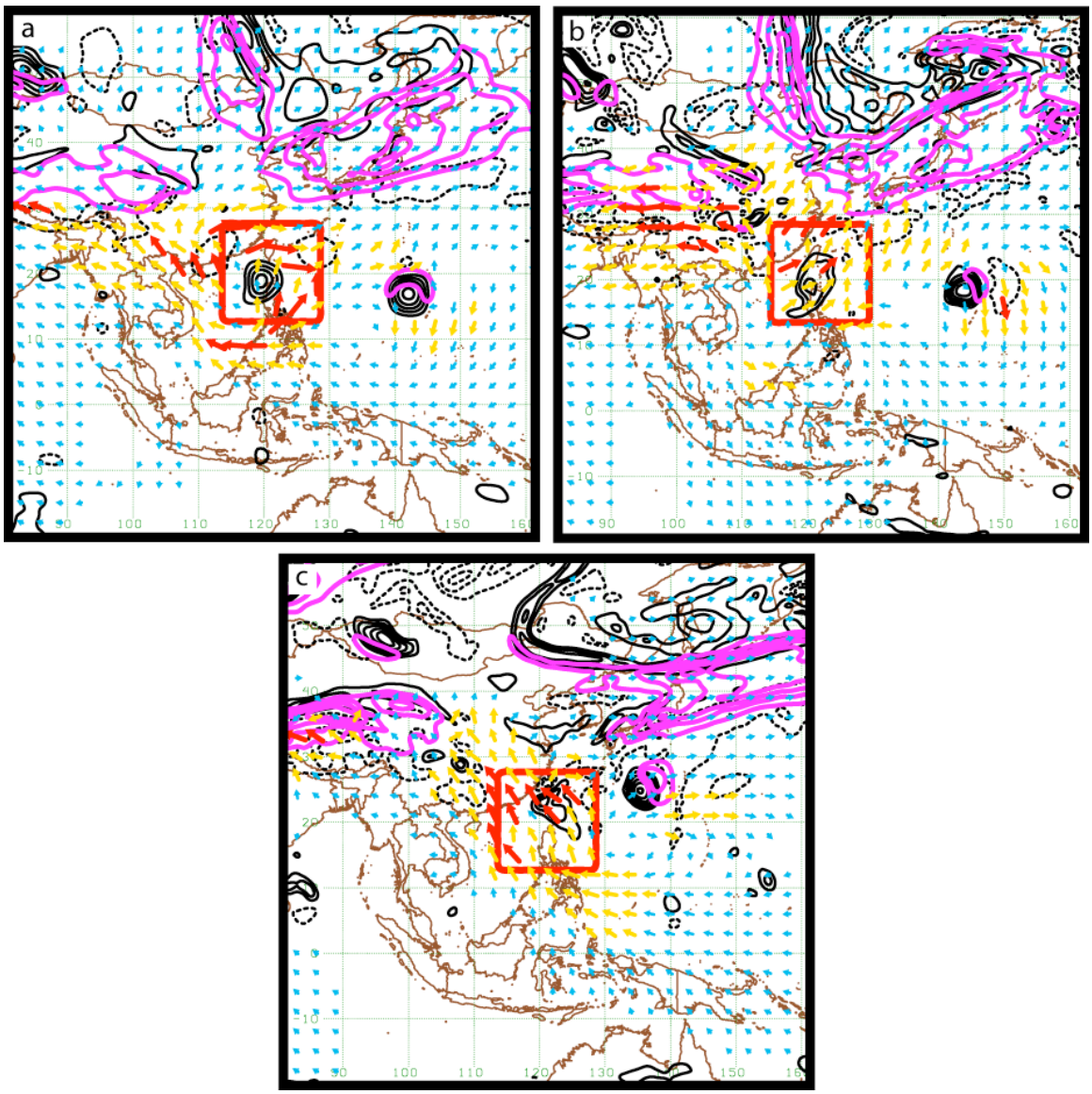

Figure 3.10. Vorticity ADSSV at the 0.4718 sigma level, corresponding roughly to the 500mb level. Basic-state vorticity (black contours every 4 s^{-1}, negative contours dashed), basic state isotachs (magenta contours every 6 ms^{-1} greater than or equal to 24 ms^{-1}). The red contour is the location of the response function box. Computed for a 108hr simulation of Typhoon Parma (2009) initialized at 12 UTC 02 October 2009 and valid at (a) model initialization (b) 36 hours (c) 72 hours corresponding to sensitivities derived for the steering of the TC 36 hours in the future.

from Melor that would steer Parma, resulting in a positive *perturbation* to the meridional steering of Parma relative to the unperturbed (control) run. These ADSSV suggest that the zonal steering of Melor modulates the meridional steering of Parma at this time. ADSSV from the 36hr period before (Fig. 3.10a) or after (Fig. 3.10c) show that the steering of Parma is not as sensitive to this effect during these times, and sensitivities are localized about Parma or upstream of the TC.

e) Comparisons

ADSSV of the Meari (2004), Longwang (2005), and Choi-Wan (2009) in the middle troposphere (Fig. 3.11) provide another perspective. Large differences between ADSSV for Typhoon Meari (2004) (Fig. 3.11a) and Typhoon Choi-Wan (2009) (Fig. 3.11c) are observed, despite the similarities in track and environment. While the upstream trough is clearly visible in both plots, it appears to only be barely significant to the steering of Meari at this level, while for Choi-Wan the strongest sensitivity again exists just in the lee of the trough. Significant subsidence exists upstream of the trough in both simulations.

The difference may have to do with the location of the trough. In the Meari simulation, the trough interacts directly with Meari, and even at model initialization, the vorticity of the trough is well within the response function box. The trough in the Choi-Wan simulation, on the other hand, is outside of the response function box. Recall that the response function presupposes that vorticity within the response function box is considered vorticity associated with the TC. This vorticity is removed when calculating the vorticity of the environment. Any perturbation just in the lee of the trough in the initial conditions of the Meari simulation would most likely end up in the response function box by model

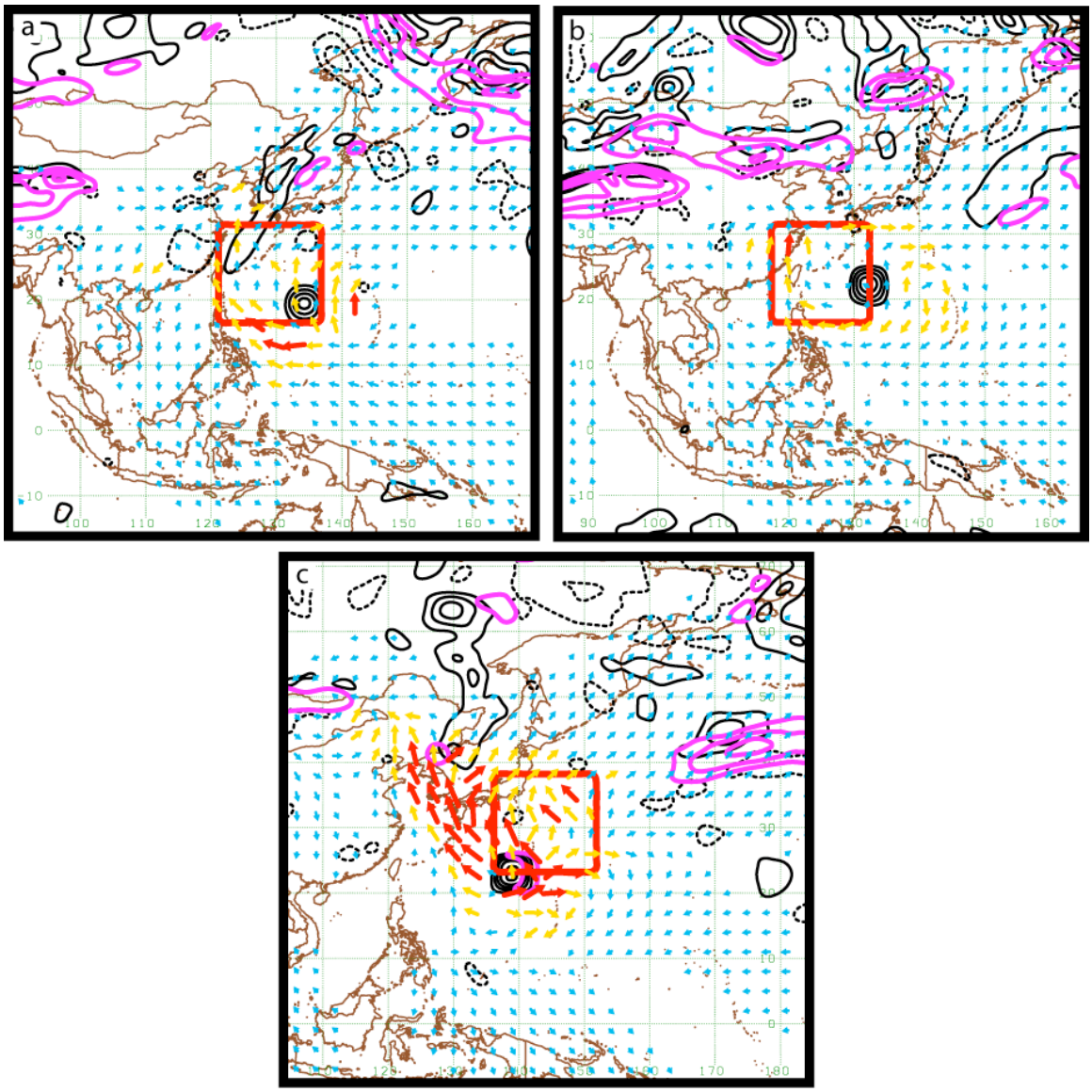

Figure 3.11. Vorticity ADSSV at the 0.4718 sigma level, corresponding roughly to the 500mb level. Basic state vorticity (black contours every 4 s^{-1}, negative contours dashed), basic state isotachs (magenta contours every 6 ms^{-1} greater than or equal to 24 ms^{-1}). The red contour is the location of the response function box. Valid at model initialization for 36 hour simulations of (a) Typhoon Meari (2004) initialized at 00 UTC 24 September 2004 (b) Typhoon Longwang (2005) initialized at 00 UTC 30 September 2005 (c) Typhoon Choi-Wan (2009) initialized at 00 UTC 18 September 2009.

verification and have no impact. Perturbations placed in the lee of the trough in the Choi-Wan simulation do not experience this effect.

What is being observed is an effective "blind spot" in the sensitivities that arises as a result of how the response function is defined. Sensitivities are also likely to vary depending on the size of the response function box because perturbations that yield the largest effect on steering will most likely create perturbation vortices that exist just outside of the response function box at model verification, where they can impose the maximum amount of influence on the flow in the box. Repeating the calculation of sensitivities for Meari (2004) using an 11^{o}x11^{o} box results in an eastward shift in the meridional steering sensitivity with respect to vorticity, putting it just to the west of the midlatitude trough (not shown).

3.5 Conclusions

Through careful choice of response functions representing the steering of a TC, adjoint models can provide valuable *a priori* information about the sensitivity of TC steering to features in all previous model states. While these sensitivity gradients cannot explicitly determine the importance of a particular feature of the model state in terms of its contribution to the response function *in the basic state*, sensitivity information provides insight into how small perturbations of the model state will change the response function, and in which features of the basic state perturbation would be of greatest import.

It is found in this study that the ADSSV technique is able to effectively describe the speed and direction change of steering to perturbations of vorticity in the initial conditions over a trajectory length of 36 hours. Furthermore, a dynamical interpretation of these sensitivities is possible; the rule established by Langland et al. (1995) can be applied here: features of the basic state are "important" if they are found in regions of strong sensitivity to

the model state (**x**) and are responsible for large *time-tendencies* of the model state. In this study, the subsidence region in the lee of a passing midlatitude trough is found to be a region of significant sensitivity with respect to vorticity. In addition, it is found that the reason for this sensitivity is the ability for a small vorticity perturbation to be stretched by the subsidence, leading to a large growth of the vorticity over time. We can therefore employ this rule to identify this subsidence region as an important feature of the basic state to the steering of a TC. Likewise, the ADSSV technique is able to distinguish when a binary interaction is significant in a simulation of Typhoon Parma (2009) and Typhoon Melor (2009).

The most practical application of this technique is in the deployment of targeted observations for the explicit purpose of improving TC track prediction. Owing to the dearth of in-situ observations of TCs and their surrounding environment, numerical weather prediction (NWP) forecasts of TC track suffer from poorly defined initial conditions with large uncertainties. Track errors can be mitigated by deployment of targeted observations in the TC's environment to reduce error in the initial conditions near the TC (Aberson 2003). However, lacking any *a priori* information concerning the potential impact of an observation on TC steering, it is not clear where these observations should be taken. The addition of good observational data into the model's initial conditions would not necessarily lead to a significant forecast improvement if those observations were taken in the wrong places (Aberson 2002), or improperly assimilated. A strategy for defining optimal targets for observation is required to ensure that the effort and expense in obtaining these observational data improves the TC forecast in a significant way.

Adjoint-derived sensitivity gradients clearly show where small perturbations to the model initial conditions can have the largest impact on the steering of the TC; this information is vital if one wishes to objectively deploy observations that have the (desired) effect of making small but meaningful innovations to a model background state. While this sensitivity information says nothing about the uncertainty in the model background state, which clearly modulates the impact of deployed observations (Buizza et al. 2007), this information can be provided through the application of the adjoint of the observation assimilation system, a method known as 'observation-space targeting' (Langland 2005), which also provides valuable information on the impact of a single observation based on how the information from that observation is assimilated into the initial conditions (Langland and Baker 2004).

Starting with the firm foundation established in this study, it is hoped that dynamical sensitivity information provided by the adjoint of an NWP model can be combined with information about initial condition uncertainty and the assimilation of observational data provided by the adjoint of an assimilation system to provide a fully comprehensive, objective targeting strategy for the improvement of TC track prediction. Furthermore, response functions can be developed for the purpose of defining sensitivities for a variety of other forecast challenges, such as TC intensity prediction. The development of such a technique would provide an objective, robust method for defining flight plans and target locations for reconnaissance aircraft, as well as valuable dynamical information for researchers and forecasters who wish to better understand the physical processes at work in TC steering and intensity change.

Acknowledgments

The authors wish to thank Dr. Rolf Langland at the Naval Research Laboratory for his help with the NOGAPS model and its adjoint. The first author is supported by the National Science Foundation under grant No. 0529343 and the Office of Naval Research under grant N000141610563PR.

Chapter 4: Identifying an Appropriate Response Function for Tropical Cyclone Intensity and Genesis

Abstract

Adjoint models can provide detailed sensitivity information about a specific aspect of the model forecast state, but only if the response function chosen to represent that forecast aspect is appropriate. Moreover, a function can be appropriate to describe the forecast aspect and *also* be inappropriate as a response function for calculating sensitivity gradients; this is often caused by auxiliary assumptions made about the forecast trajectory that may or may not be valid (e.g. the location of a particular synoptic scale feature at model verification). Oftentimes, one or more mechanisms exist that can make small alterations to the forecast trajectory, resulting in changes to the chosen response function in ways that have nothing to do with the forecast aspect being investigated. These mechanisms can generate inappropriate sensitivity gradients that are difficult or impossible to differentiate from "real" sensitivities that are related to the forecast aspect of interest.

An adjoint model is used to calculate sensitivity gradients for several response functions designed to describe the intensity of a tropical cyclone. These response functions are tested for their appropriateness by perturbing the initial conditions of the model based on these sensitivities and observing the result. Inappropriate response functions lead to perturbations that have the desired impact on the response function but do not have the desired impact on the intensity of the TC. The reasons for this inappropriateness are investigated, and a response function is chosen that performs the most appropriately.

4.1 Introduction

Tropical cyclone (TC) intensity can be defined through any number of metrics; however, for the purposes of defining a response function to compute adjoint-derived sensitivities, additional criteria must be considered. First, the function must be differentiable with respect to variables of the model state. Second, it must be tested for its appropriateness to the task at hand; as has already been shown, a function can be defined that adequately describes some aspect of the forecast (e.g. TC steering as the horizontal flow averaged over a column centered on the TC) but that same function fails to function properly when used as a response function to calculate sensitivity to that aspect of the forecast. The response function may be changed in ways that have nothing to do with the aspect of the forecast under consideration, in which case sensitivities computed from that response function are not entirely appropriate.

Several functions have been defined to measure the intensity of a tropical or extratropical cyclone for the purposes of calculating sensitivity to cyclone intensity. These include lower-tropospheric kinetic energy (Doyle et al. 2010), lower-tropospheric vorticity (Vukicevic and Raeder 1995), and sea level, terrain, or bottom-level perturbation pressure (Langland et al. 1995, Ancell and Hakim 2007). Each of these functions makes physical sense in that one can imagine how the chosen metric increases or decreases as a modeled cyclone intensifies or weakens. However, these functions are rarely tested for their appropriateness as *response functions* for the purpose of calculating *sensitivity gradients* of cyclone intensity.

In this study, several metrics of cyclone intensity are tested for their appropriateness as response functions by calculating sensitivity of each response function to perturbations of

initial condition vorticity. The vorticity is perturbed based on these sensitivities, and the result is analyzed. A description of the model and case study is provided in section 2. Methodology for testing each response function is given in section 3. Results are described in section 4. Conclusions are provided in section 5.

4.2 Model and Case Study

The Navy Operational Global Atmospheric Prediction System (NOGAPS; Hogan and Rosmond 1991, Rosmond et al. 2002), a global spectral model and its adjoint, at T159 resolution and 30 vertical (sigma-) levels. Model state variables are zonal wind (u), meridional wind (v), temperature (t), specific humidity (sh), vorticity (ζ), divergence (δ), terrain pressure (p_o), and terrain temperature (t_o). Any response function chosen for the calculation of sensitivity gradients must be differentiable with respect to these variables, or to variables derived from these variables.

The basic state is chosen as a 24 or 36 hour simulation of Hurricane Noel (2007) initialized at 0000 UTC 03 November 2007. Noel (2007) is an intensifying TC off the east coast of the United States as it recurves into the midlatitudes, interacting with an upper-level trough to its west and a blocking anticyclone to its east. During this time, the cyclone technically enters extratropical transition (Brown 2007), though as it continues to intensify it maintains a warm core, displaying more of a hybrid TC/extratropical cyclone structure (Fig. 4.1). The varied interactions of this cyclone with the midlatitude synoptic features of its environment as it takes on some characteristics of extratropical cyclones make this an interesting case to consider.

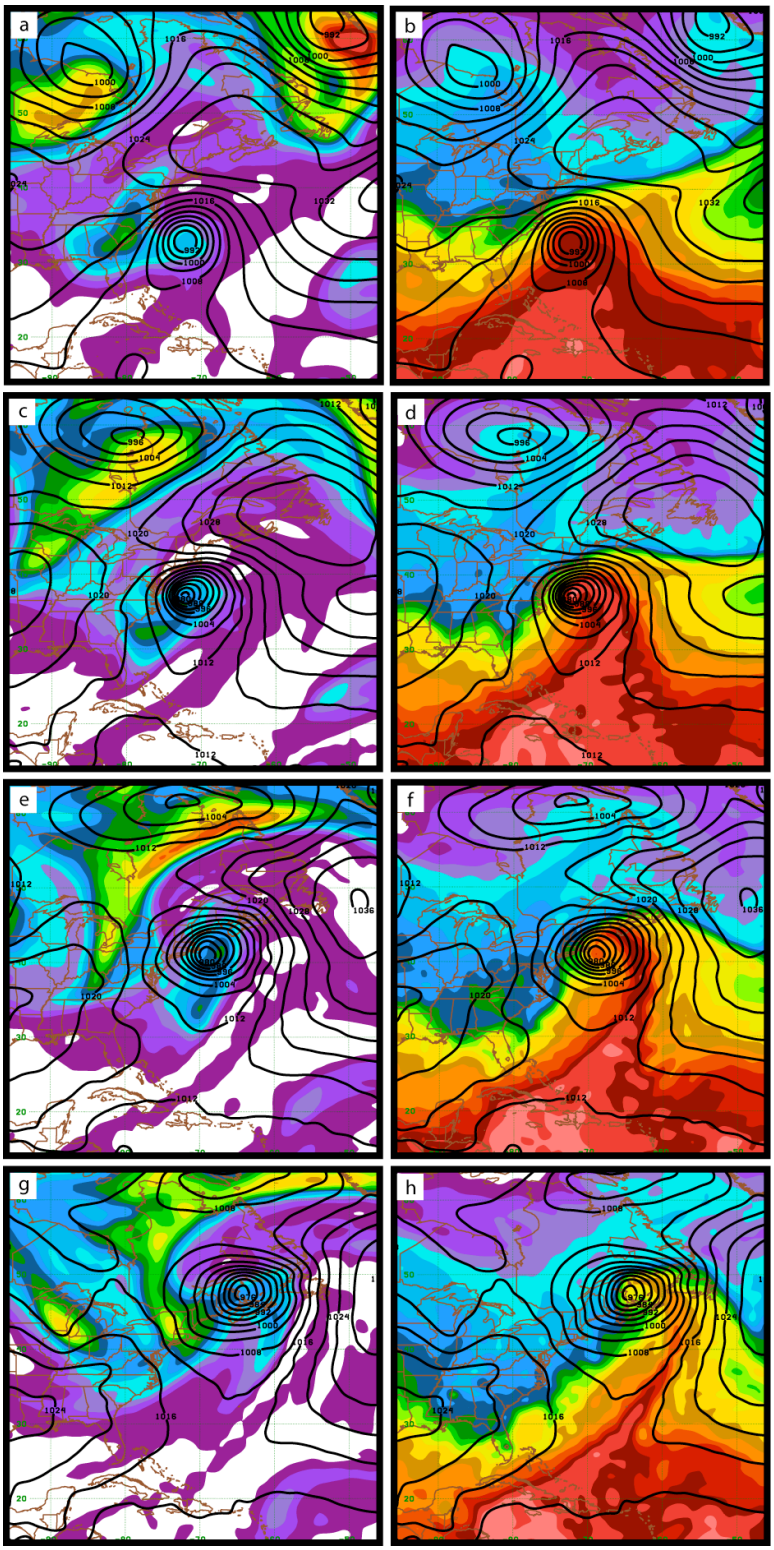

Figure 4.1. Synoptic overview of simulation of TC Noel (2007) initialized at 0000 UTC 03 November 2007. Potential Vorticity (left) between 500-250 hPa shaded every 0.25 PVU and equivalent potential temperature (right) at 900 hPa. Sea level pressure contoured every 4 hPa. Plots valid 0 (a, b), 12 (c, d), 24 (e, f), and 36 hours (g, h) into the simulation.

4.3 Methodology

a) Perturbations

The nonlinear NOGAPS model is run 24 hours to establish a basic-state; the adjoint model is run backward from this point to compute sensitivity gradients of each response function (see below), valid at 24 hours into the simulation, with respect to model initial conditions. The initial condition *vorticity* is perturbed based on these sensitivities:

$$\zeta'_{i,j} = \frac{S\left(\partial R/\partial \zeta\right)}{\partial R/\partial \zeta\big|_{\max}} \qquad (1),$$

With $\partial R/\partial \zeta\big|_{\max}$ representing the maximum absolute value of the sensitivity with respect to vorticity at any point in the model domain, and S representing a scaling factor. For all experiments, $S=2.5x10^{-5}$, such that the maximum vorticity perturbation in the entire model domain has an absolute value equal to S, and all other points have a vorticity perturbation relative to that point based on the magnitude of the sensitivity. Equation 1 creates a vorticity perturbation field with maximum amplitude of S, with positive (negative) perturbations in regions of positive (negative) sensitivity. All perturbations are intended to *increase* the intensity of the cyclone; for any response function that *decreases* in value as the cyclone intensifies (e.g. sea level pressure), $S=-2.5x10^{-5}$.

The model is run 24 hours with the perturbed initial conditions to observe the impact of the perturbations on the cyclone, as well as to calculate the change in the response function relative to a "control" simulation where no perturbation is present. Several questions are considered. First, do the perturbations actually have a *positive* impact on the cyclone's intensity? This will mainly be analyzed with respect to the change in sea-level pressure at 24 hours due to these perturbations. Secondly, what is the impact of these

perturbations on the *response function*? An inappropriate response function may produce sensitivities such that, when the model is perturbed based on those sensitivities, the response function is changed in ways that have little or no impact on the intensity of the cyclone. We wish to determine which of these response functions produces sensitivities that *principally* describe the impact of perturbations on *cyclone intensity*, and not some other process. Some response functions are then tested again with a 36-hour basic state trajectory to observe a longer-timescale result.

b) Response function definitions

Four response functions are used in this study: Low-Level Vorticity (LVR), Low-Level Kinetic Energy (LKE), Subset Kinetic Energy (SKE), and a proxy for Sea Level Pressure (SLP). Each response function is differentiable with respect to model state variables. Response functions are defined within a "response function box" (D) 21°x21° centered on the final-time location of the TC at 24 hours into the model simulation:

$$LKE = \sum_{0.8544-\sigma}^{0.8078-\sigma} \sum_{i,j \in D} \frac{1}{2} u_{i,j}^2 + \frac{1}{2} v_{i,j}^2 \quad (2)$$

$$LVR = \sum_{0.8544-\sigma}^{0.8078-\sigma} \sum_{i,j \in D} \zeta_{i,j} \quad (3)$$

$$SKE = \sum_{0.8544-\sigma}^{0.8078-\sigma} \sum_{i,j \in D} \frac{1}{2} \tilde{u}_{i,j}^2 + \frac{1}{2} \tilde{v}_{i,j}^2 \quad (4)$$

$$SLP = \sum_{i,j \in D} p_o \quad (5),$$

with each response function being defined over all points, indexed zonally by i and meridionally by j, existing in D and between the 0.8544 and 0.8078 sigma levels, roughly centered at 850 hPa. While LKE uses the full wind-field (u,v) to compute kinetic energy, SKE uses only a subset portion of the wind field induced by the vorticity and divergence inside of the response function box ($\tilde{u}$,$\tilde{v}$). These are computed by setting all vorticity and

divergence outside of the response function box to zero and computing the wind field from this subset of vorticity and divergence. Routines exist within the NOGAPS model and its adjoint to do these calculations, as well as the adjoints of these calculations. The subset wind-field is calculated using spherical harmonics.

In addition, one can calculate the change in the response function by computing the function for each of the perturbed and unperturbed model simulations and computing the difference:

$$\Delta R = R\big|_{perturbed} - R\big|_{unperturbed} \qquad (6).$$

This can be compared to the expected change given the limitations of the adjoint model by computing the inner-product of the sensitivity with respect to model initial state and the perturbation to model initial state:

$$\delta R = \left\langle \frac{\partial R}{\partial \zeta}, \zeta' \right\rangle \quad (7),$$

where in our case the product is only done over vorticity. For a model trajectory that is perfectly linear and devoid of moist physics missing in the tangent and adjoint models, $\delta R = \Delta R$. In real application, some amount of discrepancy will exist between these two values due to nonlinear and moisture physics effects in the nonlinear model that are not accounted for in the tangent and adjoint models. This comparison (equations 6 and 7) will be performed to make sure that no systematic errors have been made (e.g. perturbations being calculated incorrectly resulting in the opposite of desired outcomes), and that the case under consideration is (subjectively) determined to operate well enough within the limitations of the adjoint model so as to make its application meaningful.

4.4 Results

a) LKE and SKE perturbations

Perturbations based on LKE sensitivity yields only a 2 hPa deepening of the cyclone by verification time, from 978 hPa to 976 hPa. Despite this, there is a significant increase in kinetic energy in the response function box, a change of 4.54×10^4 m^2 s^{-2}. This appears to be largely due to intensification of the height gradient between Noel and the blocking anticyclone to its east; the intensification of this gradient is due to intensification of the *anticyclone* as much as it is due to intensification of Noel (Fig. 4.2). Perturbations also appear to displace the cyclone slightly to the west; this can allow for regions of high kinetic energy existing outside of the response function box to the east of the cyclone to migrate into the box, increasing the kinetic energy within the box while having no impact on cyclone intensity. The 36-hr trajectory perturbations migrate toward this latter solution, with a large westward displacement of the cyclone, and even a *weakening* of cyclone intensity in the process (not shown). According to (6), the adjoint model predicts a change of $6.80x10^4\ m^2\ s^{-2}$, over-predicting the actual change.

This appears to be a poor response function for TC intensity. Large changes to features other than the TC (e.g. the blocking anticyclone) seem to have a significant or even dominating effect on the response function. In a case such as this, where kinetic energy is strongly biased to one side of the TC, a simple moving of the TC without intensification (or even with *weakening* of the TC) is another unforeseen solution. This problem may be solved by moving the response function box to be centered over the maximum kinetic energy, so that movement of the TC no longer has any impact. However, this would not re-focus the

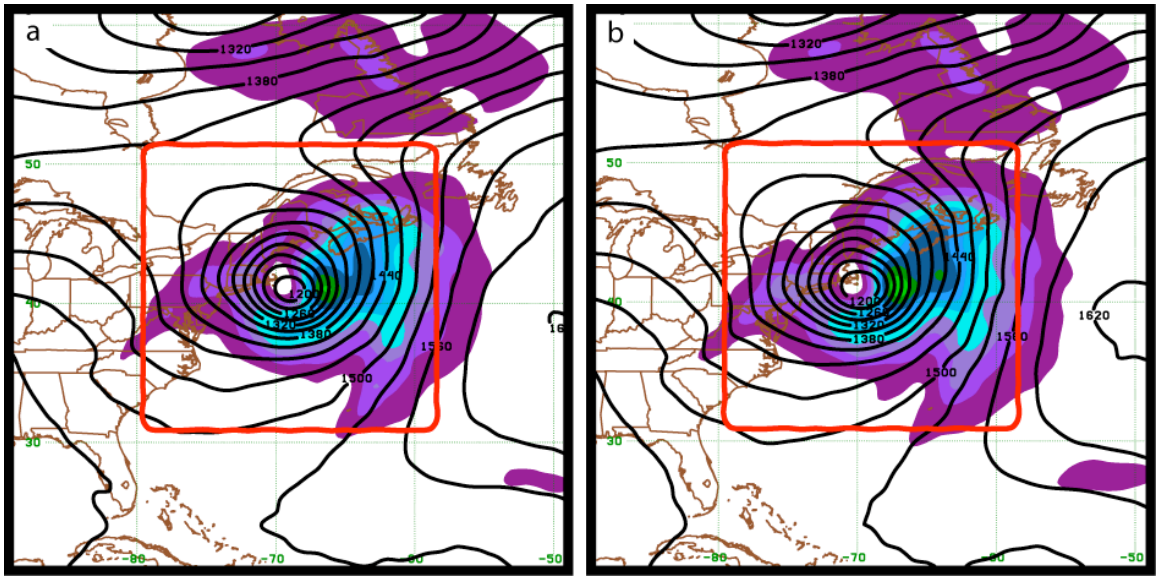

Figure 4.2. Kinetic energy (shaded every 100 m^2 s^{-2}) and geopotential heights (contoured every 30 m) at 850 hPa for unperturbed (a) and LKE perturbed (b) simulations at 24 hours. The red square designates the location of the response function box.

sensitivity away from intensification of the anticyclone and toward the intensification of the cyclone.

However, this problem could be avoided if the response function were redesigned to only include the portion of the wind field that is attributed to vorticity and divergence that exists *within* the response function box. This can be done by applying a simple operator (O) to the vorticity and divergence fields that is equal to 1 at all grid points (i,j) for which $i, j \in D$, and zero otherwise:

$$\tilde{\xi} = \xi \cdot O \quad ; \quad \tilde{\delta} = \delta \cdot O \text{ (8)},$$

where $\tilde{\xi}$ and $\tilde{\delta}$ are the vorticity and divergence (respectively) within the response function box. This operator is self-adjoint, such that:

$$\frac{\partial R}{\partial \tilde{\xi}} \cdot O = \frac{\partial R}{\partial \xi} \quad ; \quad \frac{\partial R}{\partial \tilde{\delta}} \cdot O = \frac{\partial R}{\partial \delta} \text{ (9)}.$$

The subset wind field associated with these portions of the vorticity and divergence fields are calculated with spherical harmonic routines; the adjoint of the routines to compute *vorticity and divergence from zonal and meridional flow* are used to calculate sensitivity with respect to the subset wind field.

When the model is perturbed to increase kinetic energy for this particular portion of the wind field, there appears to be no strengthening of the anticyclone; any intensification that occurs is focused on the TC (another 2 hPa deepening from 977 hPa to 975 hPa), because the anticyclone is largely outside of the response function box, and any change to features outside of the box are ignored when the response function is calculated (Fig. 4.3). However, westward displacement of the cyclone and anticyclone still exists as a solution; as

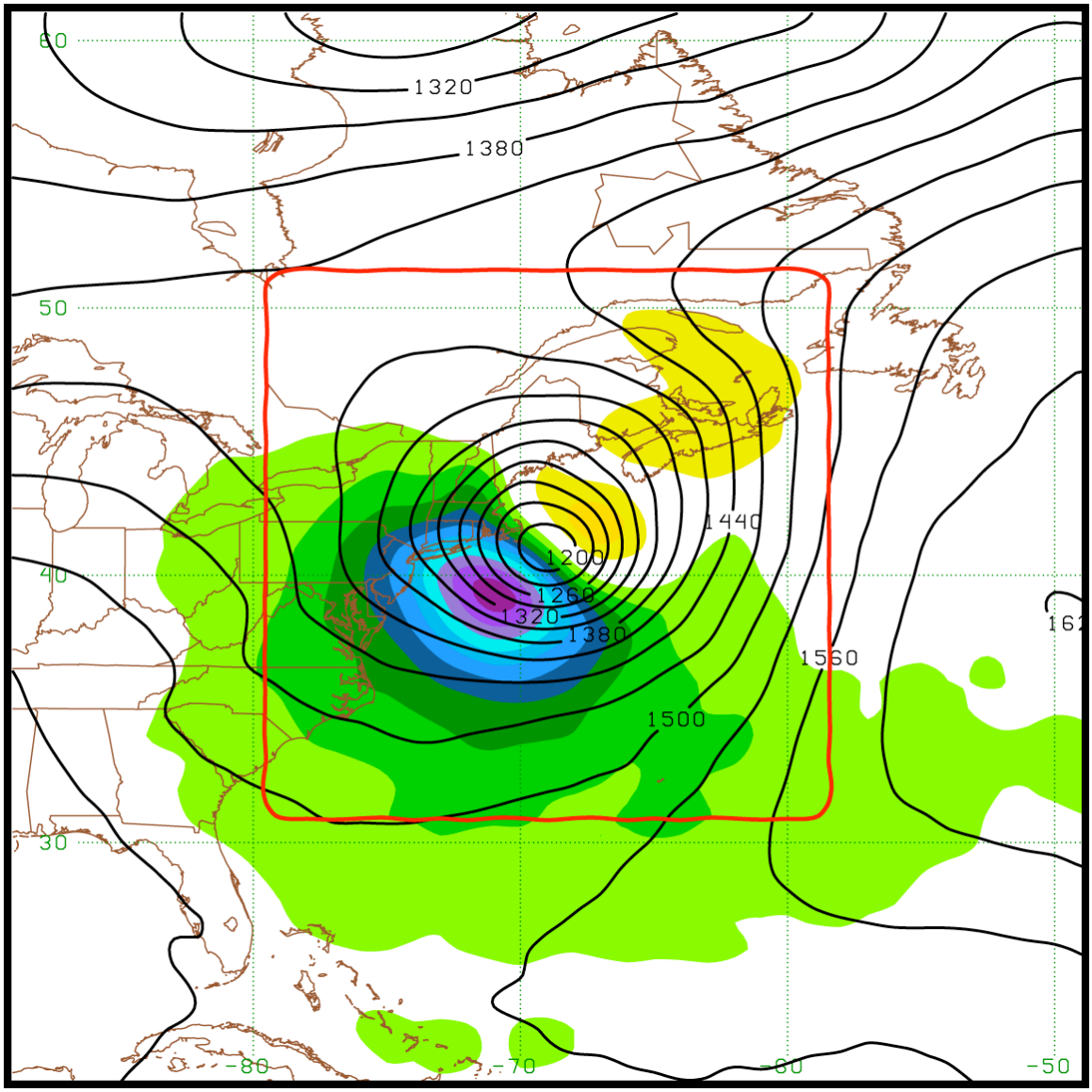

Figure 4.3. Geopotential height difference (SKE perturbed minus unperturbed; shaded every 5 m) and geopotential heights (contoured every 30 m) at 850 hPa for unperturbed simulation at 24 hours. The red square designates the location of the response function box80

.

long as some of the anticyclonic vorticity can be advected into the response function box, the high kinetic energy existing outside of the box can be brought inside and will affect the response function. This is the dominant contribution to the response function for longer (36 hour) time scales (not shown). These perturbations resulted in a change of 3.23×10^4 m^2 s^{-2}, while the adjoint model again over-predicted the impact to be 4.34×10^4 m^2 s^{-2}.

b) LVR perturbations

Perturbations designed to increase low-level vorticity again introduce a roughly 2 hPa deepening of the cyclone; the cyclone track is slightly north and east of the control run (Fig. 4.4b). An increase in vorticity of 7.49×10^{-3} s^{-1} is observed, but again, it appears the core vortex of the TC is largely unchanged. In the control run, the response function box contains the core vortex of the TC along with anticyclonic vorticity around the periphery of the TC and east of the TC, residing in the blocking anticyclone (Fig. 4.4a). The adjoint again over-predicts the change in vorticity to be 1.16×10^{-2} s^{-1}.

Changes to vorticity in the response function box are largely relegated to one of three effects (Fig. 4.4b). First, a dipole of perturbation vorticity oriented southwest/northeast implies a track change to the cyclone; this is of course simply an advection of the TC core and has no impact on the total integrated vorticity. Second, there is increased vorticity northeast of the cyclone due to enhanced frontogenesis at earlier times (Fig. 4.4c,d); this is most likely due to the more northward track the TC takes in the perturbed simulation, allowing for greater interaction with the baroclinic zone along the east coast of the United States. Finally, large amounts of the difference in vorticity between these runs is due to the

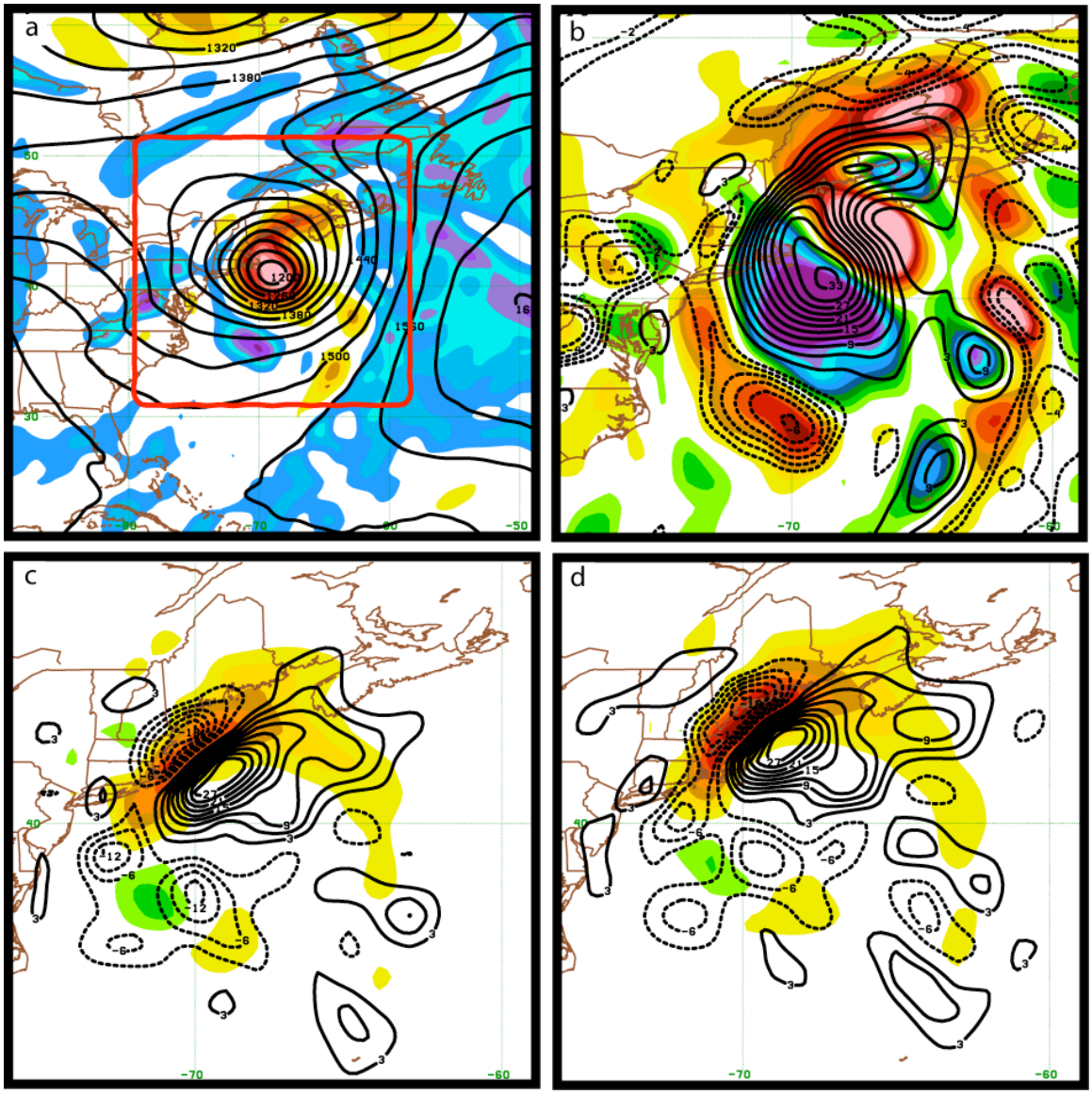

Figure 4.4. (a) Geopotential height (black contours every 30 m) and vorticity (shaded every $1x10^{-5}$ s^{-1} for negative values and every $3x10^{-5}$ s^{-1} for positive values, cool colors negative) at 24 hours and at 850 hPa in the control Noel (2007) simulation. The red box shows the bounds of the response function box. (b) Vorticity of control simulation (black contours every $1x10^{-1}$ s^{-1} for negative (dashed) values and every $3x10^{-5}$ s^{-1} for positive values) and difference between LVR perturbation and control simulations (shaded every $1x10^{-5}$ s^{-1}, cool colors negative) at 24 hours and at 850 hPa. The panel shows the region of the response function box only. (c and d) Frontogenesis at 18 hours and at 850 hPa (shaded every 1 K m^{-1} s^{-1}, cool colors negative), and time rate of change of vorticity (black contours every $3x10^{-9}$ s^{-2}, dashed contours negative) calculated as the difference between vorticity at 21 hours and 15 hours, with advection at 18 hours subtracted for the control (c) and perturbed (d) runs.

elimination of *anticyclonic* vorticity, either through vortex stretching or simply being advected out of the box.

The focus of sensitivity on affecting regions of anticyclonic vorticity rather than the core vortex of the TC may come from several sources. First, advection of the cyclone itself has no effect on the cyclonic vorticity within the box, but the advection of anticyclonic vorticity to regions outside of the box is a positive effect on the response function. Second, column-stretching may be relegated to regions of anticyclonic vorticity simply because stretching requires a divergent secondary circulation which is more easily achieved in regions of low inertial stability, rather than in the high inertially stable region of the core TC vortex. The change in sea level pressure appears to be due to only the portion of vorticity *generated*, such as through increased frontogenesis (which is clearly a process of intensification that is case-dependent), or due to superposition of vorticity as the TC is pushed up against the blocking anticyclone (which has no net effect on vorticity and is thus incidental to the response function under consideration). Again, we find that this response function contains too many processes unrelated to TC intensification to be useful as a response function for TC intensity.

c) SLP perturbations

Perturbations specifically designed to reduce terrain pressure (a suitable proxy for sea level pressure over the ocean) predictably yield the largest change in sea level pressure, a 10 hPa drop from 977 hPa to 967 hPa. The adjoint model appears to slightly under-predict the impact of perturbations, with $\Delta R = -6.99x10^3\ hPa$ and $\delta R = -7.83x10^3\ hPa$. The solution yielded by the model is very similar to the LVR solution, with a northeastward displacement of the cyclone. This makes sense from a purely advective perspective; just as an eastward

displacement of the TC pushes anticyclonic vorticity out of the box, such a displacement also pushes the high surface pressure of the anticyclone out of the box. The added benefit of vorticity superposition as the TC is pushed against the blocking anticyclone, an incidental effect for LVR perturbations since there is no additional vorticity gained through superposition, actually has a positive effect on the SLP response function.

The sensitivity of SLP with respect to vorticity looks much like the sensitivity of LVR with respect to vorticity (reversed in sign) near the cyclone, but SLP sensitivity also has a global pattern roughly centered on the equator (Fig. 4.5). These global patterns represent global-scale waves that can be excited, creating regions of low pressure much larger than the TC. If SLP perturbations are split between those near the cyclone (within a 30^o radius) and those far away (outside of this radius), the perturbations near the cyclone produce an intensification of the cyclone specifically (a 4 hPa drop from 977 to 973, Fig. 4.5c), while those perturbations made to the global-scale wave pattern produce a large region of lowered pressure covering the TC and its surrounding environment (a maximum 6 hPa drop in pressure, Fig. 4.5d). As an ad-hoc measure of linearity, one can show that the 10 hPa drop in minimum sea level pressure from the entire SLP perturbation appears to be entirely separated into a 4 hPa drop from perturbations within 30^o of the cyclone and a 6 hPa drop from perturbations outside of this radius.

4.5 Conclusions

A simple survey of several response functions typically used to define TC intensity shows that there are many issues present regarding their appropriateness. Response functions based on low level kinetic energy and vorticity are too easily affected by changes to the TC's environment that have nothing to do with TC intensification, and while some of these issues

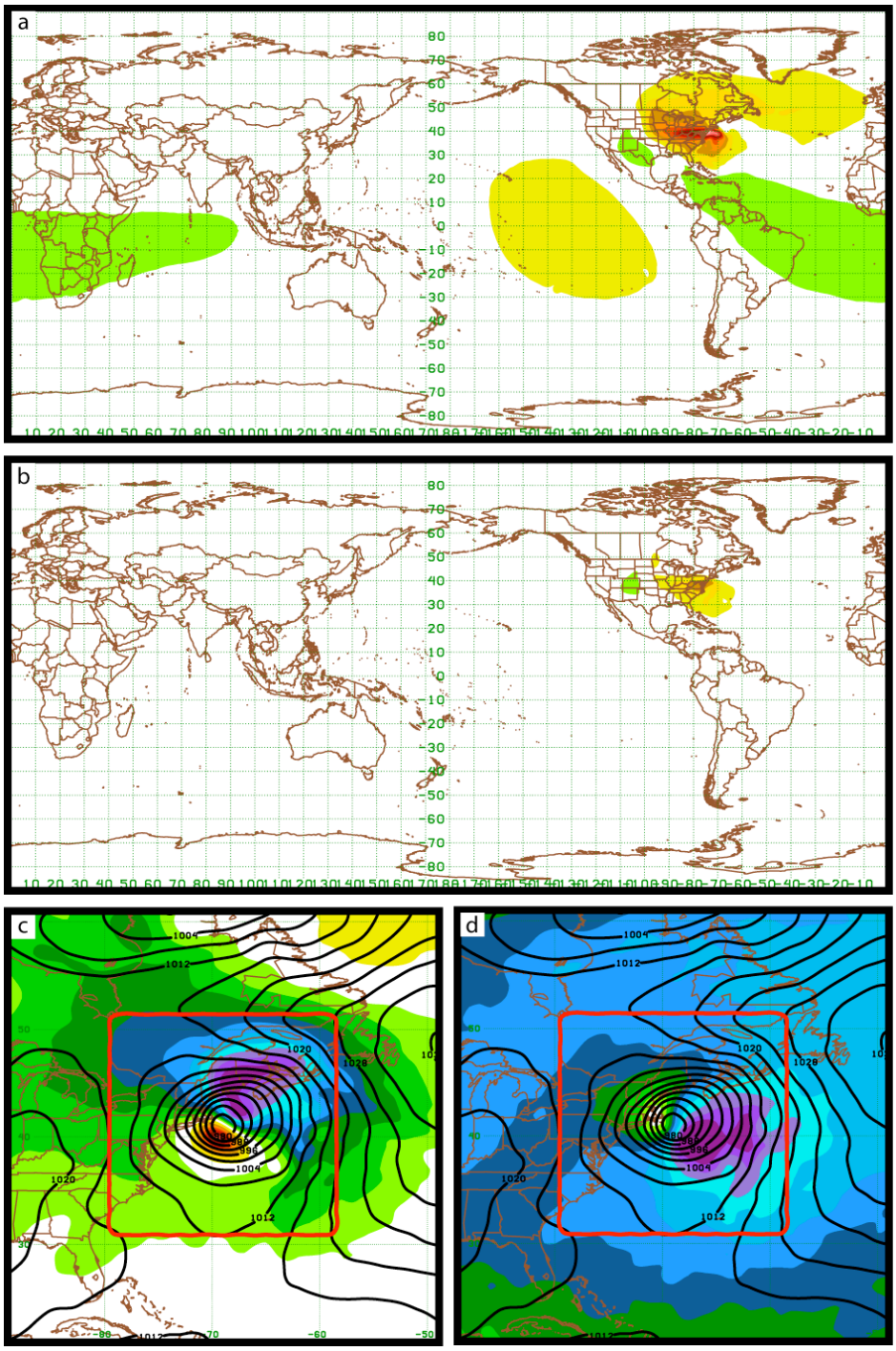

Figure 4.5. Sensitivity of SLP (a) and LVR (b) with respect to vorticity at initialization and at the 0.4718-sigma level, roughly corresponding to 500 hPa. Shading is every (a) $1x10^4$ hPa s (cool colors negative, sign reversed) and (b) 0.1 s s^{-1} (cool colors negative). Sea level pressure at 24 hours of control simulation (black contours every 4 hPa), and perturbation sea level pressure (shaded every 1 hPa, cool colors negative) for SLP perturbations (c) within 30-degree radius of cyclone, and (d) outside of 30-degree radius of cyclone.

can be circumvented by a more careful choice of how the response function is defined (such as using a subset of the wind field instead of the entire wind field to perform a kinetic energy calculation), oftentimes sensitivities represent little more than sensitivity to small changes to the geometry of the TC's location relative to other environmental features rather than to TC intensity itself.

Of all four response functions tested, the sea level pressure response function appears to be the most appropriate. Not only can the sea level pressure be affected by methods of intensification such as column stretching, which also affects vorticity, but the sea level pressure is also sensitive to the effect of vorticity superposition; this is a simple advection method of intensification that is invisible to a vorticity response function, since it does not create *more* vorticity but instead makes the cyclonic vorticity that is present more efficient by pushing it into a smaller space.

One must still be careful with how this response function is used; advection of high-pressure regions out of the response function box is still an affect that can change the response function without changing the intensity of the cyclone, and global models find sensitivity to global-scale wave patterns that may not be physically realistic. However, it appears to be easy to delineate between the global-scale pattern and sensitivity to regions within the TC's environment, and these global-scale patterns would not be present in a regional grid-point model. Keeping these concerns in consideration, we can move forward into dynamical sensitivity analysis of TC intensity and genesis knowing that the response function chosen has been tested for its appropriateness.

Chapter 5: Identifying Barotropic Growth Signatures in East Pacific Tropical Cyclogenesis with Adjoint-Derived Sensitivities

Abstract

The existence of a low-level westerly jet in the tropical eastern Pacific provides the potential for barotropic growth of vortices that could develop into tropical cyclones. Studies have shown that the number of cyclones formed in the eastern Pacific basin can fluctuate with the strength of this jet, but also that this barotropic growth mechanism is not necessary for cyclogenesis. Analysis of the hypothetical potential for tropical cyclogenesis using numerical weather prediction models by means of perturbing the initial conditions to observe the result typically suffer from arbitrariness; there is no guarantee that perturbations added to the model initial conditions will favorably interact with the low-level jet to facilitate cyclogenesis unless a priori information about the development of the cyclone is provided.

By defining a response function for the sea level pressure in the region of a modeled tropical vortex, one can calculate sensitivity gradients of the intensity of the developing tropical storm to perturbations of the model initial conditions. These gradients can then be used to provide the necessary a priori information about the location and characteristics of perturbations that have the largest impact on the developing cyclone. In this study, sensitivity gradients are calculated for 24 cases from 2008 and 2009 to determine which cases have sensitivities describing structures that can grow barotropically from the low-level jet, and two cases are run at high resolution to observe the impact of perturbations derived from these sensitivities.

5.1 Introduction

Sensible weather in the eastern Pacific is influenced by the existence of a low-level (surface to 850 hPa) westerly jet centered around 5^{o}N (Poveda and Mesa 2000); this near-surface jet feature in the deep tropics of the western Pacific is manifest as a zonally elongated region of enhanced westerly flow with a meridional reversal of the potential vorticity (PV) gradient across the jet. This presents the possibility for the growth of tropical disturbances into tropical cyclones (TCs) through barotropic energy conversion of shear to eddy kinetic energy on the cyclonic shear side of the jet (Guinn and Schubert 1993, Ferreira and Schubert 1997, Maloney and Hartmann 2001, Hartmann and Maloney 2001), though it has been shown to not be a necessary condition for eastern Pacific TCs to develop (Davis et al. 2008).

Significant questions remain unanswered regarding the role of barotropic energy conversion in the genesis of TCs in this region, such as the overall importance of this process compared to other mechanisms (air-sea interaction, baroclinic growth, etc.) for individual TCs and optimal environmental conditions for this process to function. Furthermore, while success in TC genesis and intensity prediction in numerical weather prediction (NWP) models has lagged significantly behind other aspects of TC prediction such as track (DeMaria and Gross 2003), some TCs have been predictable with high accuracy several days in advance; it is possible that the predictability of these TCs is due to synoptic features of their environment that are well defined by NWP models (Davis et al. 2008). The relative importance of barotropic growth processes may be a feature that helps delineate between more predictable and less predictable TCs.

Given a function of model-state output (a "response function"), one can employ the adjoint of a linearized NWP model to produce sensitivity of that function with respect to

small perturbations to the model-state at earlier times (Errico 1997), or to derived variables of the model state (Kleist and Morgan 2005). These sensitivity gradients provide insight into the dynamics of a modeled atmosphere that are otherwise difficult or impossible to obtain. A more traditional approach of making changes to the initial conditions of a model and comparing the resulting forecast to a "control" run where the initial conditions are undisturbed is sometimes characterized as a more robust "sensitivity study" by including several perturbations in an attempt to make the results seem less anecdotal. The advantage of an adjoint model is that the sensitivity gradients provide the necessary *a priori* information about the impact a perturbation of a particular variable in a particular geographic region would have on the chosen response function. The costly and ultimately still arbitrary technique of perturbing the initial conditions in several different ways is avoided, and instead the sensitivity gradients can be used to define perturbations that will have an impact on a *specific aspect* of the forecast (Errico 1997, Blessing et al. 2008).

Adjoint models have been used in the past to investigate sensitivity of sea-level pressure (Langland et al. 1995) or low-level vorticity (Vukicevik and Raeder 1995) in midlatitude cyclones to infer the importance of various synoptic scale features of the cyclone's environment to the intensity of that cyclone. Application of adjoint models to TC development has largely been restricted to sensitivity of TC steering (Peng and Reynolds 2006, Wu et al. 2007, Wu et al. 2009, Chen et al. 2009, Hoover and Morgan 2010); this is at least partially due to the constraints of linearity and simplified moisture physics that limit the applicability of adjoint models to tropical dynamics.

In this study the adjoint of a NWP model is employed to investigate the importance of barotropic growth to east Pacific TC genesis along the low-level westerly jet. The

identification of a "signature" in the adjoint-derived sensitivities that indicates the importance of barotropic growth of vorticity at the expense of the background shear is sought. As this analysis is primarily concerned with the *potential impact* of small perturbations with respect to the synoptic-scale, dry dynamics of this possible genesis mechanism, an adjoint model is uniquely suited to this task. A description of the model used is provided in section 2. Section 3 provides a description of the methodology used. Results of the analysis are described in section 4, and conclusions and directions for future research are given in section 5.

5.2 Model

The PSU/NCAR Mesoscale Modeling System (MM5) Version 2 and its adjoint (Zou et al. 1998) are used. The MM5 model is a non-hydrostatic, limited area, primitive equation model which uses as its vertical coordinate a terrain following sigma coordinate. For all sensitivity calculations performed, the nonlinear version of MM5 is used to create a basic state about which the tangent linear model (TLM) and adjoint model are linearized. For the TLM and adjoint integrations, the basic state is updated every time step. The model is run with the Grell cumulus convection scheme. Model simulations run at 30 km grid spacing use a 90 s time step and are initialized with NCEP 1^{o}x1^{o} final reanalysis data (ds083.2)[6], while model simulations run at 12 km grid spacing use a 36 s time step and are initialized with GFS 0.5^{o}x0.5^{o} analysis fields from the Historical Unidata Internet Data Distribution Gridded Model Data archive (ds335.0)[7].

---

[6] The data for this study are from the Research Data Archive (RDA) which is maintained by the Computational and Information Systems Laboratory (CISL) at the National Center for Atmospheric Research (NCAR). NCAR is sponsored by the National Science Foundation (NSF). The original data are available from the RDA (http://dss.ucar.edu) in dataset number ds083.2.

[7] The original data are available from the RDA (http://dss.ucar.edu) in dataset number ds335.0.

5.3 Methodology

The analysis is composed of two parts: (I) a set of 24 simulations of east Pacific tropical vortices in the 24 hours leading up to declaration as a tropical storm, and (II) an in-depth analysis of two cases run at higher resolution. Simulations in part (I) are run at 30 km grid resolution. Simulations in part (II) are run at 12 km grid resolution.

a) Part I: 30 km simulations

Model runs of 24 east Pacific TCs from 2008 and 2009 produce 24-hr simulations composed of the 24 hours before the TC is declared as a tropical storm (Table 5.1). The response function is defined as negative perturbation pressure at the lowest sigma level in a 600 km box centered on the minimum sea level pressure of the modeled cyclone at the end of the model run (24 hrs). The adjoint model then runs backward 24 hours to produce sensitivities of this response function to small perturbations of the basic state at model initialization. These "sensitivity gradients" describe how a small perturbation to the initialization will impact the response function. In this case, the sensitivities represent how small perturbations impact the intensity of the developing tropical storm; since the response function is defined as *negative* perturbation pressure, it can be inferred that a positive (negative) perturbation in a region of positive (negative) sensitivity will result in an intensification of the cyclone. A perturbation of the opposite sign in that location will result in a weakening of the cyclone.

A barotropic growth "signature" in the sensitivities is defined in the sensitivity with respect to zonal flow as a structure that tilts upshear with respect to the jet into the core of the low-level jet on either side (Fig. 5.1; see Langland 1995, Farrell and Moore 1992). Zonal perturbations with this tilted structure have the capacity to extract energy from the shear of

Name (year)	Simulation Begins	Simulation Ends
Alma (2008)	0000 UTC 28 May	0000 UTC 29 May
Boris (2008)	1200 UTC 25 June	1200 UTC 26 June
Douglas (2008)	1200 UTC 01 July	1200 UTC 02 July
Elida (2008)	0600 UTC 11 July	0600 UTC 12 July
Fausto (2008)	1200 UTC 15 July	1200 UTC 16 July
Genevieve (2008)	1800 UTC 20 July	1800 UTC 21 July
Hernan (2008)	0000 UTC 06 August	0000 UTC 07 August
Julio (2008)	1800 UTC 22 August	1800 UTC 23 August
Lowell (2008)	0000 UTC 06 September	0000 UTC 07 September
Marie (2008)	1200 UTC 30 September	1200 UTC 01 October
Norbert (2008)	0000 UTC 04 October	0000 UTC 05 October
Odile (2008)	0600 UTC 08 October	0600 UTC 09 October
Polo (2008)	0000 UTC 02 November	0000 UTC 03 November
Andreas (2009)	0000 UTC 21 June	0000 UTC 22 June
Dolores (2009)	1200 UTC 14 July	1200 UTC 15 July
Lana (2009)	1800 UTC 29 July	1800 UTC 30 July
Enrique (2009)	0000 UTC 03 August	0000 UTC 04 August
Felicia (2009)	0600 UTC 03 August	0600 UTC 04 August
Guillermo (2009)	0000 UTC 12 August	0000 UTC 13 August
Jimena (2009)	0000 UTC 28 August	0000 UTC 29 August
Linda (2009)	1800 UTC 06 September	1800 UTC 07 September
Nora (2009)	0600 UTC 22 September	0600 UTC 23 September
Patricia (2009)	0000 UTC 11 October	0000 UTC 12 October
Rick (2009)	0000 UTC 15 October	0000 UTC 16 October

Primary Barotropic Sig.	Secondary Barotropic Sig.	No Barotropic Sig.
Alma (2008)	Douglas (2008)	Elida (2008)
Boris (2008)	Marie (2008)	Genevieve (2008)
Fausto (2008)	Andreas (2009)	Julio (2008)
Hernan (2008)	Dolores (2009)	Odile (2008)
Lowell (2008)	Rick (2009)	Guillermo (2009)
Norbert (2008)		Jimena (2009)
Polo (2008)		Linda (2009)
Lana (2009)		Patricia (2009)
Enrique (2009)		
Felicia (2009)		
Nora (2009)		

Table 5.1. (Top): Beginning and ending times of 24-hour simulations for 24 east Pacific tropical cyclones from 2008 and 2009. (Bottom): Cases binned into "Primary Barotropic Signature" (PBS), "Secondary Barotropic Signature" (SBS), and "No Barotropic Signature" (NBS) based on low-level sensitivity to zonal flow.

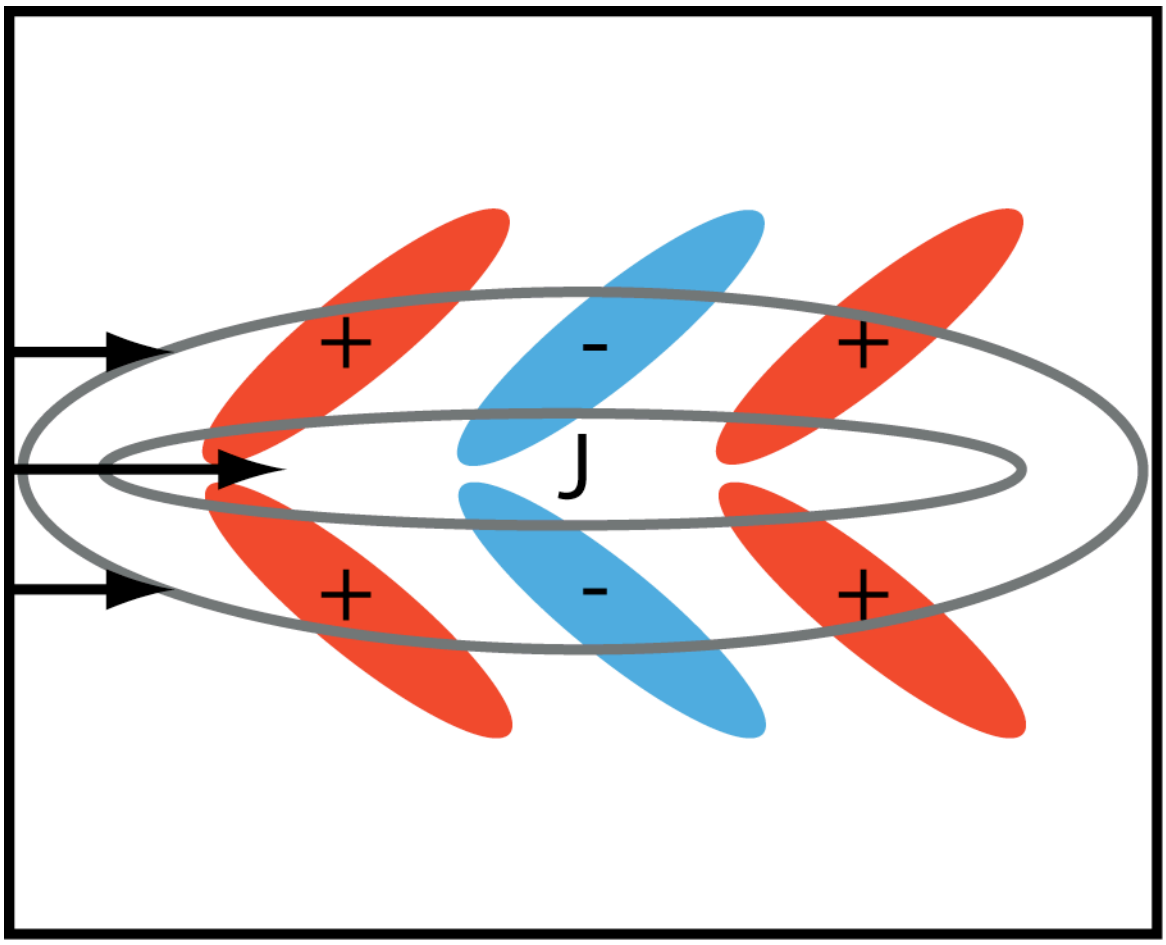

Figure 5.1. Conceptual diagram of barotropic signature in zonal wind sensitivities around a zonal jet. Gray lines are isotachs, with a "J" indicating the jet core. Vectors indicate relatively stronger zonal flow within the jet core. Sensitivity with respect to zonal flow is indicated with shaded regions representing areas of positive (red) and negative (blue) sensitivity.

their environment and grow over time. The structure of sensitivities with respect to low-level zonal flow is analyzed for each of the 24 cases in order to bin the cases into one of three categories (see section 4).

b) Part II: High-resolution perturbation experiments

The second part of the analysis is based on simulations of two TCs at 12 km grid resolution – a TC exhibiting a strong barotropic signature (Alma (2008)), and another that has no barotropic signature (Linda (2009)). Calculated sensitivities are used to define perturbations to the initial conditions of both simulations, and these perturbations are observed as they evolve in the model simulation. These simulations are run for 48 hours – the original 24 hours up to declaration as a tropical storm (when the response function is defined) as well as 24 hours after this point. This is done in order to determine if the perturbations added to the initial conditions remain favorable to the development of the cyclone for times after the response function is defined.

Since the response function is defined to represent the intensity of the developing vortex at forecast hour 24 *specifically*, the sensitivities of this response function are not representative of the effect perturbations would have on the TC at later times; in fact, it is possible that perturbations defined to increase the intensity of the TC at forecast hour 24 actually *weaken* the storm at later times. Therefore we wish to make a careful examination of how perturbations impact the intensity of the cyclone not only at forecast hour 24, but for the next 24 hours as well.

5.4 Results

a) 2008-2009 24-case analysis

1) DELINEATION OF COMPOSITE CATEGORIES

Based on subjective visual inspection of sensitivity to zonal flow at low levels cyclones were binned into one of three categories. Cyclones were classified as having a "primary barotropic signature" (PBS) if sensitivities were characterized by upshear-tilted regions of alternating sign (Fig. 5.1). Cyclones were classified as having a "secondary barotropic signature" (SBS) if an upshear-tilted structure was evident but was not the dominant structure of the sensitivities. Finally, if there was no evident sign of a barotropic growth signature in the sensitivities the cyclone was classified as having "no barotropic signature" (NBS). Of the 24 cases, 11 were classified as PBS, 5 as SBS, and 8 as NBS (see Table 5.1).

2) SENSITIVITY COMPOSITES

i) Sensitivity to zonal and meridional flow

Storm-centered composites of low-level (0.9250-sigma) zonal flow and sensitivity to zonal and meridional flow reveal large differences between each composite group with respect to the low-level jet (Fig. 5.2). The jet in the PBS composite (Fig. 5.2a,b) is zonally elongated but much more meridionally restricted than in either of the other two composites. Sensitivities with respect to zonal flow (Fig. 5.2a) are by design characterized by upshear-tilted features on either side of the jet, though positive (negative) sensitivity appears to be more dominant on the southern (northern) side of the jet core. This may be a combined effect of two structures in the sensitivity field – the upshear-tilted barotropic structure along with a general structure that indicates increased vorticity, which would be manifest as positive zonal flow to the south and negative zonal flow to the north, would be favorable for the development of the cyclone. Likewise, the sensitivity with respect to meridional flow

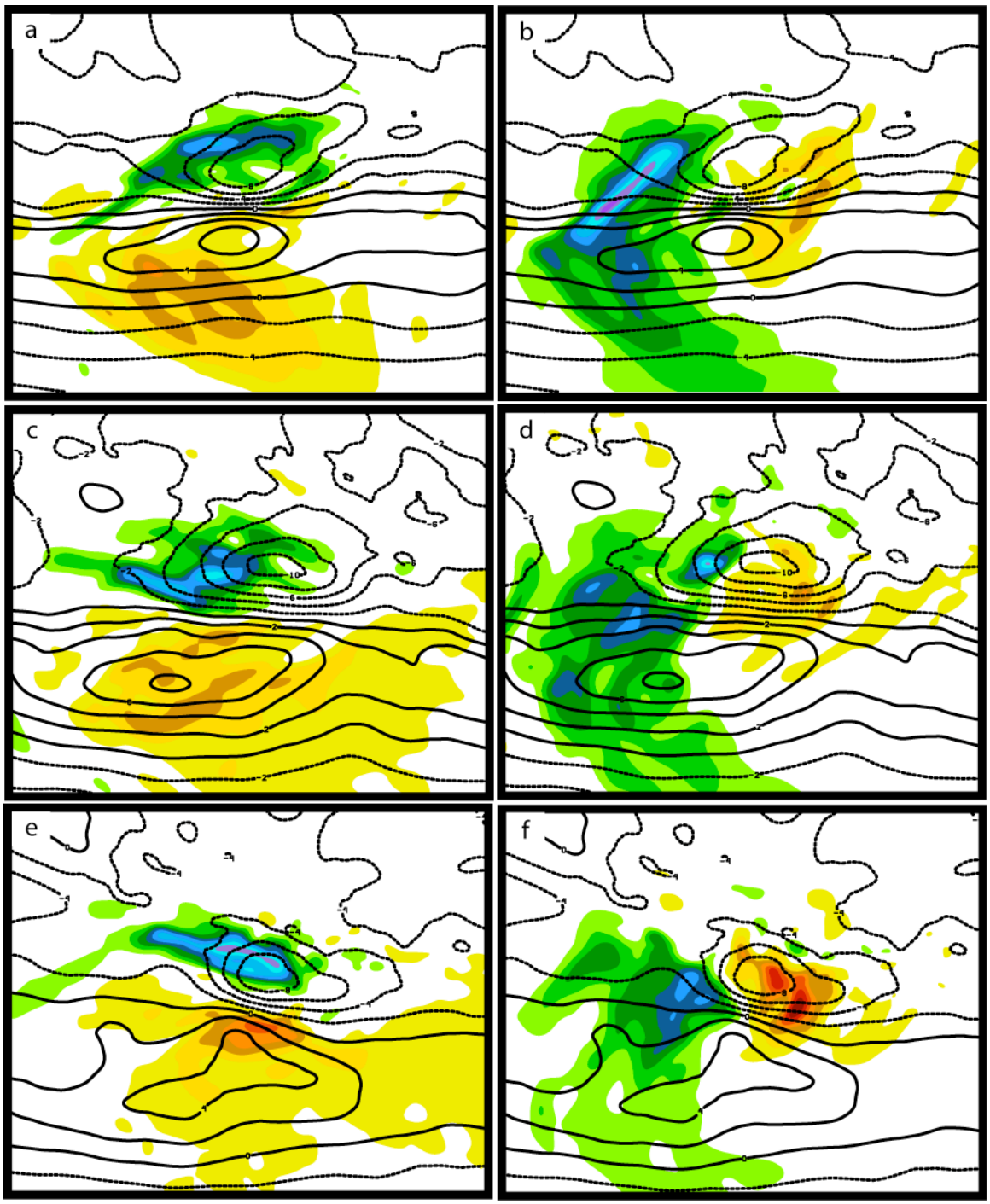

Figure 5.2. Zonal flow at the 0.9250 sigma level (black contours every 2 ms^{-1}, dashed contours negative) and sensitivity with respect to zonal flow (panels a, c, e) and sensitivity with respect to meridional flow (panels b, d, f) shaded every 0.1 Pa sm^{-1}. Warm (cool) colors indicate positive (negative) values. Panels (a) and (b) correspond to the PBS composite; panels (c) and (d) correspond to the SBS composite, and panels (e) and (f) correspond to the NBS composite.

(Fig. 5.2b) represents the superposition of an implied barotropic growth structure and a general structure that again indicates genesis is promoted by increasing vorticity in the core of the developing tropical storm.

Interestingly, despite the fact that the barotropic growth signature is strongest in the PBS composite, the most powerful westerly jet exists in the SBS composite (Fig. 5.2c,d). There is nearly no upshear-tilted structure at all in the sensitivity with respect to zonal flow (Fig. 5.2c). While the jet is stronger in this composite than in the PBS composite, it also has a much larger meridional extent; this may be an indication that simply observing a strong westerly jet is not sufficient to conclude that the potential for barotropic growth exists, and that the meridional extent of the jet must also be taken into account. The NBS composite (Fig. 5.2e,f) has the weakest and most meridionally elongated jet structure. No structure exists in the sensitivity with respect to either component of the wind except a general favorability of increased vorticity.

While it should be noted that the existence (or lack thereof) of barotropic growth signatures in these composite sensitivities is not unexpected, as this is precisely the criteria upon which each case's categorization depends, the relationship of these sensitivity structures to the characteristics of the westerly jet is striking. This analysis indicates that the *potential* for a TC to grow through barotropic conversion of energy is highly dependent upon not only the strength of the jet, but also its meridional. Therefore a simple metric based entirely on the strength of the jet would be insufficient to determine if a tropical depression has the potential to grow using this mechanism. Since barotropic conversion of energy requires significant shear in the background, a strong and meridionally restricted jet being found in

the PBS composite is consistent with the interpretation of sensitivities as describing barotropic growth from the low level jet.

ii) Sensitivity to temperature, vertical motion, and divergence

A high degree of anti-correlation exists between sensitivity with respect to temperature and with respect to vertical motion throughout the lower troposphere (Fig. 5.3). Sensitivities at low levels in both fields express the same upshear-tilted structure as was found in sensitivity with respect to both components of the wind field (Fig. 5.2), which may hint at some notion of balance within the sensitivity gradients. The strong anti-correlation between these two fields is related to the effect of adiabatic expansion and compression on the temperature field; sensitivity with respect to upward (downward) motion is found in regions of negative (positive) sensitivity with respect to temperature, because such motion promotes adiabatic cooling (warming). This relationship is clearly visible in a cross section (Fig. 5.3c,d), where positive sensitivity with respect to temperature through the core of the vortex is coincident with negative sensitivity with respect to vertical motion.

While this relationship is simple and relatable to adiabatic expansion and compression, it creates a problem when a attempting a dynamical analysis of sensitivity. While sensitivities do not usually speak to what may *cause* a perturbation to appear in a region of high sensitivity (Langland et al. 1995), vertical motion sensitivities are so well anti-correlated to temperature sensitivities that a clear cause-and-effect relationship can be established; the sensitivities with respect to vertical motion look this way precisely because such motion will cause a change in temperature. The adjoint model, being devoid of moisture physics that are necessary for the genesis of TCs, is ‘unaware’ that subsidence through the core of the tropical vortex would be quite detrimental to the future development

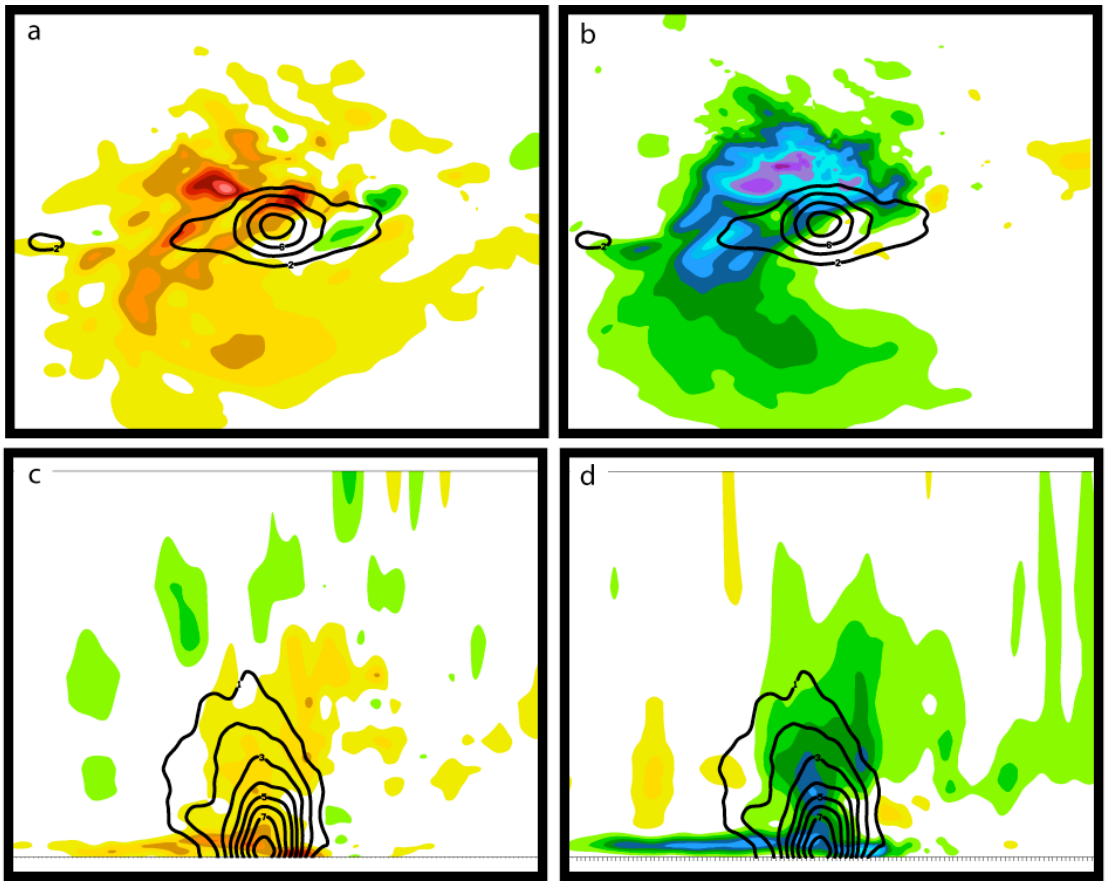

Figure 5.3. Vorticity (black contours every $2x10^{-5}$ s^{-1}) and sensitivity to temperature (panels a, c; shaded every 0.1 Pa K^{-1}, cool colors negative) and sensitivity to vertical motion (panels b, d; shaded every $2x10^{-2}$ Pa s m^{-1}, cool colors negative) for the 0.9250-sigma level (panels a, b) and a southwest to northeast cross-section through the center (panels c, d). Fields are calculated as storm-centered composites of all 24 cases valid at model initialization.

of the vortex. While one might otherwise expect that these sensitivities would show that warming the core of the vortex and increasing upward vertical motion would be beneficial for future development, they reveal a realistic sensitivity pattern with respect to temperature, but an unrealistic sensitivity with respect to vertical motion that is directly related to the temperature sensitivity. One may therefore assume that the sensitivity with respect to temperature is realistic, while the sensitivity with respect to vertical motion, being based entirely on a dry-physics, adiabatic relationship between temperature and vertical motion, is not realistic.

However, the infiltration of unrealistic sensitivities does not stop here; another direct cause-and-effect relationship allows the unrealistic sensitivity to vertical motion to extend its influence into sensitivity to the horizontal wind field. Mass-continuity dictates that subsidence must be accompanied by convergence aloft and divergence beneath. Just as sensitivity to subsidence appears because of its relationship to heating, sensitivity to divergence appears at low levels because of its relationship to subsidence (Fig. 5.4). This implies that the divergent portion of the sensitivity to the horizontal wind field is questionable; while this is clearly a small contribution to the total horizontal wind sensitivity when compared to the non-divergent portion (typically an order of magnitude smaller), this must be taken into consideration when perturbing the model (see below).

3) OPTIMAL PERTURBATIONS

i) Definition of optimal perturbations

Given sensitivity information about a response function of interest, one can construct perturbations designed to change that response function by a specified amount, optimized subject to a chosen constraint (Errico 1997, Blessing et al. 2008). We wish to construct

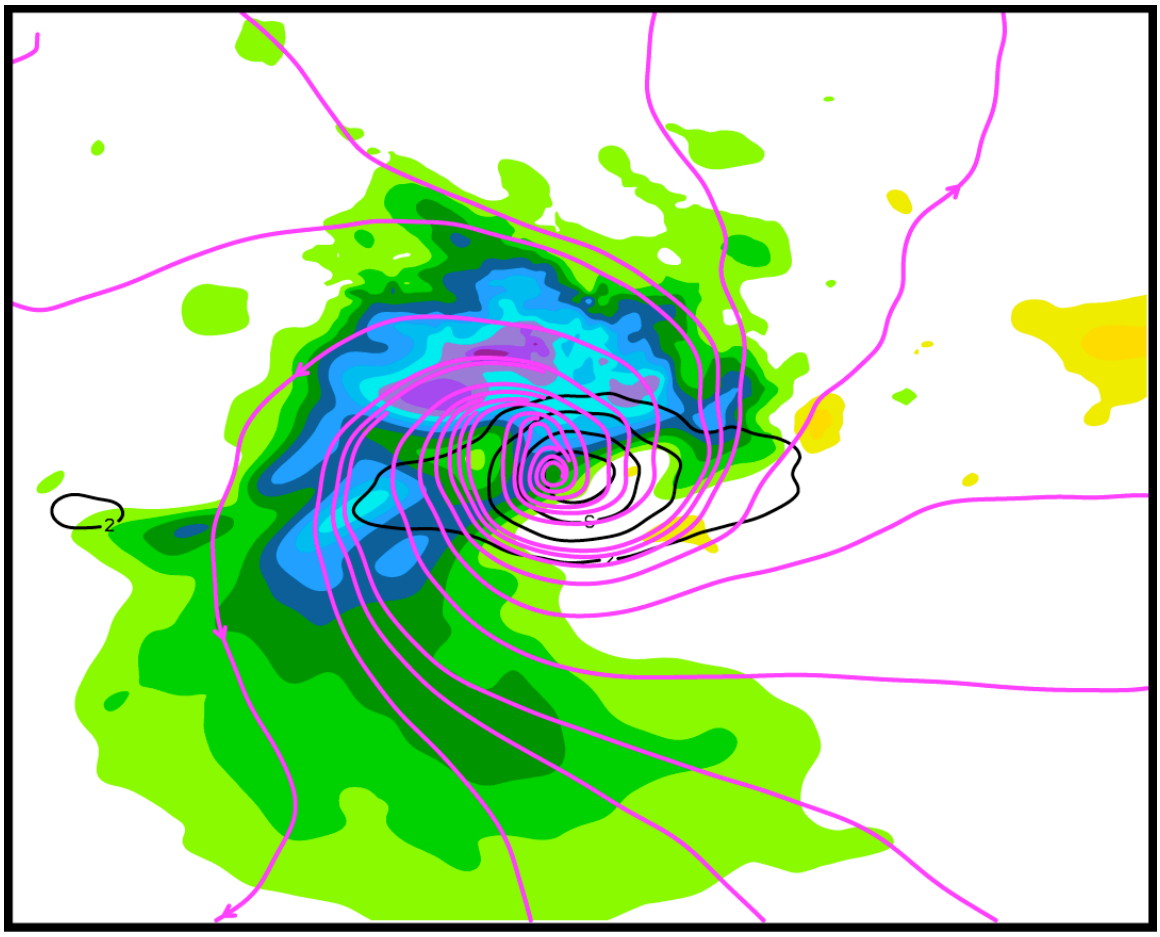

Figure 5.4. Vorticity (black contours every $2x10^{-5}$ s^{-1}), sensitivity with respect to vertical motion (shaded every $2x10^{-2}$ Pa s m^{-1}, cool colors negative), and streamlines of vectorization of sensitivity with respect to zonal and meridional wind. Vorticity and sensitivity with respect to vertical motion are at the 0.9250 sigma level. Streamlines are at the 0.9750 sigma level.

perturbations to the initial conditions subject to the constraint that these perturbations minimize a kinetic and available potential energy norm:

$$\varepsilon = \left(\frac{u'_{nd}{}^2 + v'_{nd}{}^2}{2} \right) + \left(\frac{g^2}{2\overline{N}^2 \overline{T}^2} T'^2 \right) \qquad (1),$$

where the first term represents the kinetic energy added to the system, and the second represents the available potential energy. Here, $\overline{N}^2$ is the Brunt-Vaisala frequency (calculated between every 2-sigma-level slab and averaged between slabs to approximate values on sigma levels; top and bottom slabs are directly assigned to top and bottom sigma levels), and $\overline{T}^2$ is the square of the temperature in the basic state. This energy norm constraint is based on the "approximate energy norm" used to calculate singular vectors using the MM5 adjoint model (Zou et al. 1997), with several changes. First, there is no "elastic energy" term (pressure will not be perturbed). In addition, two changes have been made to the kinetic energy term. Vertical motion is not perturbed, and so does not appear in the constraint; this is due to the unrealistic nature of vertical motion sensitivity discussed earlier. Secondly, perturbations to horizontal components of the flow $\left(u'_{nd}, v'_{nd}\right)$, are non-divergent. This again is due to the influence of unrealistic vertical motion sensitivities on the divergent component of the sensitivities to horizontal flow.

Given this constraint (1), we can seek to impose perturbations that will change the response function by ΔR while minimizing $\varepsilon = \frac{1}{2}\left\langle \mathbf{x}'_0, \mathbf{W}\Delta\mathbf{x}'_0 \right\rangle$, where $\mathbf{W}$ is a diagonal matrix of scaling factors reducing *u'* and *v'* to kinetic energy and *T'* to available potential energy. Sensitivity gradients provide information on how perturbations will impact the response

function: $\Delta R \cong R' = \left\langle \frac{\partial R}{\partial \mathbf{x}_0}, \mathbf{x}_0' \right\rangle$. This can be solved using a Lagrange multiplier with the Lagrangian (L) given by:

$$L = \varepsilon + \lambda\left(\Delta R - \left\langle \frac{\partial R}{\partial \mathbf{x}_0}, \mathbf{x}_0' \right\rangle\right) = \frac{1}{2}\langle \mathbf{x}_0', \mathbf{W}\mathbf{x}_0' \rangle + \lambda\left(\Delta R - \left\langle \frac{\partial R}{\partial \mathbf{x}_0}, \mathbf{x}_0' \right\rangle\right) \qquad (2).$$

Differentiation of L with respect to the Lagrange multiplier (λ) yields the constraint:

$$\Delta R = \left\langle \frac{\partial R}{\partial \mathbf{x}_0}, \mathbf{x}_0' \right\rangle = \lambda \frac{\partial R}{\partial \mathbf{x}_0} \mathbf{W}^{-1} \frac{\partial R}{\partial \mathbf{x}_0} \qquad (3),$$

or:

$$\lambda = \frac{\Delta R}{\left\langle \frac{\partial R}{\partial \mathbf{x}_0}, \mathbf{W}^{-1} \frac{\partial R}{\partial \mathbf{x}_0} \right\rangle} \qquad (4).$$

Optimal perturbations are yielded by differentiation of L with respect to $\mathbf{x}_0'$:

$$\frac{\partial L}{\partial \mathbf{x}_0'} = \mathbf{W}\mathbf{x}_0' - \lambda \frac{\partial R}{\partial \mathbf{x}_0} \qquad (5),$$

for $\frac{\partial L}{\partial \mathbf{x}_0'} = 0$:

$$\mathbf{x}_0' = \lambda \mathbf{W}^{-1} \frac{\partial R}{\partial \mathbf{x}_0} \qquad (6).$$

Calculation of these perturbations requires knowledge of the sensitivity to each variable, which means we must have information about sensitivity to *non-divergent* zonal and meridional flow, $\partial R/\partial u_{nd}$, $\partial R/\partial v_{nd}$. This is obtainable by computing the sensitivity with respect to vorticity, and then using this quantity to re-derive the sensitivity with respect to the horizontal wind field (Fig. 5.5).

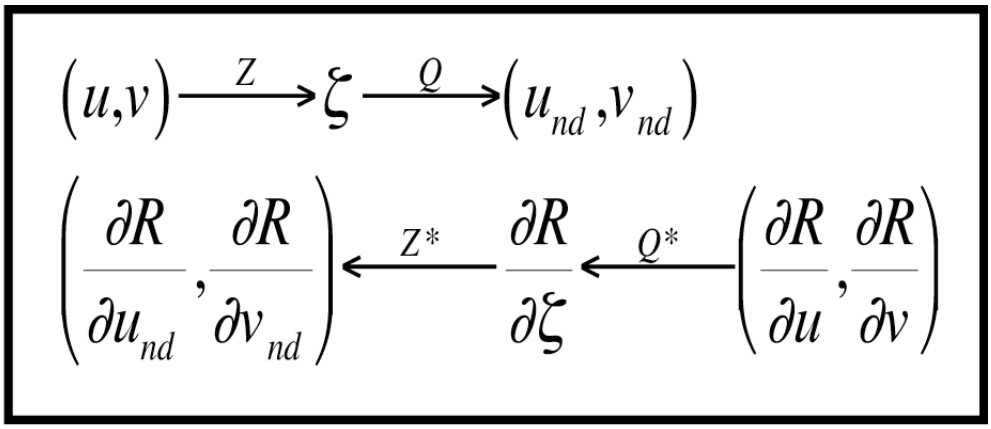

Figure 5.5. Flowchart describing routine for calculating non-divergent wind from full wind (top), and the adjoint of this procedure (bottom). Components of the full wind (u,v) are used to calculate vorticity ζ via the equation defining vorticity (Z): $Z = \frac{\partial v}{\partial x} - \frac{\partial u}{\partial y}$. Vorticity is inverted through an inverse Laplacian operator (Q) to define the non-divergent portion of the flow (u_{nd}, v_{nd}). Beginning with sensitivity to components of the full wind field, the sensitivity to vorticity can be calculated with the adjoint of the inverse Laplacian operator (Q^*). The adjoint of Z (Z^*) is then applied to calculate sensitivity to the non-divergent portion of the wind field from the sensitivity to vorticity.

Wind and temperature perturbations were calculated for $\Delta R = 22000\,Pa$, roughly analogous to a 0.5 hPa depression of sea-level pressure at each point within the response function domain, defined as a box 600 km across and centered on the tropical storm vortex at 24 hours. This modest change in intensity is intended to keep perturbations small, such that they operate linearly within the model. Perturbation experiments are performed using high-resolution model simulations (see below); the goal of calculating these perturbations for the 24 simulations at modest resolution is to determine if the structure of perturbations depends on the characteristics of the low-level westerly jet, and if there are any significant differences between perturbations calculated for barotropic cases versus non-barotropic cases.

ii) Profiles

Perturbations are separated into their kinetic energy and available potential energy components as defined by (1). Profiles of integrated perturbation energy on each sigma level (Fig. 5.6) reveal that most of the energy added to the model occurs in the lowest few sigma levels, coincident with the low-level westerly jet. Substantially more kinetic energy is concentrated at these low levels in the PBS cases than in the NBS cases, with the peak at 0.9250-sigma surpassing the 95% confidence limit. There appears to be no significant difference in the distribution of available potential energy, which seems to maximize slightly above the level of maximum perturbation kinetic energy. We can infer from these profiles that developing TCs in the PBS bin tend to be more distinctly sensitive to kinetic energy perturbations along the low-level jet, while optimal perturbations for those in the NBS bin are more spread throughout the lower troposphere.

b) High-resolution simulations: Alma (2008) and Linda (2009)

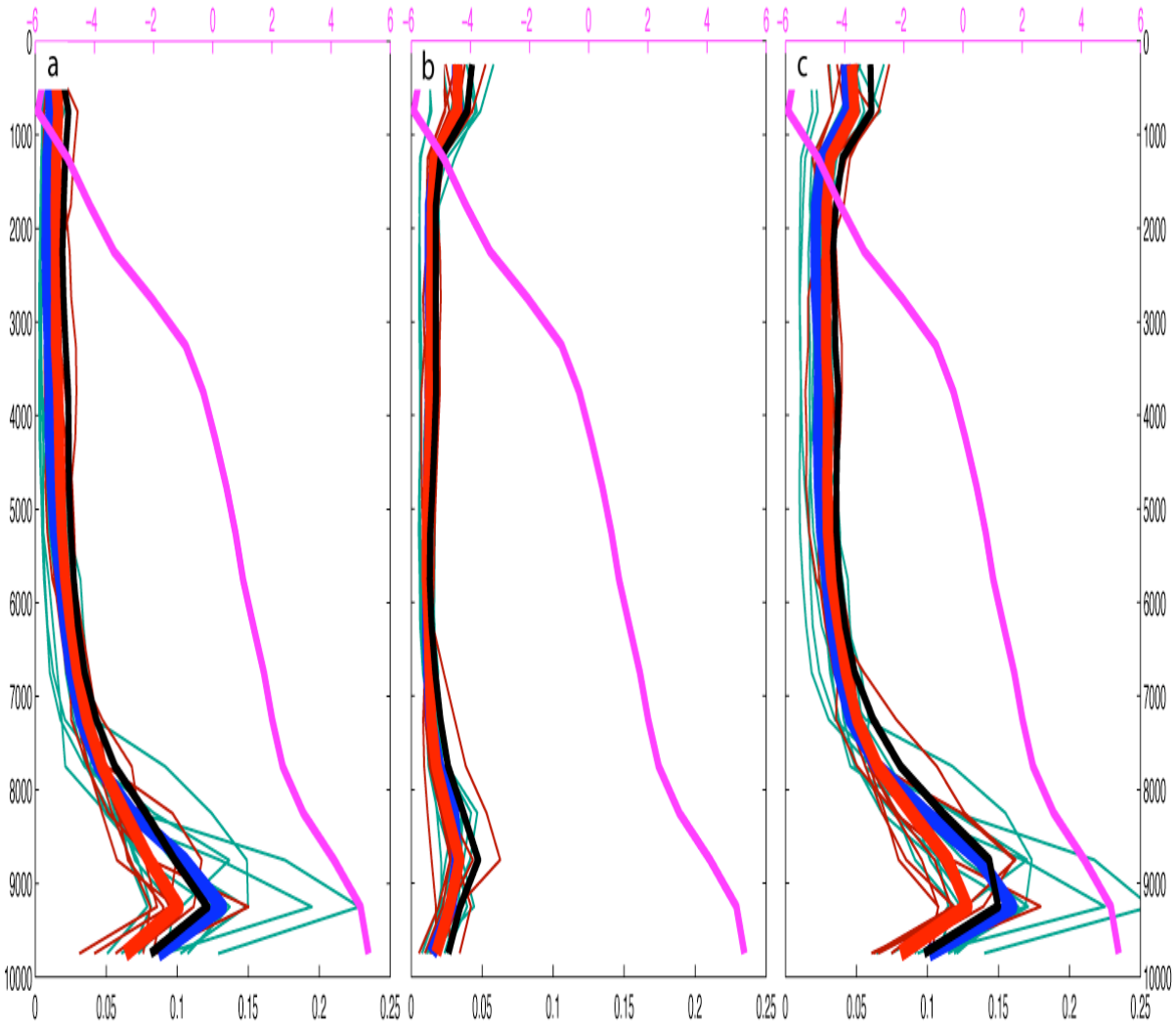

Figure 5.6. Vertical profiles of model-domain-integrated kinetic energy (a), available potential energy (b), and combined energy (c). Blue lines represent each of the 11 PBS cases, with the thick blue line indicating their average. Red lines represent each of the 8 NBS cases, with the thick red line indicating their average. The black line represent the upper limit of the 95% confidence interval on the NBS cases assuming 6 degrees of freedom in a student's T-test. The value of each curve on each level is normalized by the sum total of combined energy throughout the entire 3-dimensional model domain. Superimposed is a line (magenta) that shows the zonal jet as a zonal average of the zonal flow through the jet core with the mean subtracted.

One case was chosen to represent each of the PBS and NBS bins in higher-resolution (12 km grid spacing) simulations. The PBS cases are represented by tropical storm Alma (2008), which exhibits the strongest barotropic signature amongst all cases, while tropical storm Linda (2009) is chosen to represent the NBS cases because it appears to have no barotropic signature at all (Fig. 5.7). Simulations are run for 48 hours encompassing the 24 hours before declaration as a tropical storm and the 24 hours afterward. This is done in order to investigate the effect of perturbations on the evolution of these modeled TCs up to the time when the response function for sensitivity is defined (forecast hour 24) as well as the 24 hours afterward. It is desirable to determine if sensitivities of intensity defined for forecast hour 24 promote the general well-being of the cyclone at later times, or if perhaps these perturbations represent a highly non-balanced solution that increases intensity at verification of the response function and then quickly become a neutral or even negative influence on intensity thereafter (a phenomenon which will henceforth be referred to as "flare-out").

1) TROPICAL STORM ALMA (2008)

Tropical Storm Alma (2008) was unusual in several respects regarding its evolution and predictability (Brown 2008). Alma, having developed without the assistance of a tropical wave, formed farther east than any other east Pacific TC in history, and was the first recorded tropical storm to make landfall on the Pacific Coast of Central America. Alma was also well predicted by the National Hurricane Center (NHC), with substantially lower intensity errors for 24 and 48 hour forecasts than the average.

The environment in which Alma formed was dominated by a large cyclonic gyre on the northern side of a strong low-level westerly jet (Fig. 5.8). The gyre was positioned in the

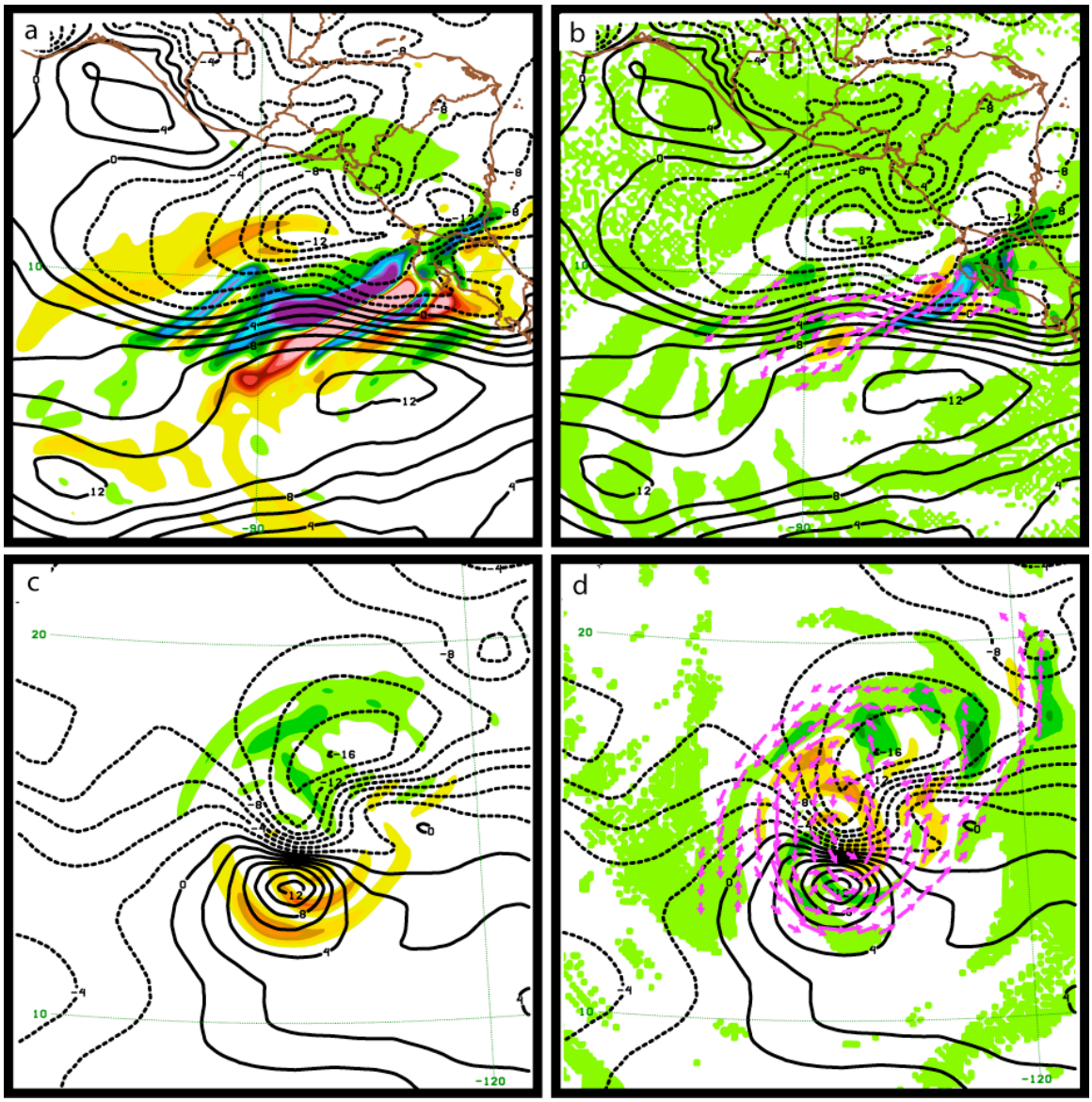

Figure 5.7. Sensitivities and derived perturbations for high-resolution simulations of Alma (2008) (panels a, b) and Linda (2009) (panels c, d) valid at model initialization. Zonal flow contoured every 2 m s^{-1} at the 0.9250 sigma level. Sensitivity to zonal flow (panels a, c) shaded every 0.2 Pa s m^{-1} (cool colors negative). Vectors (panels b, d) represent perturbation winds added to model level, and perturbation temperatures are shaded every 0.1 K (cool colors negative).

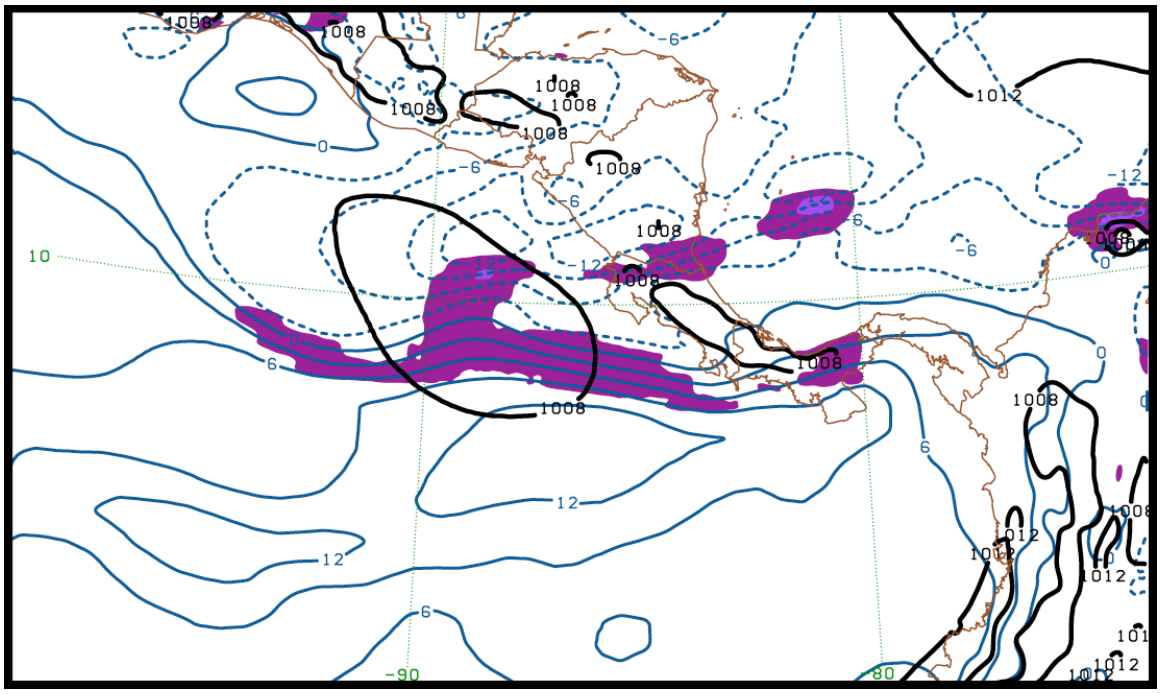

Figure 5.8. Initialization of model simulation of tropical storm Alma (2008) at 0000UTC 28 May 2008. Sea-level pressure contoured (black) every 4 hPa. Zonal flow contoured (blue, negative contours dashed) every 3 ms^{-1}, and relative vorticity (shaded) every $8x10^{-5}$ s^{-1} at the 0.8750 sigma level.

center of a zonally elongated region of shear vorticity; the amount of ambient cyclonic vorticity in the area of Alma's formation is in stark contrast to the environment surrounding Hurricane Linda (2009) (see below), and is primarily caused by the existence of the low-level westerly jet.

This shear-zone rotates within the gyre as it breaks up into many small vortices that begin to coalesce into a single major vortex by forecast hour 24 (Fig. 5.9). Throughout the next 24 hours, the cyclone is able to wrap the ambient vorticity of the environment around itself, reaching tropical storm intensity in the latter half of the 48 hr model simulation. The simulated tropical storm is slightly west, and is consistently more intense, than NHC best track (Fig. 5.10).

2) HURRICANE LINDA (2009)

A much longer-lived storm than Alma (2008), the genesis of Hurricane Linda (2009) (Berg 2009) can be traced back to an African easterly wave that entered the eastern Pacific basin on 28 August 2009. The system appeared to intensify through deep convection and, unlike Alma (2008), largely isolated from any obvious synoptic-scale environmental features. NHC forecasts showed moderate skill in prediction of Linda's intensity, with intensity forecasts at 24 and 36 hours being significantly worse than for forecasts of Alma (2008).

The tropical wave from which Linda emerged is largely the only synoptic-scale feature of its environment; nearly all cyclonic vorticity of the model domain is restricted to the vortex itself (Fig. 5.11). The low-level westerly jet is practically non-existent. The vortex intensifies modestly through the model simulation (Fig. 5.12), but lags behind NHC best track (Fig. 5.10). The lack of any ambient environmental vorticity means any

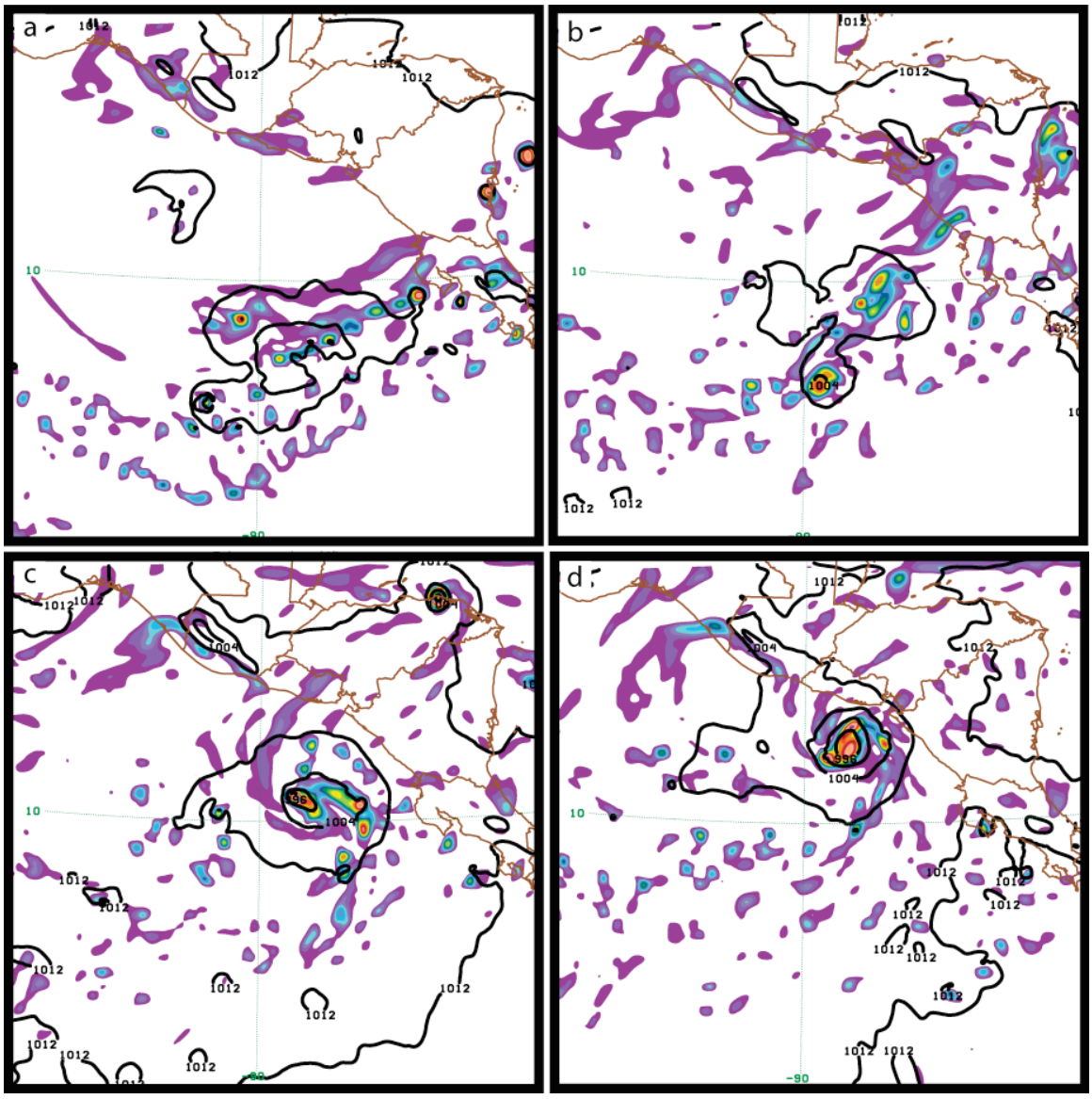

Figure 5.9. Simulation of tropical storm Alma (2008) initialized at 0000UTC 28 May 2008 at (a) 12 hours, (b) 24 hours, (c) 36 hours, and (d) 48 hours. Sea-level pressure contoured (black) every 4 hPa. Relative vorticity (shaded) every 8×10^{-5} s^{-1} at the 0.8750 sigma level.

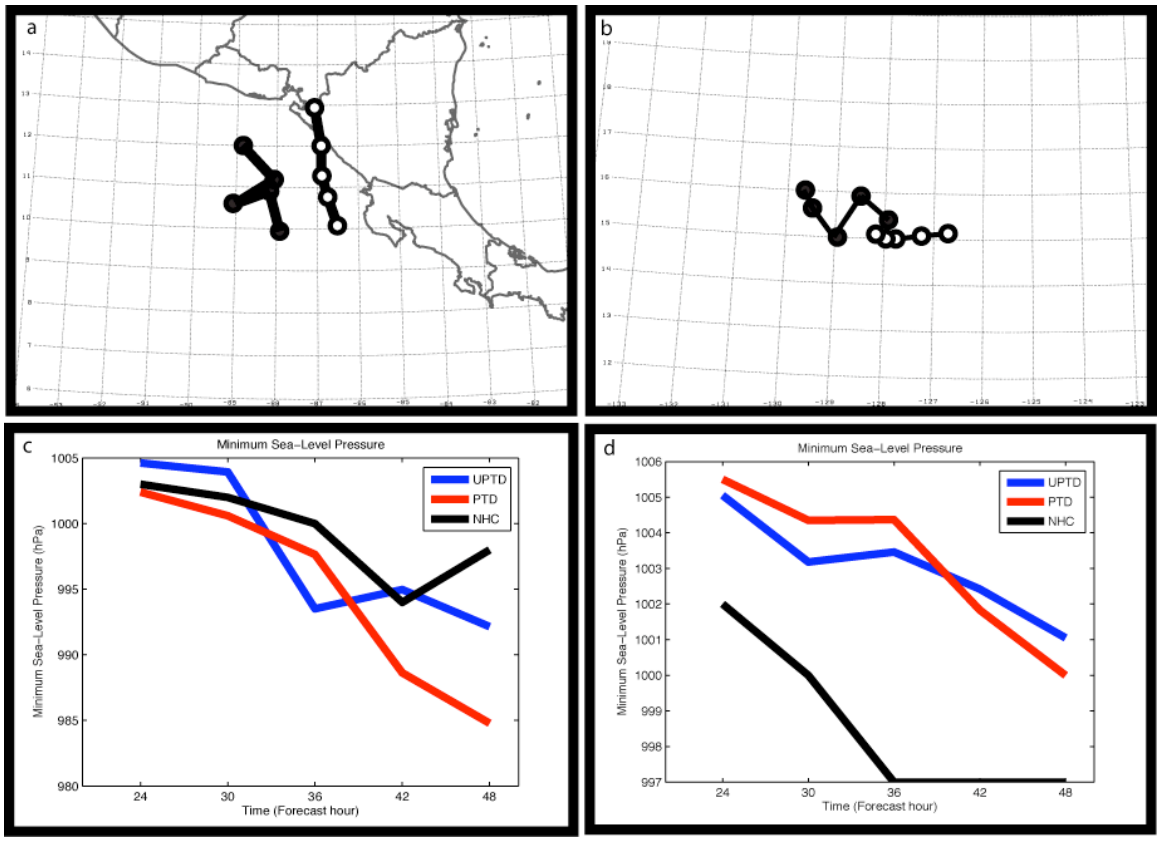

Figure 5.10. Track and intensity of Alma (2008) simulations (panels a and c, respectively) and Linda (2009) (panels b and d, respectively) compared to NHC best track for 24 hours after tropical storm declaration (forecast hour 24 to 48). (a and b) Location of minimum sea-level pressure in simulation (black) and NHC best track (white) every six hours. (c and d) Central minimum pressure (hPa) every six hours for original simulation (blue), simulation with perturbed initial conditions (red), and NHC best track (black).

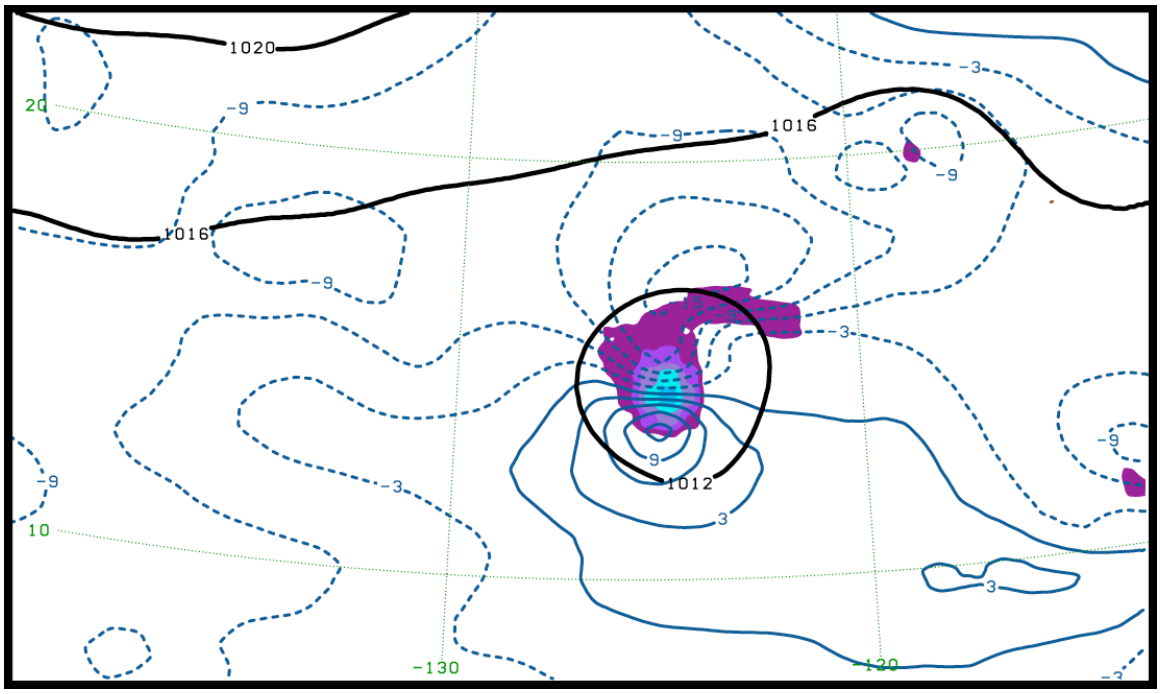

Figure 5.11. Initialization of model simulation of tropical storm Linda (2008) at 1800UTC 06 September 2009. Sea-level pressure contoured (black) every 4 hPa. Zonal flow contoured (blue, negative contours dashed) every 3 ms^{-1}, and relative vorticity (shaded) every $8x10^{-5}$ s^{-1} at the 0.8750 sigma level.

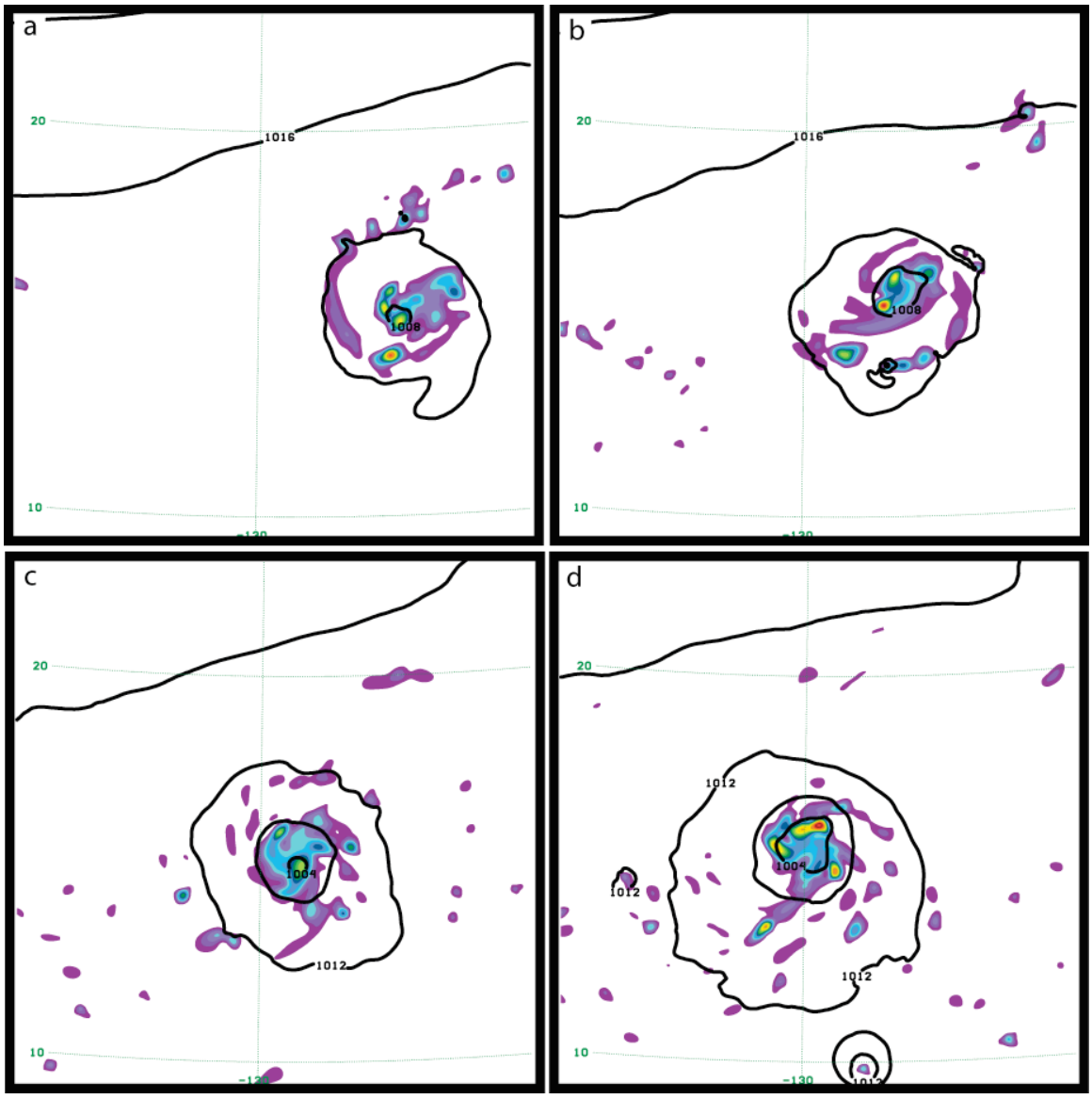

Figure 5.12. Simulation of tropical storm Linda (2009) initialized at 1800UTC 06 September 2009 at (a) 12 hours, (b) 24 hours, (c) 36 hours, and (d) 48 hours. Sea-level pressure contoured (black) every 4 hPa. Relative vorticity (shaded) every 8×10^{-5} s^{-1} at the 0.8750 sigma level.

intensification that does occur is due to storm-scale dynamics, which are notoriously poorly simulated, especially at modest model resolutions. Intensification through deep convection is also a mechanism of moist-dynamics that is not visible to the adjoint model. Hence, the sensitivity of Linda's intensity to horizontal flow is restricted to simply adding or subtracting vorticity within the tropical vortex itself (Fig. 5.7c).

3) PERTURBATIONS

Optimal perturbations are computed for $\Delta R = 22000\ Pa$. The response function box was maintained at 21x21 grid points; due to increased model resolution the physical area of this region is reduced to 240 km x 240 km. The structure of wind and temperature perturbations at low levels is illustrative of the possibility for barotropic growth in one case but not the other (Fig. 5.7). Perturbations to the initial conditions of the Alma (2008) simulation display the same upshear-tilt into the core of the low-level jet that is displayed in the sensitivities. Positive (negative) temperature perturbations are collocated with positive (negative) vorticity perturbations; this collocation is visible in sensitivities at any level throughout the evolution in both model simulations (not shown). Low-level perturbations of Linda (2009) display little beyond a general tendency to increase vorticity within the tropical wave; optimal vorticity perturbations at low levels are actually a mix of positive and negative vorticity despite sensitivity to vorticity being positive everywhere (Fig. 5.13), though negative perturbations are relegated to relative minima in sensitivity.

Profiles of normalized perturbation energy show that the characteristics of each case are similar to those of their respective PBS and NBS categories in the simulations at 30km resolution (Fig. 5.14). Perturbations for Alma (2008) are dominated by kinetic energy added

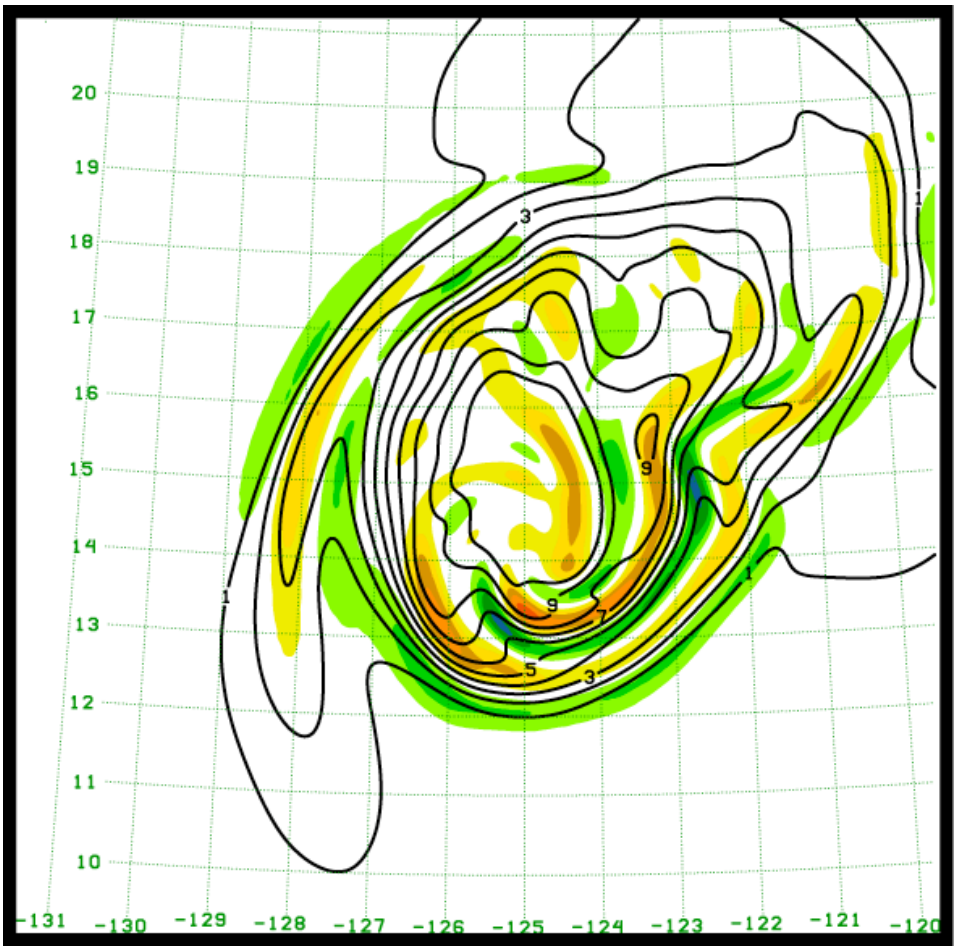

Figure 5.13. Vorticity perturbations (shaded every $5x10^{-6}$ s^{-1}, cool colors negative) and sensitivity to vorticity (black contours every $1x10^{4}$ Pa s) for initialization of Hurricane Linda (2009) simulation. Plotted on the 0.9250 sigma level.

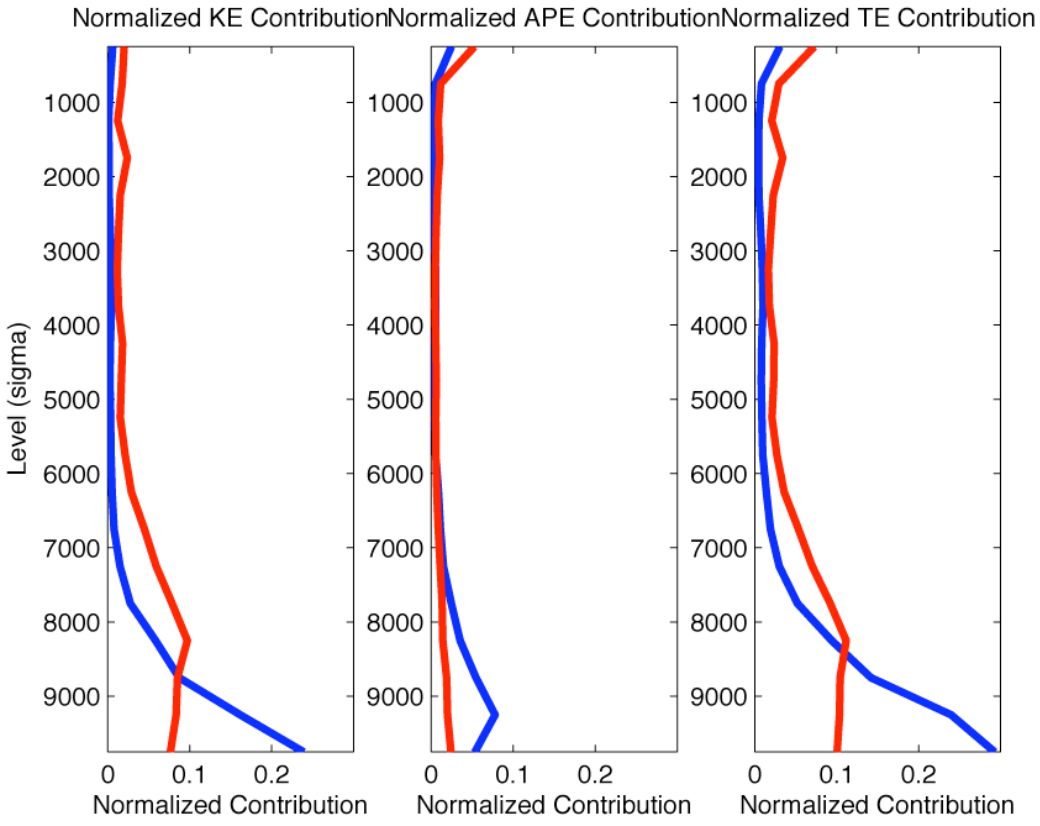

Figure 5.14. Vertical profiles of model-domain-integrated kinetic energy (a), available potential energy (b), and combined energy (c). Blue line represents the 12km resolution tropical storm Alma (2008) simulation. Red line represents the 12km resolution tropical storm Linda (2009) simulation. The value of each curve on each level is normalized by the sum total of combined energy throughout the entire 3-dimensional model domain.

at low levels, with practically no contribution added above the 0.7 sigma level. By contrast, the majority of kinetic energy in perturbations for Linda (2009) is distributed fairly evenly from the surface to about the 0.8 sigma level, then tapers off to near zero at the 0.55 sigma level. Temperature perturbations peak at low levels in Alma (2008), but are spread out throughout the depth of the atmosphere in Linda (2009). A raw (non-normalized) profile of total perturbation energy (Fig. 5.15) shows that much more energy is input into the initial conditions for Linda (2009) than for Alma (2008). This speaks to the barotropic growth mechanism present in the latter and absent in the former; with no way to *grow* vorticity once it has been input, Linda (2009) requires much more perturbation energy than Alma (2008) to yield the same result in 24 hours.

4) RESULTS

The model is run forward 48 hours with perturbed initial conditions. By design, perturbations are expected to decrease perturbation pressure in a 240 km x 240 km box centered on the developing tropical storm 24 hours into the model simulation. This expectation is based on the constraints of linearity and lack of moist physics in the adjoint model; while perturbations in the Linda (2009) case appear to hit this expected mark (Fig. 5.16), the effects of non-linearity and moist physics effect the development of Alma in ways unanticipated by the adjoint model. A time-series of evaluation of the integrated perturbation pressure in the response function box shows that this effect appears to be relegated to forestalling development in the response function box region by only an hour or so. Overall, the perturbations have the desired effect of reducing sea-level pressure at (or very close to) 24 hours into the model simulation.

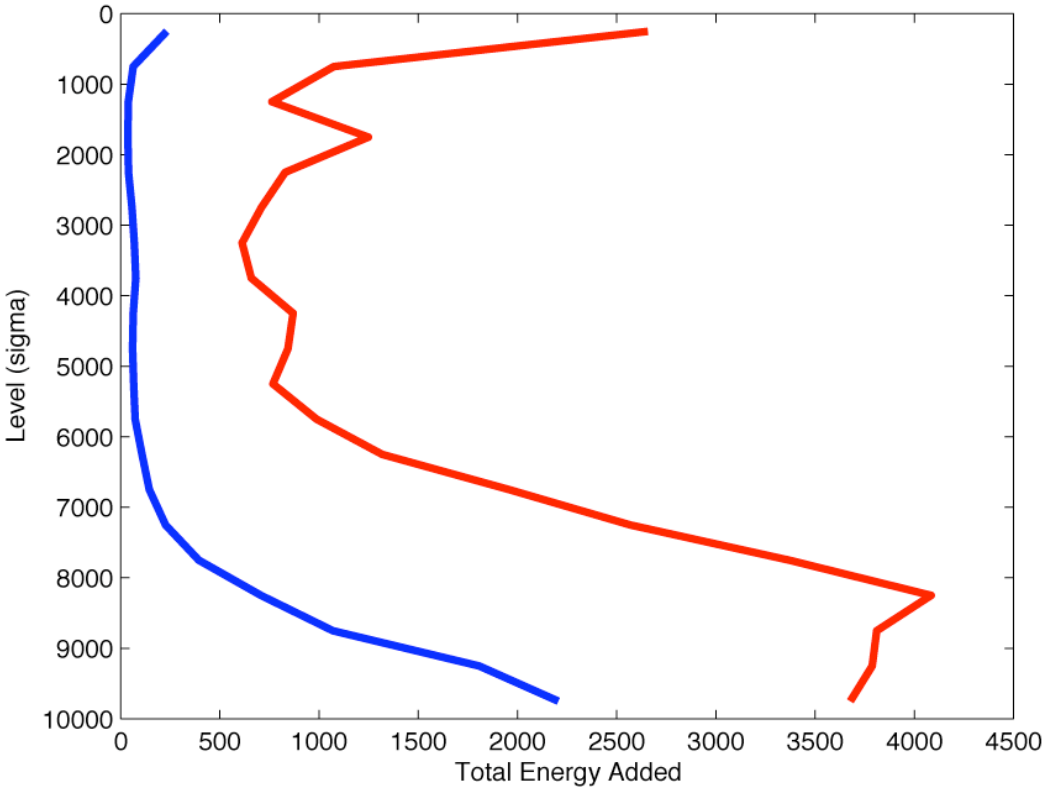

Figure 5.15. Vertical profiles of model-domain-integrated combined kinetic and available potential energy. Blue line represents the 12km resolution tropical storm Alma (2008) simulation. Red line represents the 12km resolution tropical storm Linda (2009) simulation.

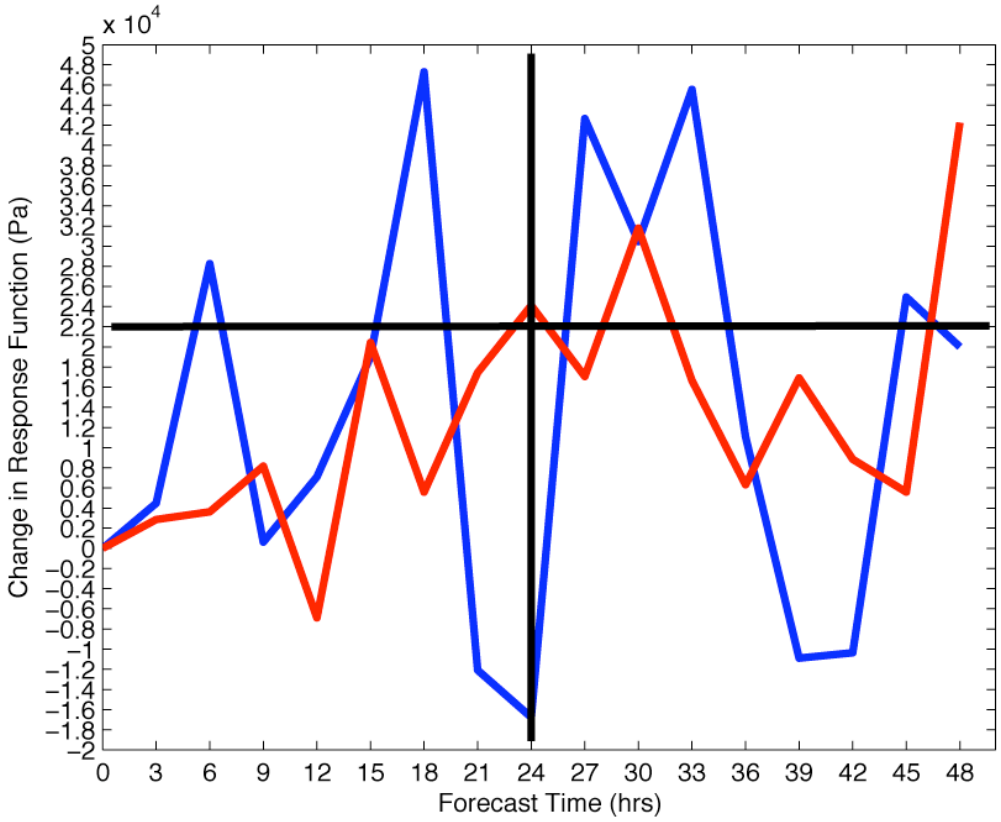

Figure 5.16. Time series of ΔR for Alma (blue) and Linda (red). Black lines cross at 24 hrs and ΔR=22000 Pa, which is the prescribed change in the response function given perturbations added to the initial conditions.

The effect perturbations impose on the simulation does not manifest as a consistent reduction of *minimum* sea-level pressure until after 36 hours (Fig. 5.10); after this time there is significant development in the Alma (2008) simulation, with a final minimum sea-level pressure reduction of 7 hPa and classifying Alma as a category-1 hurricane. Large departures from NHC best track intensity calculations beyond 42 hrs is at least partially the result of track errors that keep Alma out over the sea rather than making landfall. The perturbed Linda (2009) simulation never gets significantly deeper than the control simulation. While "flare-out" does not appear to be a problem for these simulations, it is clear that significant intensification due to these perturbations is relegated to the Alma (2008) simulation, likely due to the abundance of energy in the background that can be tapped through perturbations oriented correctly relative to the shear.

5.5 Conclusions

It has long been inferred that TCs in the eastern Pacific can take advantage of energy in the shear of their environment and grow barotropically. This *potential* for barotropic growth has since been difficult to identify; there is very little in the analysis fields themselves that can be used to conclusively show that a TC can grow barotropically in the environment provided precursor disturbances are oriented in a particular way, and the barotropic growth mechanism is not the sole cause of TC genesis in the eastern Pacific basin.

Using the adjoint of an NWP model, it has been shown that sensitivities to tropical vortex intensity often exhibit structures along the low-level westerly jet that tilt upshear, indicating the potential for barotropic growth. A survey of 24 cases of tropical storm genesis in the eastern Pacific in 2008 and 2009 show that roughly two-thirds of them exhibit some kind of barotropic-like structure. Composites of these cases into bins based on the relative

strength of this signature reveals that while the low-level westerly jet plays a critical role in whether the potential for barotropic growth exists, the strength of the jet is not the only determining factor. The strongest barotropic growth sensitivity is found in cases where the jet is not only strong, but also limited in its meridional extent. Optimal perturbations to increase intensity were found to be collocated with the low-level jet, with significantly more kinetic energy contributed at the level of the jet in PBS cases than NBS cases.

A representative case from the PBS and NBS composite bins was simulated at higher resolution to determine the impact of perturbations to the initial conditions based on these sensitivities. Relatively little perturbation energy is added to the initial conditions of the PBS case, resulting in a deepening of 7 hPa in minimum sea-level pressure by 48 hours, while in the NBS case substantially more energy was required to achieve the same result at verification of the response function (forecast hour 24), but no significant deepening was recorded after that point.

Adjoint-derived sensitivity gradients provide a wealth of dynamical information about the evolution of *specific aspects* of the model forecast that is otherwise difficult or impossible to produce. Even in the case of TC genesis, where non-linearity and the importance of moisture physics would otherwise place adjoint models at a distinct disadvantage, a sufficiently well crafted study can make use of this sensitivity information to provide direct evidence of a potentiality only hinted at by more traditional methods. When properly exercised as a *dynamical* tool, the adjoint model provides new insights and creates new directions for dynamical research.

Results of this study prompt further questions about east Pacific TC genesis, particularly with respect to predictability. Does this potentiality for barotropic growth, a

mechanism well modeled at even modest grid resolution, help delineate between TCs that are predicted far in advance from those that are poorly predicted? What kinds of precursor disturbances are most likely to take advantage of this potential growth mechanism? What kind of errors in initial conditions cause the most egregious forecast errors of TC genesis and intensity based on these sensitivities? Does this growth mechanism operate in other basins? Adjoint models may be used alongside more traditional methods in the future to answer these questions.

Acknowledgements

The first author is supported by the National Science Foundation under grant No. 0529343 and the Office of Naval Research under grant N000141610563PR.

Chapter 6: Conclusions

6.1 Dynamical Sensitivity Analysis of TC Steering and Genesis

Tropical cyclone predictability and TC forecasting encompasses a range of important problems that sit at a nexus between issues in dynamics of tropical systems and issues in data assimilation and optimization. Adjoint models are well positioned to effectively approach these questions from both dynamics and data assimilation perspectives. Beyond being a useful tool in optimizing assimilation of data into an analysis, adjoint models provide sensitivity gradients that contain large amounts of important dynamical information that can lead to new insights if the data can be properly interpreted. Due to limitations of linearity and simplified moisture physics, the adjoint model is not well suited to addressing *every* task in TC forecasting, but results indicate that well-posed questions that take these limitations into account can make use of adjoint-derived sensitivity gradients, even for some aspects of TC genesis.

Sensitivity gradients provide a lot of room for subjective, sometimes incorrect, dynamical interpretation. This is due to several aspects of their calculation. First, sensitivity gradients are calculated for a specific response function; if the response function chosen is vague or inappropriate by design for the task at hand, sensitivity gradients calculated for that response function will likewise be vague or inappropriate, and dynamical interpretation will suffer. Secondly, sensitivity gradients speak only to a *hypothetical* change in the chosen response function given a *hypothetical* perturbation to the model state. While some cause-and-effect must be established in order to make sense of these sensitivities, the adjoint model

itself provides almost no information as to *why* a response function is sensitive to one location or variable and not another.

A methodology has been established in this study that is meant to keep dynamical sensitivity analysis out of the realm of subjective conjecture, and ensure that interpretation of adjoint-derived sensitivity gradients is correct and consistent. First the nature of the study, expressed as a question being posed to the adjoint model, must be carefully considered given the limitations of the adjoint model. Studies that depend strongly on nonlinear interactions and moisture physics are obviously not well suited to an adjoint-based sensitivity analysis. However, one does not need to disregard entire branches of atmospheric science merely because nonlinearity and moisture physics play a role. Our analysis of east Pacific tropical cyclogenesis clearly shows that even within the subject of TC genesis there can be characteristics that are approachable with this technique.

Secondly, the response function must be tested for its appropriateness. This study shows that even a function that has been shown to be accurate in describing TC steering cannot automatically be trusted to behave appropriately as a response function and produce sensitivities of TC steering. This is due to the fact that the function for TC steering relies on several assumptions about the model trajectory, the most important being that the geographic region over which the steering is calculated is assumed to be centered on the TC. Since perturbations to the initial conditions can alter the track of the TC, and it is clear that the adjoint model is not restricted to only calculating sensitivities with respect to perturbations that do *not* change the TC track, sensitivity gradients for this function are strongly influenced by small perturbations to the final-time location of the TC within the response function box. Likewise, response function defining the intensity of a TC can be altered in several ways that

have nothing to do with TC intensity. These possibilities are discovered through rigorous testing of response function for appropriateness by perturbing the model initial conditions in regions of strong sensitivity and not only observing *how much* the response function changes, but observing *why* it changes. Once the reasons for a response function's inappropriateness are discovered, the function can be changed to eliminate those influences, and one can be satisfied that the sensitivities for that function are appropriate.

Finally, perturbations must also be introduced in order to observe *why* sensitivities exist in one region and not another. The mere existence of sensitivity coincident with a synoptic feature is not adequate to prove that the synoptic feature is important to the response function; typically a feature of the environment is important when it is responsible for large time tendencies (Langland et al. 1995). Several examples are available in this study. Strong sensitivity of TC steering to vorticity is found near the tropopause upstream of nearby midlatitude troughs; an analysis of perturbations in this region implies that these perturbations can grow in the subsidence region behind the trough and are advected into the middle troposphere. Perturbations at low levels near the low-level westerly jet in the eastern Pacific can have a strong impact on TC intensity in the basin because perturbations can grow at the expense of shear energy in the basic state. A combination of sensitivity gradients and perturbation experiments provides the most robust results; sensitivity gradients illustrate where perturbations will have the strongest impact, and perturbation experiments illustrate why these perturbations have such an influence.

5.2 Directions for Future Research

It is hoped that this study can galvanize future dynamical sensitivity analyses of any number of interesting dynamical problems using these or similar techniques. Some studies

that bill themselves as "sensitivity studies" by repeated but still ultimately arbitrary and subjective perturbation experiments could be replaced with adjoint-derived sensitivity analysis studies to reduce arbitrariness and provide more robust results. More theoretical work where adjoint models are considered dynamical tools are also needed in order to derive new response functions and new methodologies for calculating sensitivities to derived variables. Sensitivity with respect to potential vorticity, for example, has not been successfully derived, and the calculation of this quantity would go a long way to aiding dynamical sensitivity analysis by providing sensitivity with respect to a conserved variable (Kleist and Morgan 2005).

Future research in optimizing the deployment and assimilation of observations can greatly benefit from adjoint model techniques. Adaptive observations can greatly improve TC forecasting (Langland 2005), but the success of adaptive observations appears to lack consistency. While efforts have been made to base observation targeting on singular vector analysis (Langland 2005, Buizza et al. 2007) or reduction of mean flow variance with an ensemble transform Kalman filter (Langland 2005), little has been done in observation targeting to take advantage of the adjoint model's ability to produce sensitivity gradients for specific response functions (Wu et al. 2007, Wu et al. 2009a). It is possible that the lack of consistency in adaptive observation impact is due to poor dynamical understanding of how observations can influence TC steering and intensity forecasting and *why* observations should have a strong impact in one location but not another. This is a direction of research for which dynamical sensitivity analysis is well positioned to make great advances.

Improvement of adaptive observation and the creation of an objective, optimal targeting strategy must also consider how observations are assimilated into the analysis.

Even observational data that is obtained correctly and without substantial error can lead to forecast degradation if these observations are not assimilated properly (Aberson 2007). Again, adjoint models may be employed to address this issue. While a data assimilation system takes observations ($\mathbf{y}$) and a background model state ($\mathbf{x}_b$) to produce an optimal analysis ($\mathbf{x}_a$), the *adjoint* of a data assimilation system takes sensitivity with respect to the analysis state $\left(\partial R/\partial \mathbf{x}_a\right)$ and computes sensitivity to observations $\left(\partial R/\partial \mathbf{y}\right)$ and to the background state $\left(\partial R/\partial \mathbf{x}_b\right)$:

$$\mathbf{y},\mathbf{x}_b \xrightarrow{DA\ System} \mathbf{x}_a \quad ; \quad \frac{\partial R}{\partial \mathbf{y}},\frac{\partial R}{\partial \mathbf{x}_b} \xleftarrow{ADJ} \frac{\partial R}{\partial \mathbf{x}_a}. \qquad (1)$$

For an NWP model which is initialized with an analysis, $\partial R/\partial \mathbf{x}_a = \partial R/\partial \mathbf{x}_{in}$, such that the adjoint of the data assimilation system is initialized with the output of the adjoint of the dynamical model. This would produce sensitivities of, say, TC steering to an individual observation assimilated into the model, combining dynamical information about the sensitivity of TC steering to perturbations of the model initial state with information from the data assimilation system about how an observation is assimilated into the analysis.

Combining assimilation information with dynamical sensitivities avoids several targeting issues. For example, one would not want to take additional observations in a region where there is high confidence in the analysis state already; even if the response function were strongly sensitive to perturbations in this region one would not expect an additional observation to offer any more useful information. Likewise, observations should not be targeted in regions where observations are known to create large errors, such as data from dropsondes targeted into TC eye-walls that are assimilated assuming the dropsonde describes a straight, vertical profile (Aberson 2007). Information about observation and background

error and error covariances from the assimilation system would be present in sensitivity to individual observations that would mitigate these issues.

References

Aberson, S. D., 2002: Two years of operation hurricane synoptic surveillance. *Wea. Forecasting*, **17**, 1101-1110.

_____, 2003: Targeted observations to improve operational tropical cyclone track forecast guidance. *Mon. Wea. Rev.*, **131**, 1613-1628.

_____, 2007: Large degradations due to synoptic surveillance during the 2004 and 2005 hurricane seasons. *Mon. Wea. Rev.*, **136**, 3138-3150.

Ancell, B., and G. J. Hakim, 2007: Comparing adjoint- and ensemble-sensitivity analysis with applications to observation targeting. *Mon. Wea. Rev.*, **135**, 4117-4134.

Berg, R., 2009: Tropical Cyclone Report: Tropical Storm Linda. National Hurricane Center Tropical Cyclone Report EP152009.

Blessing, S., R. J. Greatbatch, K. Fraedrich, and F. Lunkeit, 2008: Interpreting the atmospheric circulation trend during the last half of the twentieth century: Application of an adjoint model. *J. Climate*, **21**, 4629-4646.

Brown, D. P., 2007: Tropical Cyclone Report: Hurricane Noel. National Hurricane Center Tropical Cyclone Report AL162007.

_____, 2008: Tropical Cyclone Report: Tropical Storm Alma. National Hurricane Center Tropical Cyclone Report EP012008.

Buizza, R., C. Cardinalli, G. Kelly, and J.-N. Thepaut, 2007: The value of observations II: The value of observations located in singular-vector-based targeting areas. *Quart. J. Roy. Meteor. Soc.*, **133**, 1817-1832.

Cardinalli, C., R. Buizza, G. Kelly, M. Shapiro, and J.-N. Thepaut, 2007: The value of observations III: Influence of weather regimes on targeting. *Quart. J. Roy. Meteor. Soc.*, **133**, 1833-1842.

Carr, L. E. III, and R. L. Elsberry, 1990: Observational evidence for prediction of tropical cyclone propagation relative to environmental steering. *J. Atmos. Sci.*, **47**, 542-546.

Chan, J. L., 2005: The physics of tropical cyclone motion. *Annu. Rev. Fluid Mech.*, **37**, 99-128.

_____, and W. M. Gray, 1982: Tropical cyclone movement and surrounding flow relationships. *Mon. Wea. Rev.*, **110**, 1354-1374.

_____, F. M. F. Ko, and Y. M. Lei, 2002: Relationship between potential vorticity tendency and tropical cyclone motion. *J. Atmos. Sci.*, **59**, 1317-1336.

Chen, J. H., M. S. Peng, C. A. Reynolds, and C. C. Wu, 2009: Interpretation of tropical cyclone forecast sensitivity from the singular vector perspective. *J. Atmos. Sci.*, **66**, 3383-3400.

DeMaria, M., and J. M. Gross, 2003: Evolution of tropical cyclone forecast models. *Hurricane! Coping with Disaster*, R. Simpson, Ed., Amer. Geophys. Union, 103-126.

Davis, C., C. Snyder, and A. C. Didlake, 2008: A vortex-based perspective of eastern Pacific tropical cyclone formation. *Mon. Wea. Rev.*, **136**, 2461–2477.

Doyle, J. D., C. M. Amerault, C. A. Reynolds, and J. R. Moskaitis, 2010: Initial condition sensitivity and predictability of tropical cyclogenesis. American Meteorological Society 29th Conference on Hurricanes and Tropical Meteorology.

Errico, R. M., 1997: What is an adjoint model? *Bull. Amer. Meteor. Soc.*, **78**, 2577-2591.

_____, and T. Vukicevic, 1992: Sensitivity analysis using an adjoint of the PSU-NCAR mesoscale model. *Mon. Wea. Rev.*, **120**, 1644-1660.

Farrell, B., 1990: Small error dynamics and predictability of atmospheric flow. *J. Atmos. Sci.*, **47**, 2409-2416.

Fehlmann, R., and H. C. Davies, 1997: Misforecasts of synoptic systems: diagnosis via PV retrodiction. *Mon. Wea. Rev.*, **125**, 2247-2264.

Ferrell, B. F., and A. M. Moore, 1992: An adjoint method for obtaining the most rapidly growing perturbation to oceanic flows. *J. Phys. Oceanogr.*, **22**, 338-349.

Ferriera, R. N. and W. H. Schubert, 1997: Barotropic aspects of ITCZ breakdown. *J. Atmos. Sci.*, **54**, 261-285.

Fiornio, M., and R. L. Elsberry, 1989: Some aspects of vortex structure related to tropical cyclone motion. *J. Atmos. Sci.*, **46**, 975-990.

Flatau, M., W. H. Schubert, and D. E. Stevens, 1994: The role of baroclinic processes in tropical cyclone motion: the influence of vertical tilt. *J. Atmos. Sci.*, **51**, 2589-2601.

Gelaro, R., R. Buizza, T. N. Palmer, and E. Klinker, 1998: Sensitivity analysis of forecast errors and the construction of optimal perturbations using singular vectors. *J. Atmos. Sci.*, **55**, 1012-1037.

Guinn, T. A. and W. H. Schubert, 1993: Hurricane spiral bands. *J. Atmos. Sci.*, **50**, 3380-3403.

Hall, M. C. G., and D. G. Cacuci, 1983: Physical interpretation of adjoint functions for sensitivity analysis of atmospheric models. *J. Atmos. Sci.*, **40**, 2537-2546.

_____, 1986: Application of adjoint sensitivity theory to an atmospheric general circulation model. *J. Atmos. Sci.*, **43**, 2644-2651.

Hartmann, D. L. and E. D. Maloney, 2001: The Madden-Julian Oscillation, barotropic dynamics, and north Pacific tropical cyclone formation. Part II: Stochastic barotropic modeling. *J. Atmos. Sci.*, **58**, 2559-2570.

Hogan, T., and T. E. Rosmond, 1991: The description of the Navy Operational Global Atmospheric Prediction System's spectral forecast model. *Mon. Wea. Rev.*, **119**, 1786-1815.

Holland, G. J., 1983: Tropical cyclone motion: environmental interaction plus a beta effect. *J. Atmos. Sci.*, **40**, 328-342.

Hoover, B. T., 2009: Comments on "Interaction of Typhoon Shanshan (2006) with the midlatitude trough from both adjoint-derived sensitivity steering vector and potential vorticity perspectives". *Mon. Wea. Rev.*, **137**, 4420-4424.

_____, and M. C. Morgan, 2010: Validation of a tropical cyclone steering response function with a barotropic adjoint model. *J. Atmos. Sci.*, **67**, 1806-1816.

Kleist, D. T. and M. C. Morgan, 2005: Interpretation of the structure and evolution of adjoint-derived forecast sensitivity gradients. *Mon. Wea. Rev.*, **133**, 466-484.

Langland, R. H., 2005: Issues in targeted observing. *Quart. J. Roy. Meteor. Soc.*, **131**, 3409-3425.

_____, and N. Baker, 2004: Estimation of observation impact using the NRL variational atmospheric data assimilation adjoint system. *Tellus*, **56A**, 189-201.

_____, R. L. Elsberry, and R. M. Errico, 1995: Evaluation of physical properties in an idealized extratropical cyclone using adjoint sensitivity. *Quart. J. Roy. Meteor. Soc.*, **121**, 1349-1386.

_____, and R. M. Errico, 1996: Comments on "Use of an adjoint model for finding triggers for Alpine lee cyclogenesis". *Mon. Wea. Rev.*, **124**, 757-760.

Lewis, J. M., and J. C. Derber, 1985: The use of adjoint equations to solve a variational adjustment problem with advective constraints. *Tellus*, **37**, 309-322.

Lorenz, E. N., 1963: Deterministic nonperiodic flow. *J. Atmos. Sci.*, **20**, 130-141.

_____, 1965: A study of the predictability of a 28-variable atmosphere model. *Tellus*, **17**, 321-333.

Maloney, E. D. and D. L. Hartmann, 2001: The Madden-Julian Oscillation, barotropic dynamics, and north Pacific tropical cyclone formation. Part I: Observations. *J. Atmos. Sci.*, **58**, 2545-2558.

McTaggart-Cowan, R., J. R. Gyakum, and M. K. Yau, 2004: The impact of tropical remnants on extratropical cyclogenesis: case study of Hurricanes Danielle and Earl (1998). *Mon. Wea. Rev.*, **132**, 1933-1951.

Peng, M. S., and C. A. Reynolds, 2006: Sensitivity of tropical cyclone forecasts as revealed by singular vectors. *J. Atmos. Sci.*, **63**, 2508-2528.

Poveda, G. and O. J. Mesa, 2000: On the existence of the Lloro (the rainiest locality on Earth): enhanced ocean-land-atmosphere interaction by a low-level jet. *Geophys. Res. Lett.*, **27**, 1675-1678.

Rosmond, T. E., 1997: A technical description of the NRL adjoint modeling system. NRL/MR/7532/97/7230 Available from the Naval Research Laboratory, Monterey, CA 93943-5502, 62 pp.

_____, J. Teixeira, M. Peng, T. Hogan, and R. Pauley, 2002: Navy Operational Global Atmospheric Prediction System (NOGAPS). *Oceanography*, **15**, 99-108.

Shapiro, L. J., 1992: Hurricane vortex motion and evolution in a three-layer model. *J. Atmos. Sci.*, **49**, 140-154.

Thompson, C. J., 1998: Initial conditions for optimal growth in a coupled ocean-atmosphere model of ENSO. *J. Atmos. Sci.*, **55**, 537-557.

Velden, C. S., and L. M. Leslie, 1991: The basic relationship between tropical cyclone intensity and the depth of the environmental steering layer in the Australian region. *Wea. Forecasting*, **6**, 244-253.

Vukicevic, T., and K. Raeder, 1995: Use of an adjoint model for finding triggers for Alpine lee cyclogenesis. *Mon. Wea. Rev.*, **123**, 800-816.

Wu, C. C., and K. A. Emanuel, 1993: Interaction of a baroclinic vortex with background shear: application to hurricane movement. *J. Atmos. Sci.*, **50**, 62-76.

_____, and _____, 1995: Potential vorticity diagnostics of hurricane movement. Part I: a case study of Hurricane Bob (1991). *Mon. Wea. Rev.*, **123**, 69-92.

_____, J. H. Chen, P. H. Lin, and K. H. Chou, 2007: Targeted observations of tropical cyclone movement based on the adjoint-derived sensitivity steering vector. *J. Atmos. Sci.*, **64**, 2611–2626.

_____, and Coauthors, 2005: Dropwindsonde observations for typhoon surveillance near the Taiwan region (DOTSTAR): An overview. *Bull. Amer. Meteor. Soc.*, **86**, 787-790.

_____, S. G. Chen, J. H. Chen, K. H. Chou, and P. H. Lin 2009a: Interaction of Typhoon Shanshan (2006) with the midlatitude trough from both adjoint-derived sensitivity steering vector and potential vorticity perspectives. *Mon. Wea. Rev.*, **137**, 852-862.

_____, and Coauthors, 2009b: Intercomparison of targeted observation guidance for tropical cyclones in the northwestern Pacific. *Mon. Wea. Rev.*, **137**, 2471-2492.

Wu, L., and B. Wang, 2000: A potential vorticity tendency diagnostic approach for tropical cyclone motion. *Mon. Wea. Rev.*, **128**, 1899-1911.

Zou, X., F. Vandenberghe, M. Pondeca, and Y. H. Kuo, 1997: Introduction to adjoint techniques and the MM5 adjoint modeling system. NCAR TN-435-STR.

_____, W. Huang, and Q. Xiao, 1998: A user's guide to the MM5 adjoint modeling system. NCAR TN-437+IA.